BEHAVIORAL AND THEORETICAL EVIDENCE THAT NON-DIRECTIONAL MOTION DETECTORS UNDERLIE THE VISUAL ESTIMATION OF SPEED IN INSECTS.

by

Jonathan P. Dyhr

A Dissertation Submitted to the Faculty of the

GRADUATE INTERDISCIPLINARY PROGRAM IN NEUROSCIENCE

In Partial Fulfillment of the Requirements
For the Degree of

DOCTOR OF PHILOSOPHY

In the Graduate College

THE UNIVERSITY OF ARIZONA

2009

THE UNIVERSITY OF ARIZONA
GRADUATE COLLEGE

As members of the Dissertation Committee, we certify that we have read the dissertation prepared by Jonathan P. Dyhr
entitled Behavioral and Theoretical Evidence that Non-directional Motion Detectors Underlie the Visual Estimation of Speed in Insects.
and recommend that it be accepted as fulfilling the dissertation requirement for the Degree of Doctor of Philosophy.

Date: 9 October 2009
Charles M. Higgins

Date: 9 October 2009
Wulfila Gronenberg

Date: 9 October 2009
Timothy Secomb

Date: 9 October 2009
Nicholas J. Strausfeld

Date: 9 October 2009
Joseph Watkins

Final approval and acceptance of this dissertation is contingent upon the candidate's submission of the final copies of the dissertation to the Graduate College.
I hereby certify that I have read this dissertation prepared under my direction and recommend that it be accepted as fulfilling the dissertation requirement.

Date: 9 October 2009
Dissertation Director: Charles M. Higgins

STATEMENT BY AUTHOR

This dissertation has been submitted in partial fulfillment of requirements for an advanced degree at the University of Arizona and is deposited in the University Library to be made available to borrowers under rules of the Library.

SIGNED: Jonathan P. Dyhr

ACKNOWLEDGEMENTS

This work would never have been completed without the help of many different individuals. I am thankful to my advisor Chuck Higgins who dedicated much time and red ink in helping me with this work. Also, I would not have been able to accomplish any of this work without the help of my fellow graduate students, particularly Vivek Pant, Angelique Paulk, Andre Riveros, Lise Johnson and Tim Melano who have all assisted, guided and critiqued my research. I would also like to thank my committee members Wulfila Gronenberg, Joe Watkins, Nick Strausfeld and Timothy Secomb for their patience and assistance over the course of my dissertation research.

I am also extremely grateful to Erin Wolfe for her administrative expertise which have greatly simplified my life as a graduate student and Konrad Zinsmaier for striving to improve graduate education in the Neuroscience program.

Finally, and most importantly, I would like to thank my friends and family. My parents and brothers have been an unfailing source of support and love and I cannot express how much of a blessing they have been in my life. I am also grateful to Lise Johnson for helping make the past six and a half years more enjoyable than they had any right to be and helping me figure out what is really important in life. I am thankful for the friendship and camaraderie of Vivek Pant who has encouraged and challenged me throughout graduate school. I would also like to thank my friends Carrie, Duke, Jenna, Jill, Matt, my fellow Neuroscience graduate students and the Graduate Christian Fellowship for keeping me grounded and helping me have fun and escape school and research every once and a while.

DEDICATION

This work is dedicated to my family for their unending love, support and encouragement.

TABLE OF CONTENTS

TABLE OF CONTENTS – *Continued*

LIST OF FIGURES

ABSTRACT

Insects use an estimate of the angular speed of the visual image across the eye (termed optic flow) for a wide variety of behaviors including flight speed control, visual navigation, depth estimation, grazing landings, and visual odometry. Despite the behavioral importance of visual speed estimation, the neuronal mechanisms by which the brain extracts optic flow information from the retinal image remain unknown. This dissertation investigates the underlying neuronal mechanisms of visual speed estimation via three complementary strategies: the development of neuronally-based computational models, testing of the models in a behavioral simulation framework, and behavioral experiments using bumblebees. Using these methods I demonstrate the sufficiency of two non-directional models of motion detection for reproducing real-world, speed dependent behaviors, propose potential neuronal circuits by which these models may be physiologically implemented, and predict the expected responses of these neurons to a range of visual stimuli.

CHAPTER 1

Introduction

1.1 Motivation

For many animals, the visual system plays a vital role in detecting important features in the environment for tasks such as navigation, recognition of threats, and the identification of potential food sources and mates. The visual portion of these tasks are accomplished using only the discretely sampled, two-dimensional intensity pattern incident upon the retina. While extracting information about the three-dimensional world from a two-dimensional visual image is a difficult problem in itself, issues such as a limited sampling of the available light spectrum and luminance levels that vary over more than ten orders of magnitude provide further complications (Land and Nilsson, 2002). The apparent ease with which the visual system addresses these problems belies their complexity and that of the underlying neuronal architecture. Even our most advanced artificial systems have yet to approach the full capabilities of even 'simple' biological systems.

Understanding the different aspects of visual processing has required input from diverse fields of study including mathematics, engineering, physics and biology. This multidisciplinary approach has led to a tremendous increase in our knowledge about the general organization of visual systems, but we still lack a detailed mechanistic understanding of some of the most fundamental neuronal computations. For example, while we know that different types of information, such as color, form and motion, are segregated at the earliest stages of visual processing, we do not understand how they are combined to segment the visual world into different objects (Pinto et al., 2008). What is clear is that similar anatomical organization and computational

strategies of the visual system have evolved independently in many different organisms, suggesting that these solutions are, in some sense, evolutionarily optimal (see Section 2.5).

Because of this evolutionary convergence, investigations into smaller organisms whose brains contain many fewer neurons, such as insects, have contributed greatly to our understanding of visual processing. The typical fly brain contains on the order of one million neurons, half of which are contained in the optic lobes (Strausfeld, 1976; Osorio and Bacon, 1994), compared to the approximately one hundred billion neurons in the human brain (Koch, 1999). In contrast to mammalian systems, neurons in the insect brain are individually identifiable, allowing one to record from and stain the same neuron across multiple preparations. Homologous neurons can also be identified across different species, allowing one to determine the critical components of a neuronal circuit via comparative studies and to relate behavioral differences to neuronal variations (Buschbeck and Strausfeld, 1996). Combined with a wide repertoire of interesting visual behaviors, many of which are shared with primates (Section 2.5), insects can serve as excellent model systems for studying visual processing.

One aspect of vision that has been of particular interest to scientists and engineers is the detection of visual motion. As organisms move through their environment, they experience a large amount of self-generated visual motion, termed *egomotion*. While this movement degrades the ability to identify slow-moving objects, it also generates useful information about the relative distance of objects, movement speed and distance traveled. Externally generated changes in the visual field are equally important, whether it is an object moving in the environment or an external force displacing the organism. These different types of motion must all be parsed out from the intensity fluctuations of the two-dimensional visual image. Evidence suggests that in order to accomplish this, the insect visual system has multiple motion pathways for processing different types of motion, whether it is the

speed of the visual image due to egomotion (Srinivasan and Zhang, 2004), externally generated drift (Hassenstein and Reichardt, 1956), or the tracking of small targets (Land and Collett, 1974).

In the present work, I am specifically interested in how the insect brain calculates *optic flow*, defined as the angular velocity of a single point in the visual image (Horn and Schunck, 1981). The computation of optic flow is critical for many behaviors (reviewed in Section 2.2), but a definitive underlying neuronal circuit remains unidentified. In this work we combined a top down approach, in which I used behavioral studies to identify the properties of the neuronal mechanisms, with a systems level analysis of our current electrophysiological and anatomical knowledge of the early visual pathways to develop comprehensive, neuronally-based models of visual speed estimation. I then tested the efficacy of these models to reproduce real-world behaviors in a behavioral simulation framework so that results could be compared directly to previous experimental findings and to make specific model predictions to guide future experimental design.

1.2 Guide to Thesis

I first review previous work on visual motion detection in insects (Chapter 2), beginning with the directionally selective motion pathway responsible for the image stabilizing optomotor response (Section 2.1). As one of the earliest studied motion detection behaviors, much of our knowledge of the neural processing of motion stems from studies of the optomotor system, making it important for framing the problem of visual speed estimation. In addition, the combination of top-down modeling (Hassenstein and Reichardt, 1956; Borst and Egelhaaf, 1989) and the discovery of direction-selective neurons involved in the production of optomotor behavior (Hausen, 1981; Hausen and Wehrhahn, 1983) has led to the identification of a putative neuronal circuit (Higgins et al., 2004) providing a template for neuroethological studies, in which one attempts to identify the neuronal circuits responsible for spe-

cific behaviors.

Next, I provide a comprehensive review of optic flow dependent behaviors (Section 2.2) identifying the response properties of the visual speed estimation mechanism and differentiating it from that of the optomotor response. In Section 2.3 I survey the neuroanatomy of the insect visual system in order to provide a basis for the identification of potential neuronal correlates of these behaviors. I then review previous modeling studies, both of the optomotor and optic flow systems, connecting the behavioral results to the underlying neuronal circuits (Section 2.4). In particular, I focus on a class of non-directional, motion sensitive models, whose responses increase proportionally to speed but are insensitive to the direction of motion, that we believe may underlie the visual speed estimation system (Higgins, 2004; Rivera-Alvidrez, 2005; Pant, 2007). Finally, in Section 2.5 I compare the visual systems of insects and primates to support the applicability of our work to more complex organisms.

My contribution to the field is divided into three papers provided in the appendices. Appendix A presents a behavioral simulation framework in which to test the efficacy of different models of motion detection for reproducing the visual speed dependent behaviors described in Section 2.2. Appendix B is dedicated to the further development of the non-directional models presented in Section 2.4.4 and their subsequent testing in the behavioral simulation framework. Finally, Appendix C describes behavioral experiments with live bumblebees conducted in order to provide further support for the biological relevance of the non-directional models.

1.3 Summary

Previous biologically-based models of motion detection have been insufficient to explain how insects are capable of estimating the angular speed of an image using only the two-dimensional intensity fluctuations incident upon the retina, despite clear behavioral evidence that optic flow plays a critical role in visual navigation.

The goal of this dissertation is to further develop neuronally-based models of visual speed estimation consistent with the available behavioral, electrophysiological and neuroanatomical data. With these models, we can guide further behavioral and electrophysiological investigations by targeting specific neuronal populations and predicting behavioral and electrophysiological responses to different visual stimuli. Depending on the success of these predictions, the mechanisms discussed in this dissertation may be more broadly applicable to visual processing in other organisms.

CHAPTER 2

Background

2.1 The Optomotor Response

One of the most well known examples of a computational model predicting neuronal responses comes from the seminal work of Hassenstein and Reichardt (1956) who studied the turning response of the *Chlorophanus viridis* beetle in response to the rotation of a striped drum, termed the *optomotor response*. As part of this work they developed the Hassenstein-Reichardt (HR) model, which has since been elaborated to model motion detection in many other animals, including humans (van Santen and Sperling, 1985). In this section, we describe the optomotor response and the experimental methods used to investigate the underlying mechanisms, and introduce the HR model.

The optomotor response is a gaze stabilization behavior elicited by slow, wide-field drift of the visual field due to rotation or lateral translation, such as would be caused by a gust of wind blowing a flying insect off course. By turning in the direction of the apparent visual motion and stabilizing the visual image, the insect counteracts the change in its course. This behavior is particularly important for accurate navigation because mechanosensors cannot detect constant translatory movement, only acceleration, deceleration, and rotational movements (Buchner, 1984).

Early "cybernetic" investigations of the optomotor response treated insects as a "black box" in which a visual input was presented to an insect in a controlled environment and the insect's response was measured. A method first developed by Hassenstein (1951) was to measure the turning behavior of a tethered *Chorophanus* beetle in response to a rotating stimulus using a "y-maze" sphere, pictured

in Figure 2.1. The branch points in the y-maze forced the insect to "turn" either right or left and allowed the experimenters to quantitativly describe of the insect's turning response. These early studies in which the insect had no control over the visual stimulus were termed "open-loop" experiments. More sophisticated methods were subsequently developed for controlling the visual stimulus, such as projecting a panoramic visual stimulus (Götz, 1968) or using arrays of LEDs (Strauss et al., 1997; Lehmann and Dickinson, 1997; Reiser and Dickinson, 2008), and for measuring the turning responses of flying via either a torque meter (Götz, 1964) or through optical analysis of the insect's wing beats (Götz, 1987). An example optomotor behavioral setup is shown in Figure 2.2. The precise and automated measurement of the optomotor response then enabled investigators to perform "closed-loop" experiments in which the response of the insect could be used to control the visual stimulus (Götz, 1964). Using these methods, optomotor behaviors have been studied extensively in many different insect species, most notably honeybees (Kunze, 1961), fruit flies (Götz, 1972; Buchner, 1984), and houseflies (Fermi and Reichardt, 1963). It is also believed that other motion dependent behaviors, such as the leg extension reflex used for landing (Borst and Bahde, 1987), are controlled by a similar mechanism.

In parallel with the behavioral investigations, directionally-selective lobula plate tangential cells (LPTCs) were discovered and characterized in flies (see Section 2.3.2; Hausen, 1981, 1982; Reichardt et al., 1983). The responses of these cells match those predicted by Hassenstein and Reichardt (1956), and lesion studies have shown that LPTCs play an important role in the production of optomotor behaviors (Hausen and Wehrhahn, 1983), suggesting that they underlie optomotor behaviors (Egelhaaf and Borst, 1993). Because of this, electrophysiological investigations of these cells have been used to further study the properties of the optomotor mechanism. These electrophysiological investigations have typically presented computer-controlled stimuli to large areas of the visual field while recording from one of the approximately 60 tangential cells present in the lobula plate (Egelhaaf and Borst,

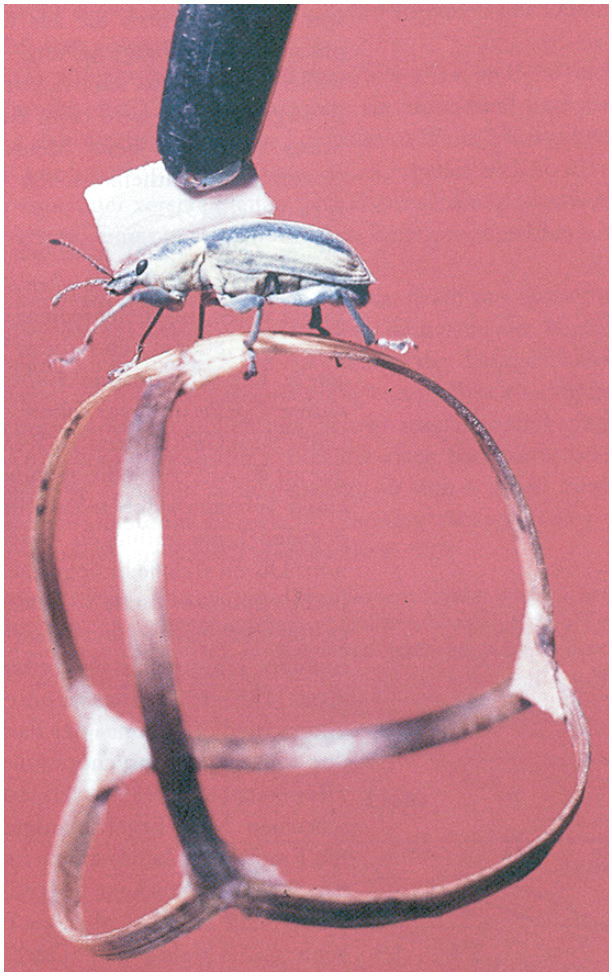

Figure 2.1: Tethered *Chlorophanus* preparation. Experimental preparation of a *Chlorophanus* beetle used in the studies of Hassenstein (1951); Hassenstein and Reichardt (1956). The turning response of the tethered beetle was measured as it crawled along a y-maze, a wire sphere with four y-shaped forks. The proportion of left versus right turns in response to a rotating drum was used to quantify its turning response. Reprinted by permission from Macmillan Publishers Ltd: Nature Neuroscience (Borst, 2000), copyright 2000.

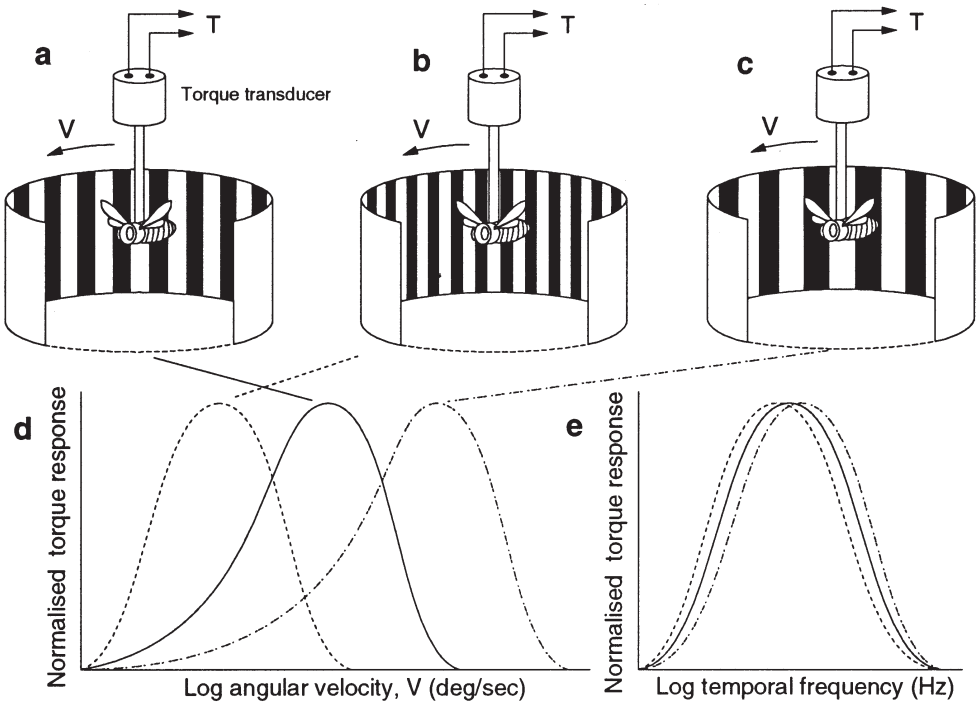

Figure 2.2: Example optomotor response experiments. Panels (a-c) A fly is fixed to a torque meter within a striped drum rotating at a constant velocity. The fly will attempt to turn in the direction of the rotating pattern in order to counteract the visual motion. Experiments can either be open-loop, in which the response of the fly does not change the velocity of the rotating pattern, or closed-loop, in which the velocity of the drum is modulated using the torque response. (d) The magnitude of the turning response is not tuned to stimulus speed because the insects' response to a pattern moving at a fixed speed is a function of the pattern spatial frequency. (e) Instead, the response appears to be tuned to the temporal frequency of the moving pattern. Reprinted from Srinivasan et al. (1999a) with permission from Elsevier.

1993).

Using these techniques it has been shown that the optomotor response is elicited by coherent motion in a single direction using a directionally selective wide-field mechanism that integrates the motion over large patches of the visual field. Although tangential cells are sensitive to sequential stimulation of individual photoreceptors (Franceschini et al., 1989), such small stimuli are not sufficient to elicit a behavioral turning response. There is evidence of specialization in different areas of the eye. Moore and Rankin (1982) found that, for honeybees, the preferred direction for eliciting a characteristic yaw torque response was different for different areas of the eye. When they occluded the lateral portion of the eyes of the bees, so that only the frontal visual field received visual input, the optomotor response was elicited only by back-to-front motion. In contrast, the lateral visual fields elicited stronger optomotor responses and were sensitive only to front-to-back motion.

These apparently contradictory results are addressed by studies of *Drosophila* by Tammero et al. (2004), who presented horizontal motion stimuli to different quadrants of the visual field. They found that the optomotor response of the fly was greatest when a rotational stimulus was presented only to the frontal visual field as opposed to when a rotating stimulus was presented to the entire visual field. When rotational motion was presented only to the rear visual field, the fly turned against the direction of motion, opposite of the normal optomotor behavior. In fact, the response to rotation of the entire visual field was equal to the linear sum of the responses measured when just the frontal or rear visual fields were stimulated (Tammero et al., 2004). Next they tested the responses of the flies to contracting or expanding visual stimuli, in which two grating stimuli presented to half the visual field are moved in the same direction such that they appear to either converge or diverge, respectively. The flies turned in the towards an expanding stimulus presented in the lateral visual field, but turned away in response to a contracting stimulus. Because an expanding stimulus results in back-to-front motion in the

frontal visual field and front-to-back motion in the rear visual field, these results appear to match those of Moore and Rankin (1982). These stimuli would typically be seen during translatory side-slip when an insect moves laterally while maintaining a forward head position, suggesting that the directional motion detection system is specialized to counteract involuntary, sideways movement. However, the differing sensitivities of eye regions for motion in different directions does not compromise the optomotor response to wide-field rotational motion (Tammero et al., 2004).

Intuitively, one would expect the magnitude of the optomotor response to be dependent on the speed of a stimulus, so that the insect could accurately compensate its path against externally generated movements. However, this is not the case. Experiments using square wave and sinusoidal stimuli have shown that the magnitude of the optomotor response to a grating moving at a fixed speed will change as the spatial frequency of the grating is varied. Indeed, the optomotor response appears to be tuned to the temporal frequency (or contrast frequency) of the stimulus, as can be seen in Figure 2.2d (Buchner, 1984; Srinivasan et al., 1999a), resulting in a bell shaped tuning curve as the temporal frequency of a fixed pattern is varied. The optomotor response is maximal at frequencies between 25-50 Hz and drops off at around 100 Hz, consistent with its role in counteracting gradual course changes (Egelhaaf and Borst, 1993).

Studies have also shown that LPTCs do not respond to flicker stimuli, in which the contrast of a visual stimulus is reversed at a set temporal frequency. In the studies of Riehle and Franceschini (1984), individual ommatidia were stimulated by targeted light pulses, such that two adjacent ommatidia could be activated in sequence while simultaneously recording from a directionally-selective LPTC. The cells responded with excitatory potentials when the ommatidia were activated sequentially in the preferred direction of the cell and inhibited when the pulses were presented in the null direction. Exciting both ommatidia simultaneously did not significantly alter the membrane potential.

The spectral sensitivity of the optomotor system was first investigated by Schlieper (1928) who proposed by that the optomotor system was "color-blind", meaning that the system was not sensitive to relative intensity differences between different wavelengths of light. Only later could this be explained by the involvement of only one class of photoreceptors corresponding to the green spectral channel (Kaiser and Liske, 1974). However, the optomotor system is sensitive to differences in overall intensity and the magnitude of the response increases gradually with the contrast of a stimulus (Buchner, 1984).

One of the most important results of these investigations of the optomotor response was the development of the HR model (Figure 2.3b) and its subsequent elaboration. The HR model is composed of two superimposed, mirror-symmetrical subunits (Figure 2.3a), each of which contains two photoreceptor channels. Both subunit channels contain temporal high-pass filters (HPF) that remove sustained illumination components from the incoming photoreceptor signal, while only one of the channels contains a temporal low-pass filter (LPF) that acts as a temporal delay. Multiplying the filtered outputs from each channel yields a large positive response to motion in one direction (because of the temporal delay in the LPF channel) and a small response in the opposite direction. By superimposing two of these subunits and subtracting their outputs, one gets a positive response to motion in one direction, a negative response to motion in the opposite direction and, because of the final subtraction stage, no response to flicker. Although not part of the original HR model (Hassenstein and Reichardt, 1956), the HPFs are consistent with the physiology (Egelhaaf and Borst, 1993) and they make the model significantly more robust to signals common to both eye, such as changes in background illumination (van Santen and Sperling, 1984, 1985).

The wide-field sensitivity of optomotor behaviors combined with the large dendritic trees of LPTCs suggest that the optomotor response is generated via the averaged responses of many small-field elementary motion detectors (EMDs), each

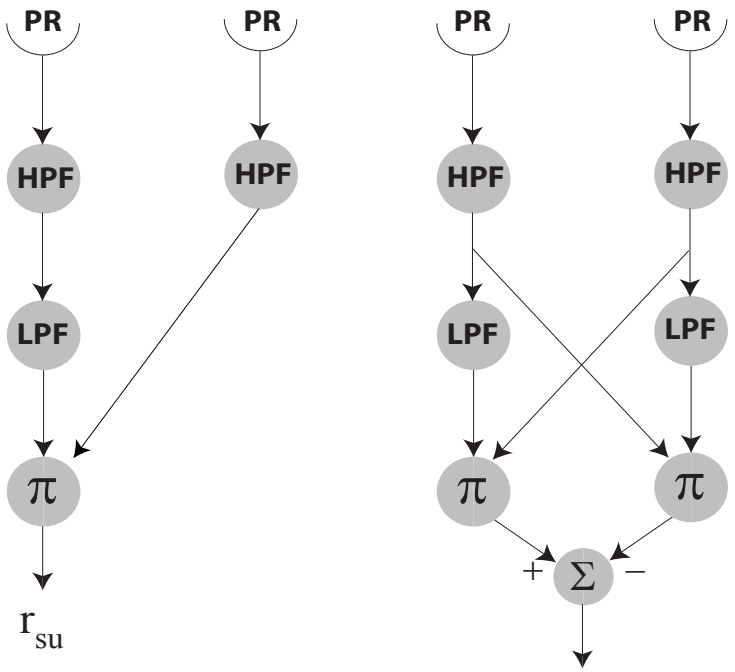

Figure 2.3: HR model and subunit. (a) An HR model containing two channels whose photoreceptor (PR) outputs are high-pass filtered (HPF) after which one of the channels is time-delayed via a low-pass filter (LPF). The outputs from the two channels are then multiplied (π) to yield a directionally selective output. (b) The HR model combines two mirror-symmetric subunits whose outputs are subtracted (Σ).

modeled as a small HR-like motion sensor (Borst and Egelhaaf, 1989). In order to better match this data, and to eliminate the temporal fluctuations of the local detectors, the outputs of multiple, spatially offset HR detectors are generally averaged to yield constant steady state responses (Borst and Egelhaaf, 1989).

While the LPTCs have been clearly identified as the neurons responsible for integrating the EMD outputs, they have provided little insight into how the brain actually computes motion. Anatomical (Buschbeck and Strausfeld, 1996) and electrophysiological studies (Douglass and Strausfeld, 1995, 1996) have identified a putative, evolutionarily conserved neuronal circuit for the EMD with small-field, directionally-selective outputs (Higgins et al., 2004). The averaged responses of these EMDs result in an output equivalent to that of the integrated HR detector. While this model does not fully describe all of the peculiarities of the actual biological responses, it does provide a comprehensive map of directional motion detection from photoreceptor to behavior and serves as a model for neuroethological investigation. The details of this model will be covered in Section 2.4.

2.2 Visual Speed Estimation

Because of the success of the HR model in explaining many motion-dependent behaviors and the relative ease of recording from LPTCs, the temptation has been to assign all motion dependent behaviors to the optomotor system. In this section I review the evidence that a distinct motion detection subsystem is responsible for estimating the angular speed of the visual image across the retina, termed optic flow. I begin with a general survey of optic flow dependent behaviors and move on to discuss various properties of the underlying mechanisms.

2.2.1 Survey of Optic Flow Dependent Behaviors

The first experiments hinting at an independent speed estimation system were performed by David (1982) who placed *Drosophila* inside a horizontally oriented, cylindrical wind tunnel. The walls of the tunnel held a spiral 'barber's pole' pattern that created the illusion of horizontally moving bars when the tunnel was rotated. He found that flies would effectively 'hover' while flying against a headwind when the pattern on the walls appeared to move at a specific speed. The flies continued to hover at this preferred speed even when the spatial period of the grating was changed from 40 to 72 degrees, contrary to what would be expected from an optomotor-like mechanism.

Comprehensive studies of the speed estimation system were first performed on honeybees trained to fly through narrow tunnels. While the bees generally flew through the center of the tunnel, Kirchner and Srinivasan (1989) noted that the lateral flight path of the bees could be manipulated by moving the pattern on the tunnel wall in the direction of flight or vice versa (Figure 2.4). This *centering response* could be explained if the honeybees were balancing the apparent image motion on each eye, such that the honeybees would fly closer to whichever wall appeared to be moving slower. Lining one of the walls with a uniform gray pattern or horizontally oriented axial stripes, thereby removing motion cues, resulted in bees flying closer to that wall (Kirchner and Srinivasan, 1989; Srinivasan et al., 1991). Further investigations showed that the behavior was dependent on a speed-tuned mechanism whose response was relatively independent of the spatial frequency of the grating pattern on the tunnel walls, contrary to what would be predicted by an optomotor-like mechanism (Srinivasan et al., 1991).

Using similar tunnel experiments it was shown that honeybees also use the apparent image speed to control their flight speed. Srinivasan et al. (1996) found that honeybees trained to fly through tapered tunnels, in which the spacing between walls decreased towards the center of the tunnel, maintained a constant rate of optic flow

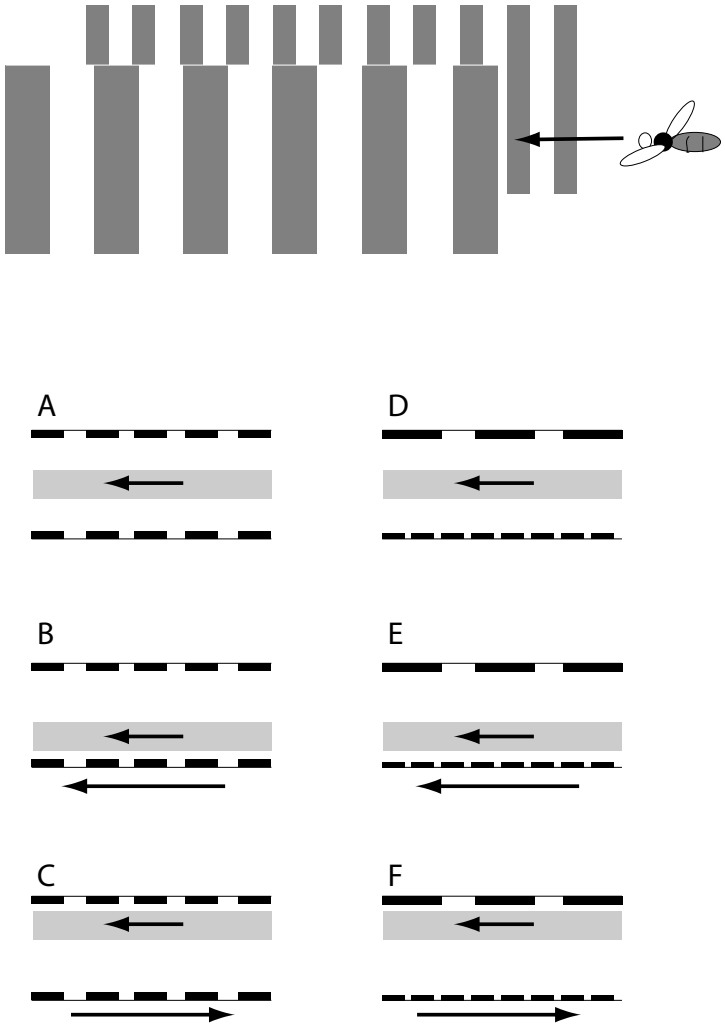

Figure 2.4: Summary of centering experiments. Honeybees were trained to fly through a narrow tunnel whose walls were lined with square wave gratings. A) When the walls are stationary honeybees will, on average, fly through the center of the tunnel. B) When one wall is moved in the direction of flight, decreasing the apparent speed, the honeybee will fly closer to the moving wall. C) When the wall is moved opposite the direction of flight so that it appears to be moving faster, the bee will fly closer to the stationary wall. D-F) The centering behavior remains unchanged even when the spatial frequencies of the square wave gratings on each wall are different. Figure reproduced from Srinivasan et al. (1996) with permission from the Journal of Experimental Biology.

by reducing their flight speed as the tunnel narrowed (Figure 2.5). The same visually mediated flight speed control has been observed in straight tunnels; honeybees will modify their flight speed to keep optic flow constant when both walls are moved at a constant speed (Baird et al., 2005) or when they are flying against a headwind (Barron and Srinivasan, 2006). When motion cues are reduced by lining the walls of the tunnel with axial stripes, honeybees fly up to three times faster (Barron and Srinivasan, 2006). However, even in these visually impoverished conditions, the bees are still able to pick up enough motion cues to modify their flight speed in order to counteract changes in wall speed (Baird et al., 2005). This flight control mechanism appears to be conserved across insects, as fruit flies have also been shown to use optic flow to control their flight speed (David, 1982; Fry et al., 2009).

The interplay between the centering response and flight speed control has been elucidated by experiments varying the size of the tunnels. When the width of the tunnel was increased to 95 cm from the typical range of 14-22 cm, Serres et al. (2008) found that the centering response shifted to a wall-following behavior. The switch to wall-following was dependent on the honeybee's starting position in the tunnel; when the starting position was close to one wall, the bee moved away from the wall until the apparent optic flow from that wall reached a preferred value of approximately 230 degrees/second, even when the opposite wall was removed. If the flight started at the center of the tunnel, the bee reverted to the centering behavior and modified its flight path through the tunnel by balancing the lateral optic flow from each wall at a much reduced rate of 140 degrees/second (Serres et al., 2008). One possible explanation for the apparent reduction in the preferred lateral optic flow from 230 to 140 degrees/second is that the bees were using motion cues from the ground instead of from the wall. It has been shown previously that the ventral visual field also contributes to the flight speed control system (Baird et al., 2006). Hence, the bee may still be holding the global estimate of optic flow constant, but the relative contribution of the lateral visual fields are simply decreasing. This suggests

that while both the centering and flight speed control behaviors are dependent on the rate of optic flow, the actual control systems for the two behaviors are relatively independent.

The discovery of the visual speed estimation system also helped settle a long-standing debate started with the Nobel Prize winning work of Karl von Frisch, who demonstrated that honeybees communicate the distance and direction of a food source to other honeybees in the hive via a "waggle dance" (reviewed in von Frisch, 1993). Two primary hypotheses were proposed for how the distance estimate was acquired: the "energy hypothesis", postulating that honeybees gauge the distance to a food source by the energy expended during flight (Heran and Wenke, 1952; Heran, 1956) and the "optic flow hypothesis" proposing that honeybees integrate the apparent motion of the visual image across the retina over the course of the foraging flight to acquire an estimate of distance (von Frisch, 1993; Esch and Burns, 1995).

Conclusive evidence that the honeybee odometer relies on the visual system, and not energy expenditure, came from studies in honeybees trained to forage from a feeder situated on a weather balloon (Esch and Burns, 1995). The hive was located on the ground, at a fixed *horizontal* distance of 70 meters from the feeder. Over the course of the experiments, the feeder was slowly raised from the ground up to an altitude of 90 meters. Esch and Burns (1995) found that the returning bees communicated *decreasing* distances as the height of the balloon was *increased* despite traveling a greater overall distance (Figure 2.6). This is consistent with the optic flow hypothesis because the optic flow cues will be much smaller at higher altitudes, whereas the energy hypothesis would predict a larger estimate due to the increased absolute distance traveled. In followup experiments, a hive was placed on top of a tall building and the honeybees were trained to forage from a feeder located on the top of an adjacent building. The waggle dances of these honeybees, flying at high altitudes from building to building, signaled significantly lower distances than

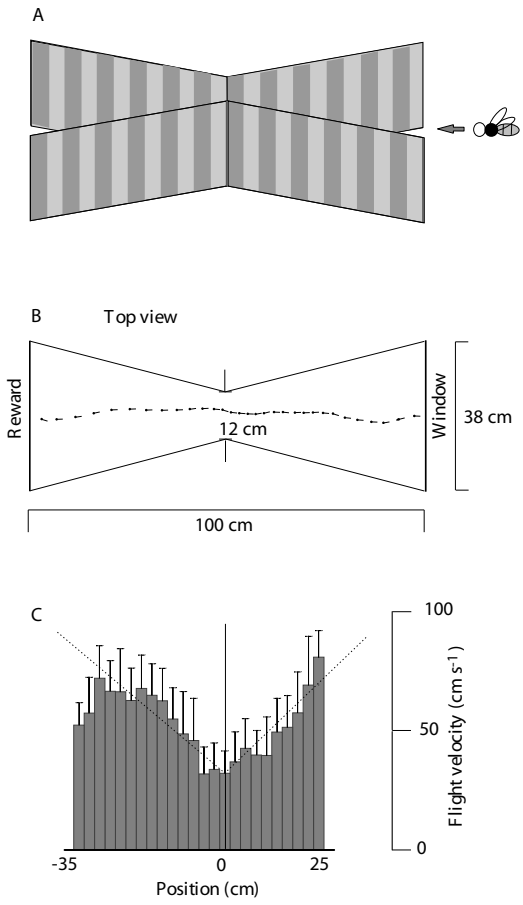

Figure 2.5: Tapered tunnel experiments. A) Honeybees were trained to fly through a tapered tunnel whose walls were lined with square wave gratings of equal periods. B) Honeybees simultaneously center their flight path while decreasing their flight speed as the walls contract. The position of the bee (dots) was sampled at regular time intervals, such that closely spaced dots indicate slower flight speeds. C) The mean flight speed and standard error of the mean for 18 flights are plotted versus the position of the bee within the tunnel (2.5 cm bins). Figure reproduced from Srinivasan et al. (1996) with permission from the Journal of Experimental Biology.

bees housed at ground level trained to fly up to the feeder (Esch and Burns, 1996). A decrease in the distance estimated is also observed when the ground holds very little visual texture, such as when a honeybees flies over water (Tautz et al., 2004).

Other related behaviors have also been shown to be dependent on visual estimates of speed. Honeybees use the relative speed of objects in the ventral visual field to infer the distance of the objects independent of their size (Srinivasan et al., 1989) and use the speed of the ventral visual field to control their flight altitude (Baird et al., 2006). This altitude control mechanism is used for grazing landings, in which honeybees slowly decrease their speed and altitude simultaneously by holding the apparent image motion constant as they approach the ground (Srinivasan et al., 1996, 2000b).

2.2.2 Directionality

The numerous optic flow dependent behaviors have facilitated in-depth investigation of the properties of the mechanisms underlying the visual speed estimation system, one of which is that the speed estimates appear to be based on a small field, non-directionally sensitive mechanism. Honeybees will still match the apparent speed of two tunnel walls even if the speed of one of the walls exceeds that of the honeybee, so that the apparent motion of the wall on one eye is back-to-front instead of the normal front-to-back motion seen during flight (Srinivasan et al., 1991). The same behavior was noted by Fry et al. (2009) in their *Drosophila* flight speed control experiments (discussed in detail in Section 2.2.6), in which the flies responded similarly to patterns with positive and negative temporal frequencies (refer to Figure 2.10). Furthermore, Srinivasan et al. (1993) performed centering experiments in which a small section of both of the tunnel walls removed and replaced with a computer monitor displaying a moving grating pattern on one side and a camera on the other. As the honeybees flew through this section of the tunnel they exhibited a characteristic 'movement avoidance' response away from the computer monitor

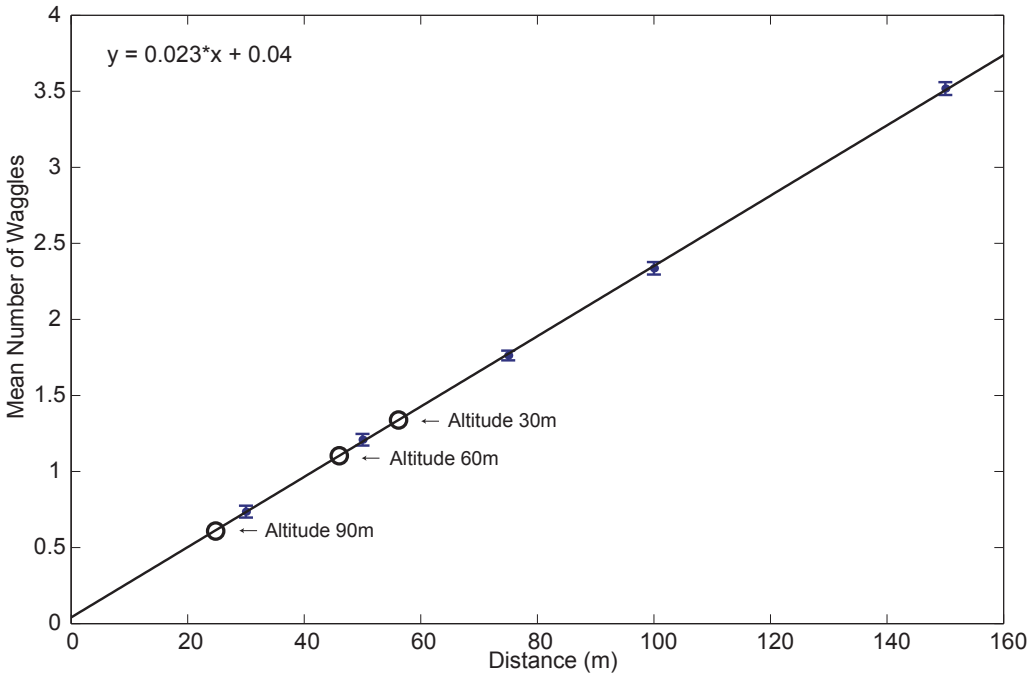

Figure 2.6: Visual odometry en route to a balloon. The distance communicated by the waggle dances of bees collecting food from a feeder of varying height 70 m from the hive (open circles) are plotted versus the distances communicated by bees foraging at ground level (solid dots). The line represents the linear regression line for the ground level feeders. As can be seen, the distance estimate decreases with feeder height, indicating that honeybees use optic flow, and not energy expenditure, to estimate travel distance. Error bars represent the standard error of the mean number of waggles. Data presented in the figure is based on the results of Esch and Burns (1995).

(Figure 2.7a) towards the relatively empty gap on the opposite wall. The response could be evoked by motion in both the horizontal and vertical directions and the magnitude of the response was dependent on the speed of the moving pattern. While a flickering stimulus also elicited a behavioral response, the magnitude was approximately half of that to moving stimuli (Srinivasan et al., 1993). The authors then presented a pattern of interleaved rows moving in opposite directions, such that the entire pattern had zero average speed. The movement avoidance response to this stimulus was equal in magnitude to that of a single grating moving at the same speed, suggesting a non-directional, small-field mechanism (Srinivasan et al., 1993). In other work, Dacke and Srinivasan (2007) trained honeybees to collect rewards from vertically sloped and L-shaped tunnels that required both horizontal and vertical flight. The waggle dances of these honeybees communicated the same distance regardless of the proportion of vertical versus horizontal flight, indicating that they are measuring image speed without regard to direction (Figure 2.7b).

Work on the *Drosophila* genetic variant *rol sol*, containing the mutant genes *reduced optic lobes* KS221 (textitrol) and *small optic lobes* KS58 (*sol*), has lent further support for a non-directional motion subsystem. While the mutant flies were believed to be motion blind because they did not exhibit an optomotor response, Wolf and Heisenberg (1986) found that *rol sol* flies were able to effectively compensate for the motion of rotating stripe during closed-loop, tethered flight experiments. The flies accomplished this via a non-directional estimate of the displacement of the rotating stripe that the authors believed was acquired through a mechanism distinct from that responsible for the optomotor response (Wolf and Heisenberg, 1986).

2.2.3 Receptive Field

Many studies have shown that both the lateral and ventral visual fields contribute to the speed estimate, with the lateral visual fields having much stronger contributions (Srinivasan et al., 1997; Si et al., 2003; Baird et al., 2006). Additionally, centering

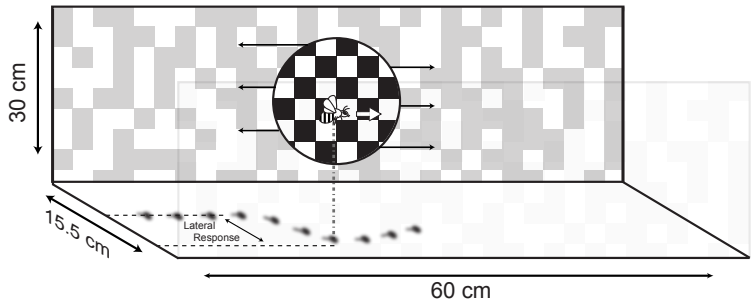

(a)

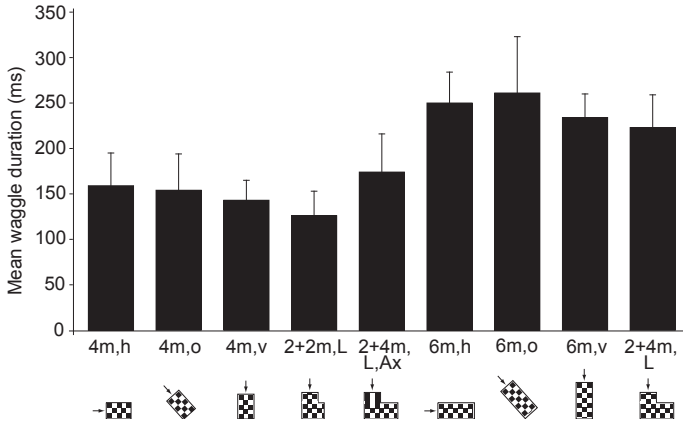

(b)

Figure 2.7: Non-directional behavioral experiments (a) Experimental setup from Srinivasan et al. (1993) in which a computer monitor was visible through a hole cut into one side of the tunnel (circle with checkerboard pattern). Honeybees displayed a stereotyped 'movement avoidance' response away from the monitor whose magnitude could be modulated by the speed of the pattern. The response was maintained even when the monitor displayed a pattern of interleaved rows moving in opposite directions (as shown) so that it had zero average speed, suggesting an underlying small field, non-directional mechanism. (b) Experiments from Dacke and Srinivasan (2007) in which honeybees were trained to travel through tunnels requiring different amounts of vertical and horizontal flight to collect a sugar reward. The distance estimates of the bees, as interpreted from the mean waggle duration, was dependent on the amount, but not direction, of the optic flow. Figure reproduced with permission from the Journal of Experimental Biology (Dacke and Srinivasan, 2007).

studies have shown that honeybees flying through a tunnel whose walls each contain a single, narrow black bar will not alter their flight paths until the bars are almost directly lateral to the bee (Srinivasan et al., 1991), suggesting that the frontal visual field plays very little role in the optic flow computation. However, since this coincides with the area of the visual field that will naturally experience the highest image speed during forward flight, it is not clear if this is because the lateral regions of the eye are specialized for visual speed estimation or if this simply occurs because they are receiving a stronger motion signal. Further free flight investigations into specialized eye regions have been prevented because honeybees are unwilling to fly when significant portions of their eye are occluded (Srinivasan et al., 1998).

In addition, based on the size of the 'checks' of the interleaved pattern used in the movement avoidance response experiments of Srinivasan et al. (1993), it has been concluded that the receptive field of each speed estimator does not exceed 20° (Srinivasan and Zhang, 1997) .

2.2.4 Preferred Angular Speed

As previously mentioned, honeybees appear to adjust their flight speed in order to maintain a preferred rate of optic flow. In their tapered tunnel experiments, Srinivasan et al. (1996) found the preferred rate of lateral optic flow to be approximately 320 degrees/second. These results are in good agreement with those of Barron and Srinivasan (2006) who found that bees maintained lateral angular image speed of between 290-320 degrees/second despite headwinds of up to 3.8 meters/second and Srinivasan et al. (1991) whose data suggest a mean rate of optic flow between 280-373 degrees/second. Serres et al. (2008) found that in a wider tunnel, honeybees maintained a unilateral optic flow of approximately 230 degrees/second, except when flying through the center of the tunnel at which point the lateral optic flow was reduced to 140 degrees/second (as discussed in Section 2.2.1). A preferred speed is observed even when the walls of the tunnel are lined with axial stripes, although

it is up to three times higher (Barron and Srinivasan, 2006).

The most comprehensive study of visual flight speed control was that of Baird et al. (2005), who found that honeybees maintained an apparent image angular velocity of 265 degrees/second in a tunnel with stationary walls, but that they would maintain a higher rate of optic flow when the walls were moved against the direction of flight (increasing the apparent speed of the walls) and a lower rate of optic flow when the walls were moved in the direction of flight (Figure 2.8). Overall, the preferred angular image speed varied between 207-320 degrees/second (corresponding to linear speeds between 50-120 centimeters/second in Figure 2.8). They also found that the data was fit well by three different linear regression lines, one each for high positive speeds (walls moving in the direction of flight), high negative speeds or small negative and positive speeds. When there was only a small change in wall speed, none of the data points were significantly different prompting the authors to suggest that the optic flow must deviate from a preferred value by 10-15 degrees/s before bees will adjust their flight speed (Baird et al., 2005). This indicates that the flight speed control system does not respond linearly to speed. Rather, the shallower slope of the curve when the apparent speed of the walls was higher (negative pattern velocities) indicates that the bees were under compensating for the amount of image motion (Baird et al., 2005). At low apparent speed (positive pattern velocities) the slope is steeper, indicating an overcompensation of image speed.

While all of these studies agree that honeybees have a preferred rate of optic flow, the actual value varies between the studies. One possibility may be a minimum preferred forward flight speed that takes precedence when the bee is experiencing very high rates of optic flow, such as in a narrow tunnel. This could be true for aerodynamic reasons, such that lower flight speeds are energetically unfavorable or difficult to maintain. This possibility is consistent with the fact that the studies with the highest preferred rates of optic flow used the narrowest tunnels (Barron and

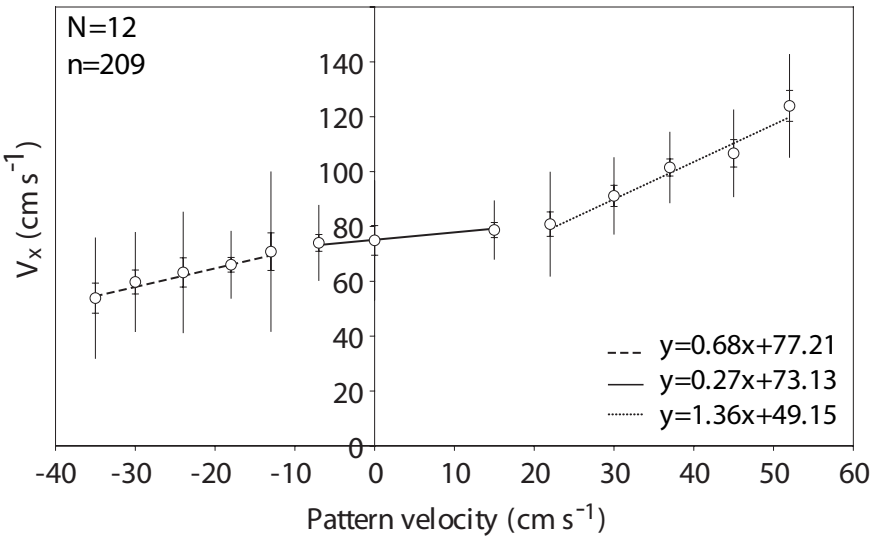

Figure 2.8: Visual flight speed control in a tunnel with moving walls. Results demonstrating the visual regulation of flight speed by honeybees flying through a 22 cm wide tunnel with moving walls. Open circles denote the average flight speed (V_x) when the walls of the tunnel were moved together either in the direction of flight (positive pattern velocities) or against the direction of flight (negative pattern velocities). The uncapped vertical bars indicate the standard deviation and the capped bars indicate the standard error of the mean. The horizontal lines represent three different linear regression fits whose equations are provided in the bottom left corner of the graph. N and n denote the number of bees and the number of flights, respectively. The range of linear flight speeds observed correspond to angular speeds between 207-320 degrees/second as seen from the center of the tunnel. Figure reproduced from Baird et al. (2005) with permission from the Journal of Experimental Biology.

Srinivasan, 2006; Srinivasan et al., 1991) and vice versa (Serres et al., 2008). Another possibility is that cues from the ventral visual field contribute more to the speed estimate when the tunnel walls are further apart and thus have lower speeds. This theory is supported by studies showing that honeybees will fly at higher altitudes and lower speeds when the floor of the tunnel is lined with a checkerboard pattern as compared to a blank or axially striped pattern (Baird et al., 2006). Bees appear to be picking up optic flow cues even when the floor is lined with white paper, as they will fly significantly faster through a tunnel with an axially striped, instead of a blank white, floor (Baird et al., 2006).

The speeds of bees flying through tunnels are much reduced from those observed in free flight in outdoor environments, but outdoor flight speeds and altitudes are consistent with the range of *image speeds* observed in tunnel experiments. Wenner (1963) estimated that unloaded honeybees flew at speeds of 7-7.5 m/s in the open field and that flight speed decreased to 5.3-6.5 m/s with nectar loads. Later studies using harmonic radar have found honeybee flights speeds ranged from 0.6-6.2 m/s, with more experienced bees flying faster (Capaldi et al., 2000). Because neither study provided altitude information, it is difficult to estimate the perceived rates of optic flow. However, studies in bumblebees (*Bombus terrestris L.*) using harmonic radar have found similar ranges of flight speeds while also supplying altitude information. Osborne et al. (1999) reported flight speeds ranging between 3.0-15.7 m/s and flight altitudes between 1-3 m for bumblebees flying in a visually varied environment with changing wind conditions. Other work reported average flight speeds of 7.1±0.43 m/s at an average altitude of approximately 2 m in an open field environment with still winds (Riley et al., 1999). In the second case, the ground would have an average angular image speed of approximately 200 degrees/s, consistent with the low range of speeds observed in tunnel experiments. The authors also noted that flight altitude decreased when the bees were flying into headwinds and increased when flying downwind as predicted by the visually mediated flight

control hypothesis.

2.2.5 Properties of the Visual Odometer

The visual odometer has been investigated further using honeybees trained to fly through narrow tunnels. Because of the close proximity of the walls, bees will perceive a greater amount of image motion when flying through a narrow tunnel than during normal flight. Srinivasan et al. (1997) trained honeybees to collect sugar water from a specific location within a tunnel and then observed the searching behavior of honeybees when placed in identical test tunnels. They found that honeybees would concentrate their searches at the approximate location of the training feeder. Furthermore, changing the width of the tunnel caused the honeybees to either undershoot (narrower tunnel) or overshoot (wider tunnel) the former location of the feeder (Figure 2.9). Patterning the walls with axial stripes effectively eliminated any search behavior: the bees would simply fly back and forth through the tunnel (Srinivasan et al., 1997). The accuracy of the odometer decreased with increasing distance, consistent with a integrative mechanism, but could be improved by adding landmarks to the tunnel (Srinivasan et al., 1997).

As with the wall-following behavior, the visual odometer still functions when only one eye is receiving significant optic flow information, as demonstrated by experiments in which one wall is lined with an axially striped pattern and the other wall is lined with a randomly textured pattern (Srinivasan et al., 1998). The estimate can also be transferred between eyes, so that if the wall patterns are switched the bee will still search for the feeder in the correct location during test trials (Srinivasan et al., 1998).

The estimated distance is represented as a linear function of the perceived optic flow (Srinivasan et al., 1999b) allowing us to acquire an approximate calibration for the visual odometer. Srinivasan et al. (2000a) trained honeybees to fly to a tunnel located a short distance from the hive and then to fly through the tunnel to collect

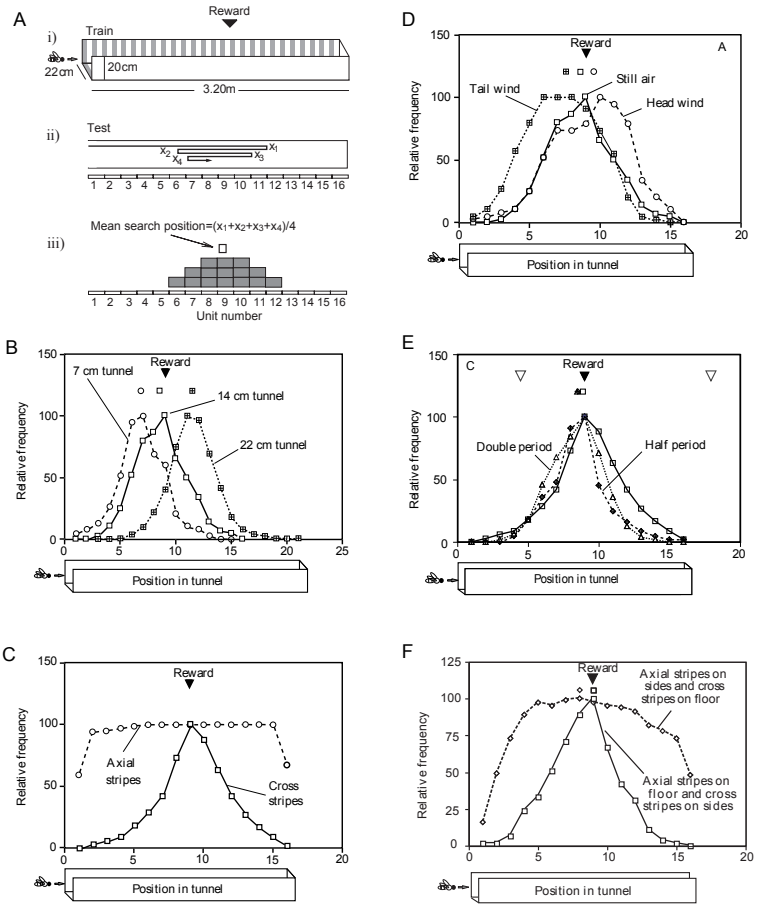

Figure 2.9: Odometer-based searching behavior. A) Honeybees were trained to collect reward from a narrow tunnel (i) and then tested in a separate tunnel (ii). The mean search position of a honeybee in the test tunnel (iii) was used to quantify the bee's estimate of distance. B) Bees either overshot (wider tunnel) or undershot (narrower tunnel) the position of the feeder (black inverted triangle) when the tunnel width was changed. C) Axially striped walls, lacking most motion cues, caused honeybees to search equally throughout the tunnel. D) The distance estimate changed with wind speed. E) Doubling or halving the 4 cm spatial period of the square wave grating used during training had no effect on search location. F) Search behavior was significantly altered when the walls, but not the floor, were lined with axial stripes. Figure modified from Srinivasan et al. (1997) with permission from the Journal of Experimental Biology.

a sugar reward. The dances of the tunnel-trained bees were then compared to those of bees trained to forage from feeders located at different distances from the hive. Honeybees foraging through the tunnel communicated much greater distances and by comparing their dances to the control groups, the authors determined that the waggle dance was calibrated such that each 1 ms of the waggle dance signals 17.7 degrees of image motion. It has since been verified that honeybees recruited by the waggle dances of tunnel-trained honeybees search at the interpreted distances (Esch et al., 2001; Riley et al., 2005). There is also evidence that stingless bees (*Melipona seminigra* Hrncir et al., 2003) and wasps (Ugolini, 1987) also use optic flow to estimate flight distances, suggesting that the visual odometer is conserved across different species of insects.

2.2.6 Spatial Frequency Dependence

Studies of the spatial frequency tuning of the visual speed estimation system have yielded mixed results. Differences in the width of the tunnels used in the various experiments makes it necessary to convert the linear spatial frequencies (cycles/m) to angular spatial frequencies (cycles/degree). For the discussion, I calculate the angular spatial frequency of all patterns as measured from the center of the tunnel. Srinivasan et al. (1991) found that the centering response was largely insensitive to differences in the spatial frequency between the walls when comparing square wave gratings of 0.02, 0.03 or 0.04 cycles/deg, although they did note significant differences when they compared *sinusoidal* gratings of 0.02 and 0.06 cycles/degree. Si et al. (2003) found that the distance estimates of honeybees, as measured by mean waggle duration, were significantly different when sinusoidal stimuli of 0.02 cycles/degree versus either 0.03 or 0.06 cycles/degree were used. However, none of the sinusoidal conditions yielded distance estimates significantly different from the checkerboard pattern control. Srinivasan et al. (1997) found no significant differences in the distance estimates of honeybees searching through tunnels with walls

lined with square wave gratings of 0.03, 0.05 or 0.1 cycles/deg. Baird et al. (2005) found that honeybees did not change their mean flight speeds when a tunnel was lined with sinusoidal gratings with spatial frequencies ranging from 0.03 to 0.11 cycles/degree. However, because the bees did not appear to adjust their flight speed until the optic flow exceeded a threshold of 10-15 degrees/second (Baird et al., 2005), it is possible that the differences in the visual speed estimates due to the spatial frequency were not large enough to cause a significant change in the flight speed. Additionally, the optic flow due to the floor of the tunnel may have helped to stabilize the speed estimate despite the changes in the spatial frequency.

The spatial frequency dependence of optic flow based behaviors has also been studied in *Drosophila*. David (1982) found that, when flying against a headwind, *Drosophila virilis* would 'hover' stationary in the center of a cylindrical wind tunnel when the apparent speed of a 'barber's pole' pattern on the wall was maintained at a preferred speed regardless of whether the spatial period of the pattern was 40 or 72 degrees. A more comprehensive study of the spatio-temporal frequency tuning of the visual flight speed control system was performed on *Drosophila melanogaster* by Fry et al. (2009). Their experimental setup consisted of two tracking cameras mounted above a wind tunnel onto whose lateral walls a computer-controlled sinusoidal pattern was projected. The speed of the visual pattern was maintained at the fly's preferred speed so that the fly 'hovered' against a headwind at the center of the tunnel. The tracked position of the fly was used to move the projected pattern to compensate for the movement of the fly within the tunnel such that the apparent spatial and temporal frequency of the pattern on the eye could be held constant. Using a 'one parameter open-loop' experimental paradigm, in which they estimated the fly's acceleration in response to a stimulus of fixed spatial and temporal frequency for a 1 second time period, they acquired a broad spatio-temporal tuning of the speed control mechanism (Figure 2.10). The limited resolution of the *Drosophila* eye restricts the range of resolvable frequencies such that behavioral responses dis-

appear above linear spatial frequencies of 20 cycles/meter, corresponding to range of angular spatial frequency of 0.012 - 0.055 cycles/degree. The speed of a stimulus is simply the ratio of the temporal frequency over the spatial frequency and one can see that the responses appear to be largely speed-tuned for spatial frequencies between 3-14 cycles/m. However, the behavioral responses show a clear drop-off outside of this range.

While these studies provide the most comprehensive spatio-temporal frequency tuning curve for any insect, there are a number of limitations on the conclusions that can be made about the general mechanism. First, the lack of resolving power of the *Drosophila* eye severely restricted the range of testable spatial frequencies compared to those resolved by honeybees. Second, Fry et al. measured the instantaneous response of the flies to a change in the speed of the stimulus as opposed to the steady state responses observed in the free flight experiments in honeybees, making it difficult to directly compare the results. The authors also noted that there appeared to be an upper limit to the acceleration response, which could be confounding their results for high speed stimuli. Finally, it has previously been noted by Baird et al. (2005) that honeybees do not adjust their flight speed until the optic flow exceeds a specific threshold, suggesting that flight speed control (and consequently acceleration responses) may not be the most accurate measures for optic flow dependent behaviors.

2.2.7 Spectral and Contrast Sensitivity

Studies have demonstrated that optic flow dependent behaviors are primarily dependent on wavelengths of light in the green regions of the visible spectrum and are relatively independent of the brightness and contrast of the pattern. Chittka and Tautz (2003) observed the dances of honeybees after flying through tunnels lined with patterns of different spectral compositions. While the bees always overestimated the distance traveled, they only performed full waggle dances (indicating dis-

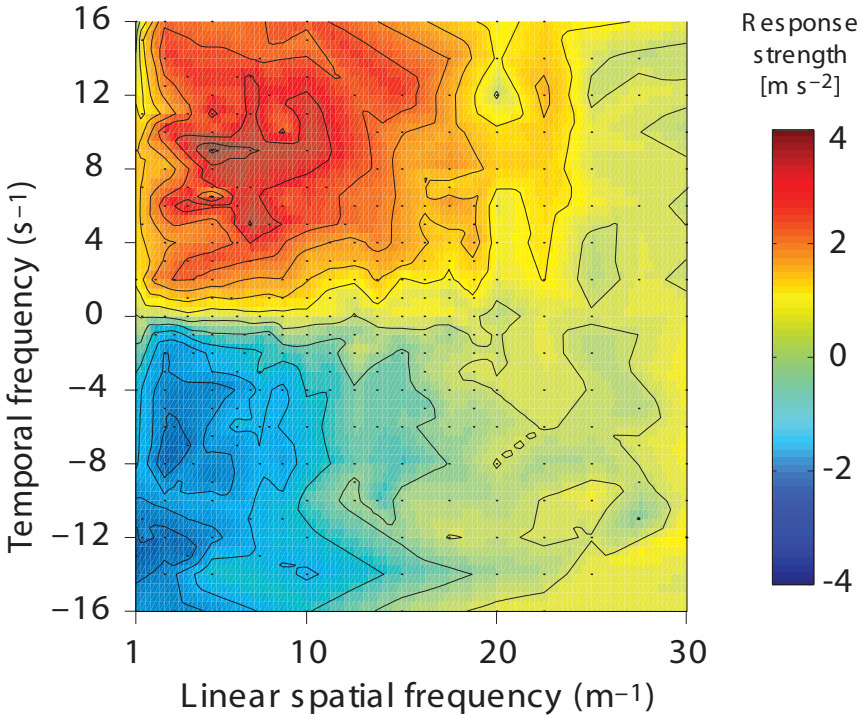

Figure 2.10: Spatio-temporal frequency tuning of *Drosophila* flight speed control behavior. The average acceleration response (contours) is plotted versus the spatial and temporal frequency of a pattern. The response surface was interpolated from trials with different parameter combinations (indicated by the black dots). Figure reproduced from Fry et al. (2009) with permission from the Journal of Experimental Biology.

tances greater 150 m) when wavelengths of light in the green region of the spectrum were present in the tunnel. Studies of the various optic flow dependent behaviors, including the centering response (Srinivasan et al., 1991), the flight speed control system (Baird et al., 2005, 2006) and the visual odometer (Si et al., 2003; Chittka and Tautz, 2003), have all demonstrated little to no dependence on the pattern contrast. The visual speed estimation system appears to fail only when contrasts are extremely low (between 0-5%) (Srinivasan et al., 1991; Baird et al., 2005). Furthermore, the visual system appears to adapt in low contrast environments so that otherwise invisible features can be used as cues for the visual speed estimation system. Honeybees appear to pick out small imperfections in uniform patterns when compared high contrast axially striped patterns (Srinivasan et al., 1991; Baird et al., 2005, 2006).

2.2.8 Summary of Optic Flow Dependent Behaviors

These studies demonstrate that a wide variety of behaviors are dependent on visual estimates of the angular speed of the retinal image and that they are conserved across species. The behaviors appear to be governed by a non-directional, small-field, contrast-insensitive mechanism that maintains a preferred level of optic flow. Speeds above and below this preferred speed are represented linearly, but the slopes of the responses are different. The mechanism is sensitive to motion in both the lateral and ventral visual fields, with motion in the lateral visual field having a larger contribution to the overall speed estimate. Furthermore, motion from the visual field directly perpendicular to the bee's long axis appears to be the most important for the optic flow estimate. Finally, the small-field mechanism estimates speeds from regions no larger that 20 degrees in angular extent and is sensitive to flicker, but the response magnitude is much smaller than that to motion.

2.3 Optics and Anatomy of the Visual System

The optics and neuroanatomy of the insect visual system provide important constraints and insights for modeling different visual processes, even at the behavioral level. The optics set limits on the acuity and sensitivity of the eye while the neuronal organization determines other properties such as color sensitivity and response latency. In this section I begin by discussing the optics and photoreceptors (Section 2.3.1) and continue on to discuss the neuroanatomy of the layers of the optic lobes responsible for motion processing (Section 2.3.2).

Before beginning this discussion, it is important to note that I am interested in identifying neuronal mechanisms for visual speed estimation that I believe are evolutionarily conserved across insects. The fact that optic flow dependent behaviors have been observed in a variety of insect species (David, 1982; Ugolini, 1987; Srinivasan et al., 1991; Hrncir et al., 2003; Fry et al., 2009) combined with the similarities of the neuronal organization across different insects (Strausfeld, 1976; Ribi and Scheel, 1981; Osorio and Bacon, 1994) suggests that the motion detecting systems are conserved. A similar view has already been advanced for the optomotor and elementary motion detection system, in which a behavior common to insects (the optomotor response), has led to a general computational model (Hassenstein and Reichardt, 1956), the identification of evolutionarily conserved motion sensitive neurons (Buschbeck and Strausfeld, 1996) and the proposal of a putative EMD circuit (Higgins, 2004). The difficulty in the present discussion is that while optic flow dependent behaviors have been studied primarily in honeybees, most of the electrophysiological recordings of motion sensitive cells in insects have been obtained from flies. Thus, while I try to focus the discussion on the optics and neuroanatomy of bees, I sometimes fill in the gaps with information obtained from flies.

2.3.1 Optics and Photoreception

The honeybee compound eye is composed of a hexagonal array of thousands of small lenses that focus light from the visual field onto a photosensitive, light-guiding structure called the rhabdom. The rhabdom is composed of the photosensitive portions of nine retinula cells (photoreceptors R1-R9) that, combined with the lens, are referred to as an ommatidium (Ribi, 1987). The honeybee has an apposition eye, meaning that each ommatidium represents a single point in the visual image and each photoreceptor in the ommatidium receives an identical stimulus due to the light-diffusing properties of the rhabdom (Land and Nilsson, 2002).

The ommatidia of the honeybee eye are arranged such that the bee has a nearly panoramic field of view, but the eye itself is not spherical. Rather, the curvature of the eye and the diameter of the lenses vary across the surface of the eye. The spacing between ommatidial axes, termed the *interommatidial angle*, changes with the curvature of the eye and also plays a role in limiting the spatial resolution of the eye. As a result of these variations, the eye is irregularly shaped and the light sensitivity and spatial resolution vary across ommatidia.

In worker honeybees, the lenses in the frontal regions of the eye tend to have larger diameters and smaller interommatidial angles, so that they are both more sensitive to light and have a higher spatial acuity, while the opposite is true as one moves dorsally and laterally across the eye (Seidl and Kaiser, 1981). There is also significant binocular overlap between the two eyes in the frontal visual field, ranging from 29 - 42° across the dorsal ventral axis (Seidl and Kaiser, 1981). This so called "acute zone" is often the area of the eye with the highest visual acuity, is present in many insects (Land and Nilsson, 2002) and plays an important role in tracking behaviors (Land and Collett, 1974).

While studies of the optics provide a maximal spatial resolution, the functional resolution of the eyes is better determined by electrophysiological and behavioral studies. The smallest interommatidial angle in the honeybee eye is approx-

imately 1° (Land, 1999) while the average interommatidial angle is approximately 2°. Recordings from retinula cells of honeybees have found an angular sensitivity of 2.5° (Laughlin and Horridge, 1971), in general agreement with the optical measurements. Behavioral studies using moving gratings suggest honeybees are unable to resolve gratings with wavelengths below 2.6° (Hecht and Wolf, 1929). Finally, single object resolution studies show that bees no longer distinguish between two points when they are less than 5° apart (Giurfa et al., 1996). Studies in the bumblebee *Bombus terrestris* have found that interommatidial angles range from 0.6 - 3.3° across the eye of a single animal. The size of the bumblebee eye also varies across individuals and is positively correlated with overall body size. This variation affects the resolution of the eyes as demonstrated by single object resolution studies in bumblebees that have found a minimum angular separation of 3.5° for large bees and 7° for smaller bees (Spaethe and Chittka, 2003).

Ommatidia in the lateral visual field of the eye have larger interommatidial angles. While this decreases spatial resolution, it can also ameliorate blurring due to motion (Land and Nilsson, 2002). Because the photoreceptor has a finite response time, a moving object will appear dimmer if it moves through the receptive field of the photoreceptor too quickly. In fact, it has been suggested that the larger ommatidial angles in the lateral portions of the eye, which will naturally experience greater amounts of image motion during forward movement, may indicate a specialization for detecting fast motion (Lehrer, 1998; Land and Nilsson, 2002).

2.3.2 Neuronal Circuitry

Because of the complexity of the insect optic lobes, I focus the discussion of neurobiology on their general organization and on specific cells that have been implicated in motion processing. I also focus my discussion on studies in honeybees except when noted otherwise.

The optic lobes of the honeybee are divided into three separate neuropils, the

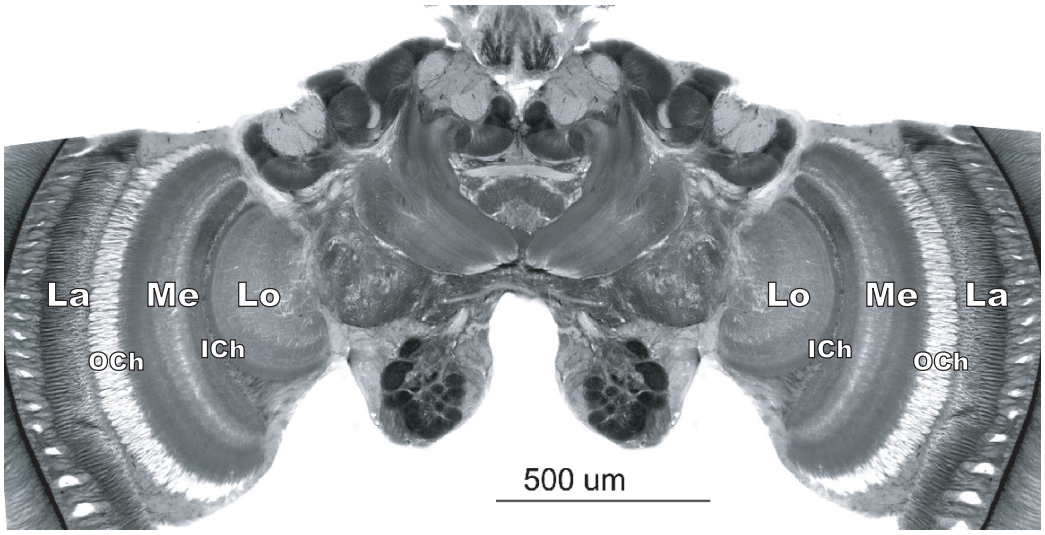

Figure 2.11: Frontal section of a honeybee brain. The majority of the photoreceptor axons from the retina project to the lamina (La). Fibers projecting from the lamina proceed through the outer chiasm (OCh) to the medulla (Me). Fibers from the medulla then cross through to the Lobula (Lo) via the inner chiasm (ICh). Image courtesy of Wulfila Gronenberg.

lamina, the medulla and the lobula (Figure 2.11). The lamina is the outermost layer and receives the majority of the projections from the photoreceptors. Fibers from the lamina project across the outer chiasm to the medulla from which fibers cross the inner chiasm to the lobula. In flies, the lobula complex is divided into two distinct neuropils, the lobula and lobula plate.

The axons of the R1-R9 retinula cells in each ommatidium group together into cartridges and remain retinotopically organized as they enter the lamina, with the blue and green retinula cells terminating in the lamina and the UV cells projecting through to terminate in the medulla (Ribi, 1987). The lamina is organized into three layers defined by the arrangement of lamina monopolar cells (LMCs), L1-L4 (Ribi, 1987). Genetic studies in *Drosophila* have suggested that the processing of rotational (L1) and translational motion (L2) is segregated into two channels at the level of the lamina (Katsov and Clandinin, 2008). In flies, the L2 cell, which receives input from a single photoreceptor (Strausfeld, 1976), responds to light with a transient hyperpolarization in response to illumination (Coombe et al., 1989) and acts to band-pass filter temporal frequency information (Laughlin, 1984). These cells are presynaptic to the Tm1 transmedullary cell in flies and have been implicated in elementary motion detection (Higgins et al., 2004). The L1 and L2 cells in bees have similar phasic hyperpolarization characteristics (Souza et al., 1992) and anatomically appear to have narrowband sensitivity to green light (Ribi, 1987). In the honeybee, two of the LMCs, L2 and L4, have collaterals in neighboring optic cartridges (Ribi, 1981). In the fly, the L4 cell has been implicated in motion detection because it is the only efferent LMC with lateral connections with multiple optic cartridges (Strausfeld and Braitenberg, 1970; Strausfeld and Campos-Ortega, 1973). Electrophysiological recordings in flies have shown that the L4 cell responds to flicker with a transient hyperpolarization and to motion with contrast frequency dependent modulations without regard to direction.

Fibers emanating from the lamina cross horizontally in the outer chiasm before

entering the medulla. The medulla is also a layered structure and contains, among many other cell types, transmedullary cells. The transmedullary cells receive input from the LMCs and are of primary interest because they are responsible for the output of the medulla (Ribi, 1987). Higgins et al. (2004) hypothesized that this is the earliest stage at which cells show preferences to motion over flicker. This theory is supported by recordings from Tm1 cells in flies that respond weakly to flicker and strongly to motion, irrespective of direction (Douglass and Strausfeld, 1995). Although less is known about specific cells in the honeybee, small-field motion-sensitive cells have been recorded from the honeybee medulla (Hertel and Maronde, 1987). Another potential cell of interest is the non-directional T4 cell that appears in a pathway parallel to the Tm1 cell (Douglass and Strausfeld, 1996) and whose potential role in speed estimation remains to be investigated.

The transmedullary cells preserve their retinotopic organization as they project to the third optic ganglion, the lobula. Before reaching the lobula, their fibers cross as they pass the inner chiasm. In the honeybee, the lobula is a six-layered structure, the first three layers of which are innervated by transmedullary fibers. Recording from bumblebees suggest that motion-sensitive lobula cells receive their inputs from four layers, while the other two layers are dedicated to color processing (Paulk et al., 2008). The motion responses of neurons in the deeper structures of the honeybee (de Voe et al., 1982) and bumblebee (Paulk et al., 2008) lobula are comparable to the responses of the wide-field, directionally-selective LPTCs believed to underlie the optomotor response in flies (Hausen, 1981). Other motion sensitive cells, including non-directionally selective cells, are present in the lobula of flies (Douglass and Strausfeld, 1995), honeybees (Hertel and Maronde, 1987) and bumblebees (Paulk et al., 2008). In honeybees, neurons in the lobula respond to wide field stimuli and begin to show spiking responses, displaying a hierarchical processing structure reminiscent of primates (Hertel and Maronde, 1987). If the transmedullary cells are indeed the non-directional motion cells responsible for speed

estimation (Higgins, 2004), then it is in the lobula that the spatial collation of their inputs and any odometric integration would take place. Outputs from the lobula then proceed to the protocerebrum and higher level processing centers (Ribi, 1987). Recordings of cells projecting from the bumblebee lobula to higher level brain centers such as the mushroom bodies and protocerebrum have complex response properties and can respond to both color and motion (Paulk and Gronenberg, 2008; Paulk et al., 2009), but no speed-tuned cells have been identified. There is some controversial electrophysiological evidence of velocity sensitive descending neurons projecting from these centers, but little is known about the origin, physiology, and organization of these cells (Ibbotson, 2001).

2.4 Models of Motion Detection

Many different models have been proposed to underlie motion detection, but they fall into three main classes: feature-based, gradient-based and correlation-based (or motion energy) models. Feature-based models require the identification and tracking of different features in the image while gradient and correlation schemes extract motion using only local intensity fluctuations. While I am primarily interested in correlation-based models that have strong biological support, I also review other theories of visual speed estimation, beginning with a very brief review of feature-based detectors. Next, I discuss velocity-sensitive, gradient-based algorithms that were originally developed from theoretical approaches to motion detection (Section 2.4.1). I then proceed with a survey of directionally-selective, correlation-based models, such as the HR model (Section 2.4.3). From here I show how the basic components of correlation models have been rearranged to improve their speed-tuning, culminating in the non-directional motion models investigated in this dissertation (Section 2.4.4). Finally, I discuss higher level simulations proposing different control systems for using the speed-tuned outputs of motion detectors to reproduce optic flow dependent behaviors (Section 2.4.5).

Before detailing the models, it is useful to define some terminology and identify limitations introduced by the biology of the visual system. I define a *motion detector* as responding more strongly to motion than to flicker, where a flickering stimulus displays no coherent variation in contrast relative to the background illumination. A *non-directional* motion detector has the further qualification of responding equally to motion in any direction. The general computation of motion detection requires at least two spatially separated points at two different times, although in artificial situations it is possible to extract motion information from a single point given sufficient constraints (Horn and Schunck, 1981). The detection of motion also requires some sort of nonlinearity, whether it be a multiplication, differentiation, or threshold operation (Buchner, 1984).

Photoreceptors provide a representation of the fluctuating light intensity within their receptive field, such that the visual image is composed of many discrete pixels. While we represent each photoreceptor as having a point-like receptive field for computational simplicity, extending the receptive fields through the addition of spatial filters can provide a more accurate representations of visual processing and eliminate *spatial aliasing*, in which high spatial frequency gratings will be perceived as moving in the opposite direction (Fermi and Reichardt, 1963; van Santen and Sperling, 1985). *Temporal aliasing*, in which the apparent direction of motion is reversed for fast moving stimuli, can also occur in simulations using discrete representations of time when a grating moves more than half its spatial wavelength over successive frames, although this would not be observed in a biological setting (Zanker et al., 1999). Finally, the spacing between photoreceptors is often represented linearly when modeling motion detector responses, but technically the visual field is better represented in angular coordinates because of the approximately spherical shape of the eye.

2.4.1 Gradient-based Models

Gradient schemes were developed to extract motion from an image via the spatial and temporal derivatives of the pattern intensity at each point in the image, denoted as I_x and I_t, respectively, for the one dimensional case (Limb and Murphy, 1975; Fennema and Thompson, 1979; Horn and Schunck, 1981). These are related to the pattern velocity v_p by the following equation

$$v_p = \frac{dx}{dt} = -\frac{I_t}{I_x} \tag{2.1}$$

This method also works for two dimensions (Horn and Schunck, 1981), although motion can only be measured in the direction of the intensity fluctuation, a phenomenon known as the *aperture problem*. Versions of the gradient model have been developed to explain biological motion detection. The first was by Marr and Ullman (1981) to explain the responses of simple cells in primates, although their model was distinct in that it primarily extracted the direction of visual motion and not the local velocity (Hildreth and Koch, 1987). Another version is that of Buchner (1984) in which the temporal derivatives are approximated by high-pass filters and the spatial derivative is approximated by subtracting the outputs of two adjacent photoreceptors, as shown in Figure 2.12.

While the speed tuning of gradient schemes makes them attractive for explaining optic flow dependent behaviors, there are some disadvantages to the models for measuring optic flow. A true spatial derivative requires that the spacing between two points becomes infinitely small. In a biological system the spacing between two photoreceptors is finite so that one cannot implement an ideal gradient model. This will cause the output of gradient-based models to become dependent on the spatial frequency of a stimulus, although this dependence is smaller than that observed in most correlation-based models (Buchner, 1984). Another disadvantage of gradient schemes is that derivatives enhance high frequencies which will amplify noise in the

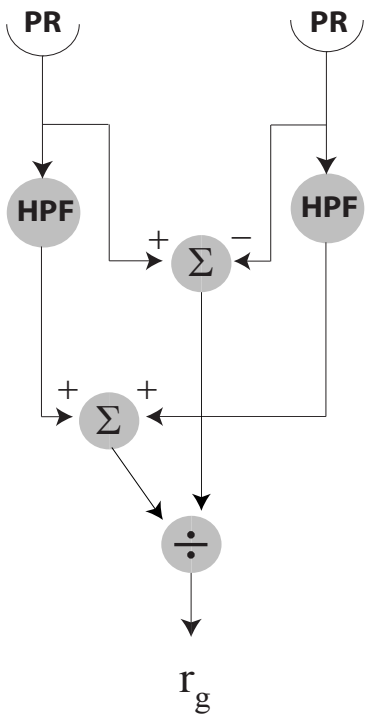

Figure 2.12: Example gradient-based detector. A directionally-selective, one-dimensional gradient-based detector as presented by Buchner (1984) in which the temporal derivatives are approximated by high-pass filters (HPF) and the spatial filter is approximated by the subtraction of two adjacent photoreceptor (PR) outputs. By dividing (÷) the spatial derivative by the temporal derivative one acquires an estimate of the local velocity as shown in Equation 2.1.

signal (Hildreth and Koch, 1987), something common in neural signals. Finally, the biggest disadvantage of gradient schemes is that they necessitate the division of two derivatives, and if the divisor becomes zero the output of the model is meaningless.

An alternative, biologically-inspired gradient model was developed by Srinivasan et al. (1991) to explain optic flow dependent behaviors. Their model, diagrammed in Figure 2.13, first converts the intensity signal of the moving visual image to a binary image via fast-saturating neurons sensitive to very low contrasts. The binary image is then spatially low-pass filtered to convert the sharp edges into ramps of constant spatial slope. The temporal derivative of the low-pass filtered image yields pulses whose amplitudes are equal to the local angular speed of the image and which can then be rectified to give an estimate of image speed independent of the direction (Srinivasan et al., 1991). The advantage of this method is that it avoids the division operation present in other gradient models, an operation that can produce indeterminate values when the gradient is small (Srinivasan et al., 1999a). It has also been argued that neurons with the necessary response properties to implement such a scheme are present in the insect optic lobes (Srinivasan et al., 1999a; Coombe et al., 1989; Srinivasan et al., 1990), although there has not been a targeted investigation into a potential pathway.

There has been some psychophysical evidence supporting the use of gradient schemes in humans (Moulden and Begg, 1986), but the majority of biological data, especially in insects, has supported correlation-based detectors as the neural underpinnings of biological motion detection. In particular, the effectiveness with which the HR model can be used to match insect behaviors and cellular responses of LPTCs has been striking.

2.4.2 Feature-based Models

Another class of models, termed 'feature-based' or 'token-matching' schemes, estimate the speed of an image by measuring the displacement of specific features in

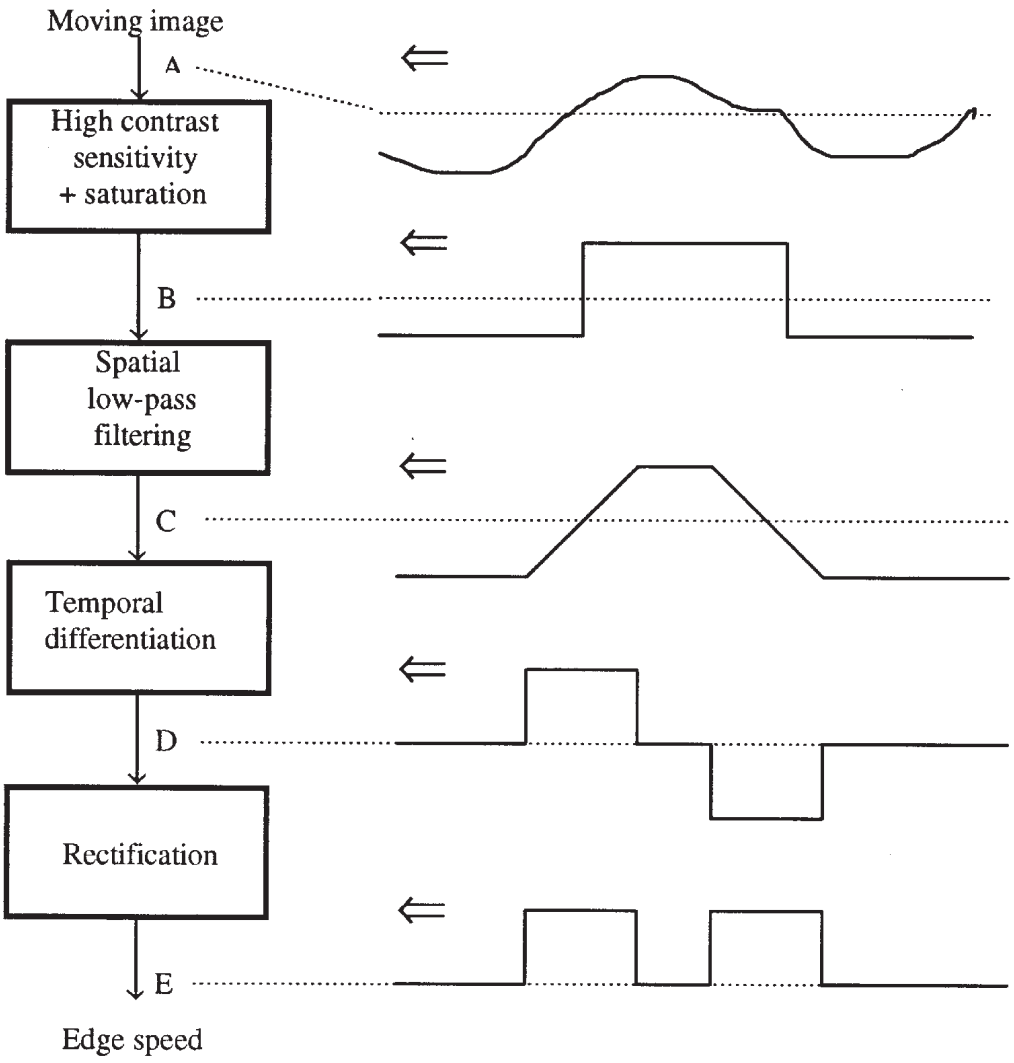

Figure 2.13: Biologically-inspired gradient model. A modified gradient scheme originally proposed by Srinivasan et al. (1991) consisting of four processing stages. (A) The moving image is represented as a time-varying intensity pattern. (B) A threshold operation converts intensity profile of the image into a binary image where the contrast is either zero or one. (C) Next, the binary image is spatially low-pass filtered to yield ramped edges. (D) Third, differentiating the low-pass filtered outputs yields pulses with amplitudes equal to the local angular velocity. (E) Finally, the angular speed is recovered by rectifying the pulses. Reprinted from Srinivasan et al. (1999a) with permission from Elsevier.

the image. These models yield very accurate measurements of image speed, but require the identification of features before this measurement can take place. In addition, once a feature is identified, one faces the 'correspondence problem' of correctly identifying the same feature as it moves through the visual image. These models are of interest primarily because they have been used to test and develop biologically-inspired, optic flow based navigational algorithms (discussed in Section 2.4.5). However, they appear to have little relevance to the early stages of biological motion processing.

One feature-based scheme is the 'facilitate and sample' method first developed by Blanes (1986) and later independently discovered by Kramer and Koch (1997). The detector is composed of two photoreceptors. Activation of the first photoreceptor by a moving edge triggers an exponentially decaying function that is sampled upon activation of the second, adjacent, photoreceptor. The sampled value of the exponential yields an estimate of the time between activations and, because the spacing between photoreceptors is fixed, an estimate of the speed of the edge. While very accurate, facilitate and sample detectors require sharp edges and will not work with gradual intensity changes. To solve this problem Aubépart and Franceschini (2007) added a preprocessing step, equivalent to that of Srinivasan et al. (1991), in which the original image is first converted into a binary image.

A second method that is not technically feature-based, but has been used in similar contexts, is the image interpolation method of Srinivasan (1994). This method calculates the optic flow by comparing the visual image to seven reference images. The reference images are chosen such that the displacement of the current image can be interpolated from the relative differences between the images. The time delay between successive frames is assumed to be constant such that the velocity of each point is simply proportional to the displacement of the image. It is not clear how this model would be implemented in a biological system.

2.4.3 Directionally Selective Correlation Models

Much of the correlation model literature has been developed in the context of studying biological motion detection systems. While correlation models have been very successful in explaining many motion dependent behaviors, their responses are not generally speed-tuned. One of the most well known correlation-based models is the HR model (Hassenstein and Reichardt, 1956) described in Section 2.1. The HR model is tuned to the temporal frequency of a stimulus and will respond differently to two sinusoidal gratings with different spatial frequencies moving at the same speed. The responses of the HR model are discussed in depth in Appendix A.

An elaborated version of the HR model has been developed by van Santen and Sperling (1984). They expanded the point-like receptive fields of the original model, replacing them with spatial filters, and added temporal filters to the photodetector outputs, corresponding to the HPFs depicted in the HR model presented in Figure 2.3b. With these modifications, the outputs of the HR model provide a much better match to the results of psychophysical studies (van Santen and Sperling, 1985).

Another correlation-type model based on the known physiology and psychophysics of the primate visual system was proposed by Adelson and Bergen (1985). In this model, the *motion energy* is extracted from an image using the squared outputs of a quadrature pair of filters, defined as two linear filters 90° out of spatial and temporal phase (Figure 2.14). Because of the differential phase relationship between the filters, the output of a quadrature pair is not dependent on the contrast of a stimulus. The elaborated HR model of van Santen and Sperling is actually a special case of the Adelson-Bergen model. By subtracting the outputs of two spatially separated quadrature pairs, one can create a directionally selective correlation model equivalent to that of the HR model (Adelson and Bergen, 1985; van Santen and Sperling, 1985).

Studies by Barlow and Levick (1965), who were interested in the neuronal cir-

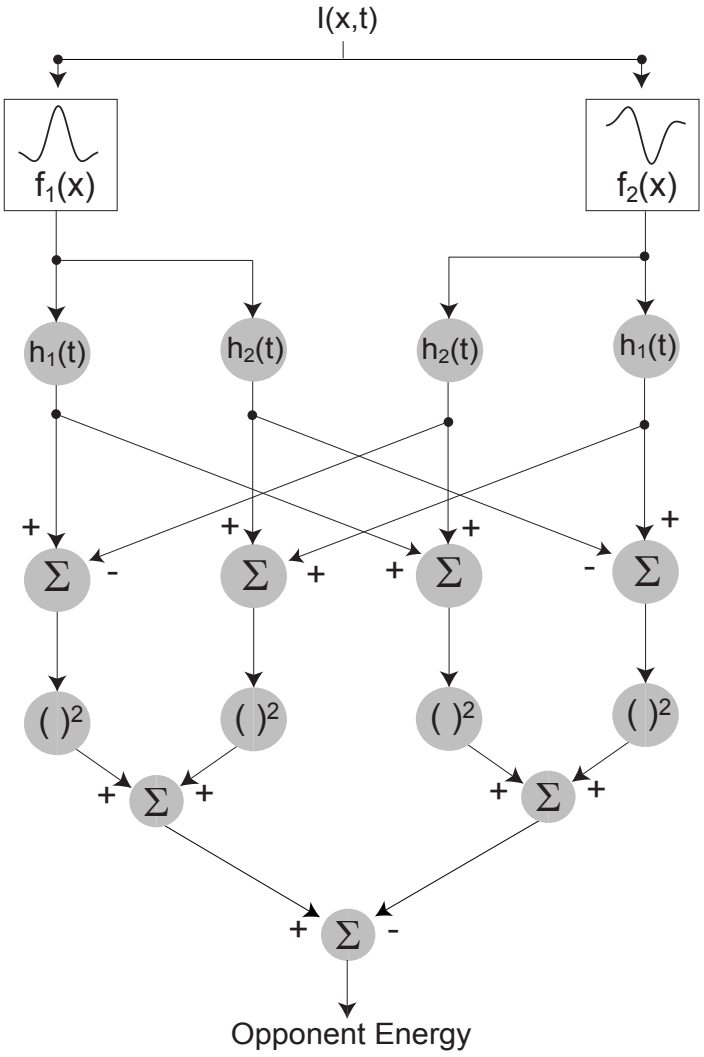

Figure 2.14: Example Adelson-Bergen motion detector. A spatio-temporally varying intensity stimulus $I(x,t)$ is spatially filtered ($f_1(x)$ and $f_2(x)$) and then temporally filtered by a quadrature pair ($h_1(t)$ and $h_2(t)$) by each photoreceptor. These outputs are then differentially summed (Σ), squared, and summed again(Σ). The outputs of this detector are equivalent to those of the HR model (Adelson and Bergen, 1985; van Santen and Sperling, 1985).

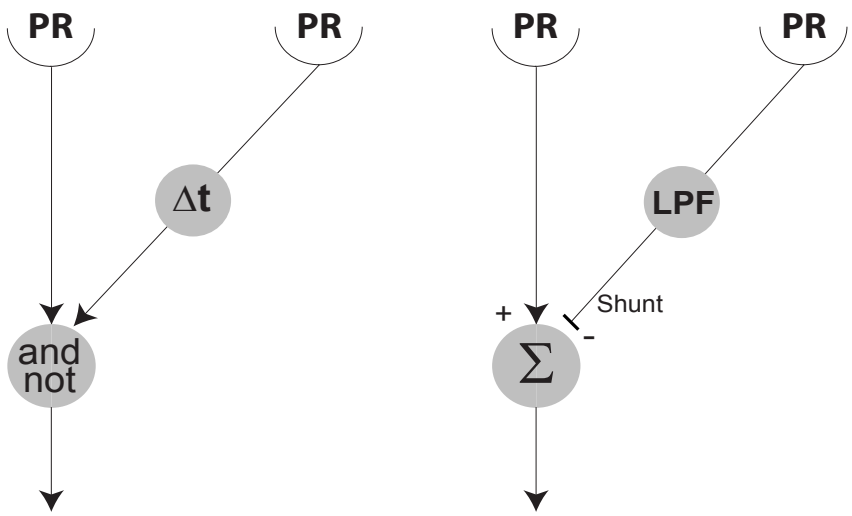

(a) (b)

Figure 2.15: Barlow-Levick Model. (a) The model as originally envisaged in which an AND/NOT logic gate relates a temporally delayed (Δt) photoreceptor (PR) output with an undelayed PR output. (b) An diagram of the Barlow-Levick model as implemented by Torre and Poggio (1978), in which the temporal delay is accomplished via a low-pass filter (LPF) and the AND/NOT logic gate is replaced by a shunting inhibitory synapse.

cuitry underlying motion sensitive retinal ganglion cells in the rabbit, led to the development of a neuronally-based Barlow-Levick (BL) model. This model was initially envisaged as correlating differentially delayed photoreceptor outputs via an AND/NOT logic gate (Figure 2.15a). Attempts to implement the model eventually led to the replacement of the AND/NOT logic gate with a shunting inhibitory synapse, which prevents the activation of an innervated cell without reducing its membrane potential, as shown in Figure 2.15b (Torre and Poggio, 1978). The delayed shunting inhibition allows a response to motion only in one direction. This is because a stimulus moving in the anti-preferred direction will first activate the time-delayed inhibition, preventing excitation of the adjacent photoreceptor. Movement in the preferred direction does not trigger the shunting inhibition prior to activating the undelayed photoreceptor channel, thereby eliciting an excitatory response. It has been argued that shunting inhibition approximates a multiplication operation for inputs with small synaptic conductance (Hildreth and Koch, 1987), making the BL model equivalent to an HR model subunit in this special case.

While these correlation models have very different implementations, the equivalence of their responses suggests there is convergence in the way that biological systems compute motion. This is highlighted by the fact that for many of proposed neuronal implementations of correlation models, a shunting inhibitory synapse is often used as the nonlinearity rather than a multiplication (Torre and Poggio, 1978; Clifford and Ibbotson, 2002; Higgins et al., 2004).

The agreement between the predictions of the HR model, the behavioral studies of the optomotor response and the responses of directionally-selective LPTCs has been striking (Egelhaaf and Borst, 1993), but there has still been some debate about the neuronal implementation of the correlation mechanism. While the high-pass and low-pass filtering operations have relatively straightforward implementations in neuronal systems, the physiological analog to multiplication is less clear (Hildreth and Koch, 1987) and different methods for approximating multiplication have been

proposed (Koch, 1999). The most straightforward method for addressing this issue is to identify the neuronal components of a motion detection circuit and observe the neuronal responses.

Higgins et al. (2004) proposed a putative, evolutionarily conserved elementary motion detection (EMD, Figure 2.16) circuit in the fly, the responses of which match those of the HR model. By combining the neuroanatomical data with the few electrophysiological recordings available from the early visual pathways of the fly, they were able to assign specific mathematical functions to each cell in the pathway. Although more complicated than the HR model, the EMD model has provided much insight into the neuronal processing of motion. One such insight was that the non-linearity in the EMD pathway is actually provided by a shunting inhibitory synapse.

Another surprise was that the computation of non-directional motion by the Tm1 cell precedes the detection of directional motion by the T5 cell (refer to Section 2.3). As previously mentioned in Section 2.2.2, the fact that optic flow dependent behaviors are sensitive to motion without regard for direction (Srinivasan et al., 1993; Srinivasan and Zhang, 1997) makes the Tm1 cell a particularly strong candidate as a potential neuronal speed sensor.

It has been shown that correlation-based motion detectors can be used to estimate image speed via a population code, in which multiple motion detectors with different spatio-temporal tunings are combined to yield a speed-tuned output (Srinivasan et al., 1999a). However, this method of speed estimation requires another layer of neuronal processing to discard the spatial frequency information. Furthermore, electrophysiological recordings from known directionally-selective cells in insect motion detection pathways do not respond to the high temporal frequencies seen during optic flow dependent behaviors (Srinivasan et al., 1999a). Thus, its seems unlikely that such a neuron intensive strategy is used by insects to visually estimate speed.

Another suggestion is that insects would not experience narrowband stimuli in

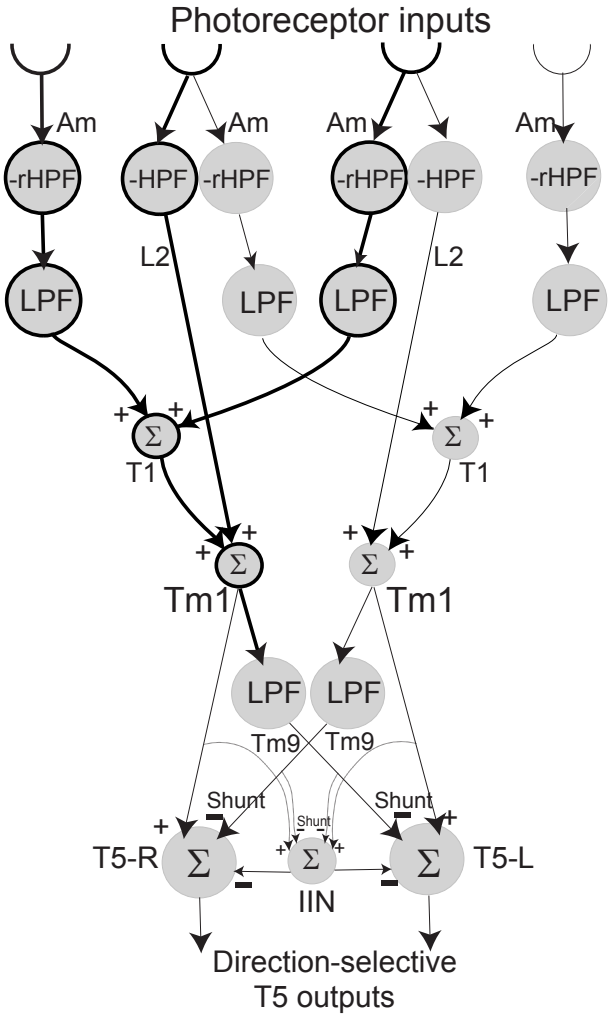

Figure 2.16: Elementary Motion Detector (EMD) model. The neuronal pathway for elementary motion detection as proposed by Higgins et al. (2004). HPF and LPF denote high-pass and low-pass filters, respectively. An rHPF denotes a relaxed high-pass filter that retains some of the sustained illumination components of the photoreceptor signal. Summing operations are represented by Σ, while "shunt" indicates shunting inhibition. Am, L2, T1, Tm1, Tm9, IIN and T5 all indicate the neurons believed to carry out the different operations. The processing steps of the non-directionally selective Tm1 cell are highlighted with bold lines. Figure modified from Higgins et al. (2004) with permission from Visual Neuroscience.

the real world and that the responses of the HR model to sinusoidal stimuli are not important. Instead, studies have shown that natural scenes have characteristic, $\frac{1}{f^2}$ frequency spectra (van der Schaaf and van Hateren, 1996) to which HR detectors have speed-tuned responses (Dror et al., 2001). Thus, the HR model can be used as an effective optic flow sensor in real-world environments (Dror et al., 2001). However, these experiments do not address the fact that honeybees are still able to estimate the speed of narrowband grating patterns (Srinivasan et al., 1991; Baird et al., 2005).

2.4.4 Speed-tuned Correlation Models

Attempts to decrease the spatial frequency dependence of the correlation models, thereby improving their speed tuning, began with the investigations of Zanker et al. (1999) who tested the speed sensitivity of the HR model while modifying the relative weights of the two mirror-symmetrical subunits. They found that a single subunit (Figure 2.3a), sensitive to motion only in one direction, responds proportionally to speed over a broader range of spatial frequencies than the full HR model.

This idea was expanded by Higgins (2004) who arranged two HR model subunits anti-symmetrically to create the non-directional motion detector shown in Figure 2.17a, which is refered to as the non-directional multiplication (NDM) model. The NDM model is sensitive to motion in any direction, has an improved speed-tuning compared to the HR subunit, and maintains residual responses to flicker, thus better matching optic flow dependent behaviors (Srinivasan et al., 1993).

It was discovered by Rivera-Alvidrez (2005) that a modified version of this model, the non-directional summation (NDS) model (Figure 2.17b), in which a summation operation replaces the final multiplication of the NDM model, was speed sensitive in its *amplitude*, as opposed to mean, response. This was a particularly interesting development, as the operations yielding the NDS model matched those proposed for the Tm1 cell in the EMD model (Figure 2.16; Higgins et al., 2004). The response

characteristics of the NDM and NDS models are further described in Appendix A.

The success of the non-directional models prompted Pant (2007) to implement them in silicon. While testing the vision chips he noted that the spatial frequency dependence of these models could be further reduced by entirely removing the low-pass filters in both the NDM and NDS models. He termed them "simplified non-directional models" and their response characteristics are described in depth in Appendix B.

A similar approach to developing a speed detector with a broad spatial frequency tuning was implemented by Riabinina and Philippides (2009), who effectively combine the simplified NDM model of Pant (2007) with a gradient scheme (Figure 2.12; e.g. Buchner, 1984). In their angular speed detector (ASD, Figure 2.18) the outputs of adjacent photoreceptors are first temporally differentiated to extract the time-varying components of the intensity signal. The differentiated outputs from one pair of photoreceptors are then multiplied, an operation that is repeated in a cascade-like fashion for a total of 60 receptors covering a 120° field of view. Next, the sum of the correlated outputs are summed and divided by the average of the differentiated photoreceptor outputs. This division reduces the temporal frequency dependence of the model, resulting in a wide-field motion detector primarily sensitive to the angular speed of the image. (Riabinina and Philippides, 2009).

The ASD shares many of the drawbacks of the gradient-based models. The final division step makes the model susceptible to division by zero when image motion is very small. Also, as with the gradient model, a temporal derivative will amplify high frequency noise. However, because a pure derivative cannot be implemented by neurons, Riabinina and Philippides (2009) used a thresholding operation to identify changes in image intensity similar to that used in the gradient-based detector of Srinivasan et al. (1991). This approximation decreases the effectiveness of the models for speed estimation.

However, the ASD also proposes a novel method for improving the speed tuning

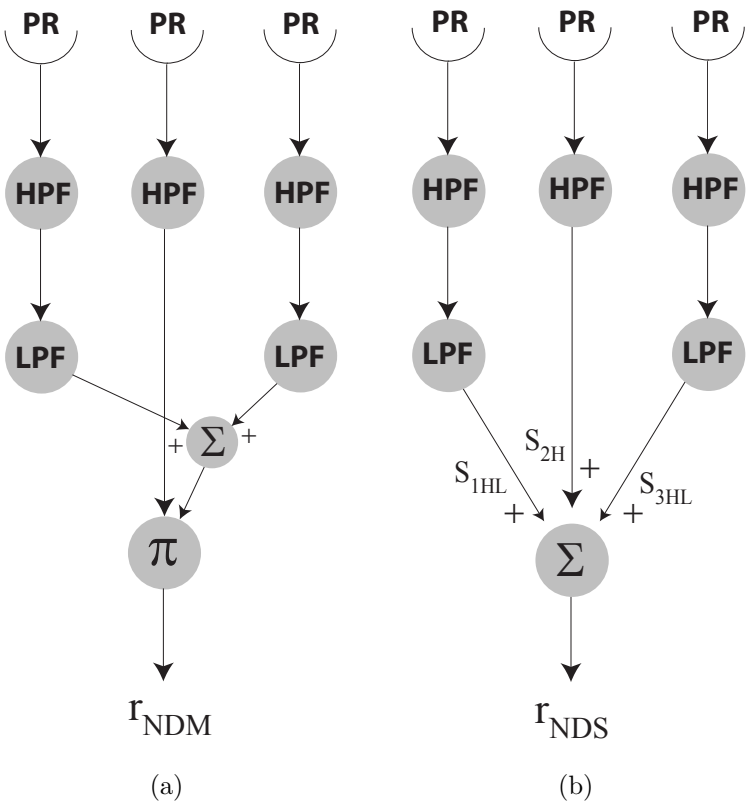

Figure 2.17: Non-directional models. (a) The NDM model comprises three photoreceptors (PR) whose outputs are first high-pass filtered (HPF). The filtered outputs from the two lateral arms low-pass filtered (LPF), summed (Σ) and multiplied (π) by the filtered output of the central channel. (b) The NDS model is identical to the NDM model except that the final multiplication is replaced by a summation.

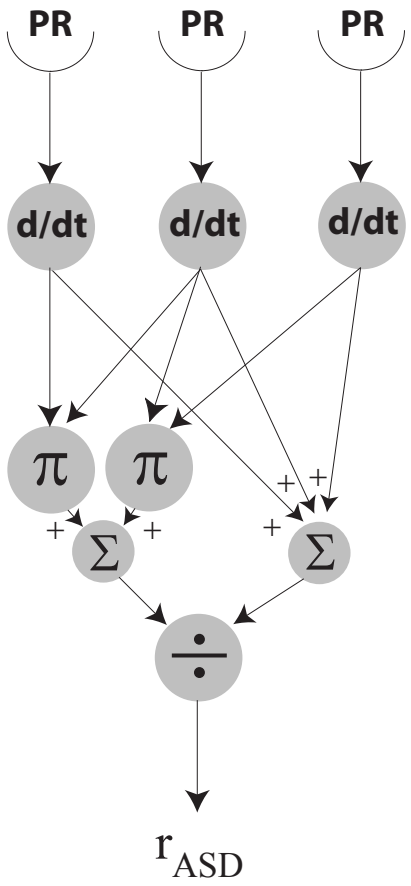

Figure 2.18: ASD motion detector. A small cross-section of an ASD detector that normally contains 60 photoreceptors (PR). The photoreceptor outputs are differentiated (d/dt) to highlight changes in image intensity. The differentiated outputs of neighboring photoreceptors are then multiplied (π) and summed (Σ). The temporal frequency dependence of the averaged correlator output is then removed by dividing ($\div$) by the sum of all the differentiated PR outputs.

of correlation models, namely the division of the motion detector responses with a temporal frequency dependent signal. If one approximates the temporal derivatives of the ASD model with high-pass filters, this effectively yields a simplified NDM model. It may therefore be possible to improve the speed tuning of the NDM model by dividing its output by the average of the high-pass filtered photoreceptor responses. This division would also help counteract fluctuations in contrast by effectively normalizing the NDM output. The speed-tuning of the HR model was also improved by taking the quotient of two detectors with different interommatidial angles (1° and 2°), but did not improve the speed tuning beyond that of the ASD (Riabinina and Philippides, 2009).

2.4.5 Higher Level Simulations

There have been a number of studies investigating how optic flow signals can be used to match the behaviors seen in insects. These higher level control algorithms are often implemented on robotic platforms that require simple but effective methods for detecting optic flow and therefore rarely use sophisticated or biologically-realistic detector schemes. However, they have provided valuable insights into the challenges of using optic flow to control behavior and can be used to demonstrate the sufficiency of different models for reproducing optic flow dependent behaviors.

One of the earliest robotic studies was performed by Srinivasan et al. (2001), who mimicked the optic flow-based landing behaviors of honeybees with a simple robotic gantry. A downward-looking camera was suspended from the gantry and viewed a random black and white pattern that was fixed to the floor. The gantry was required to descend at a fixed angle and maintain a preferred rate of optic flow. In order to achieve this preferred rate of optic flow, the global motion of the image was calculated using the image interpolation method (Srinivasan, 1994) discussed in Section 2.4.2. For each successive frame, the ratio of the preferred optic flow to the apparent optic flow was used to modulate both the forward speed and rate of

descent of the gantry. These experiments demonstrated the sufficiency of optic flow for mimicking the landing behaviors observed in honeybees (Srinivasan et al., 2000b, 2001).

A similar altitude control algorithm, named OCTAVE (Optic flow based Control sysTem for Aerial VEhicles), was implemented by Ruffier and Franceschini (2005). In their experiments, an aerial robot with a single rotor was fixed to a robotic arm, thereby simplifying the navigational problem by limiting the degrees of freedom of the system. The forward and vertical flight speed of helicopter-like robot was controlled by modulating the rotor speed as the robot flew in a circle around the base of the robotic arm. Optic flow was measured using a 'token-matching' algorithm (Section 2.4.2) with a downward looking camera. They showed that the robot would maintain a relatively fixed height above the ground by holding the apparent optic flow constant. In this case, the difference between the perceived optic flow and the preferred optic flow were used to control the rotor speed and consequently the height of the robot.

Serres et al. (2006) developed another algorithm, LORA(2) (Lateral Optic flow Regulation Autopilot), to mimic the centering response and visually mediated flight speed control. In their experiment, a hovercraft was outfitted with two laterally oriented motion detectors facing opposite walls of a tunnel. The motion detectors we token-matching EMDs consisting of two photodetectors with large receptive fields. The axis of the hovercraft was held constant so that its 'gaze' was fixed and the EMDs were always oriented perpendicular to the axis of the tunnel. A preferred rate of optic flow was used to control both the lateral and forward speed of the robot. The speed of the robot was adjusted by taking the difference between the mean rate of optic flow and the preferred rate. The lateral position of the robot was determined by taking the highest perceived optic flow from the left and right eyes, subtracting it from the preferred optic flow, and then multiplying it by the sign of the difference between the optic flow estimates. This value was then used to adjust

the lateral speed of the robot such that it moved away from the wall that appeared to be moving faster. One consequence of this control scheme was that if the speed of the faster-moving wall matched the preferred rate of optic flow, the robot did not change its lateral flight speed (or position). The result was a wall-following behavior similar to that observed in honeybees flying through very wide tunnels (Serres et al., 2008).

2.5 Parallels to Primates

Although there are numerous glaring differences between the visual systems of insects and primates, such as simple versus compound eyes, many of the computational and organizational strategies appear to be convergent. The preservation of retinotopic arrangements throughout the early visual pathways, the representation of color using receptors of three different spectral sensitivities (in honeybees and bumblebees), and the "achromatic processing" of motion are examples of the more basic principles shared by both organisms (Gribakin, 1969; Kaiser and Liske, 1972; Ribi, 1987; Hubel and Livingstone, 1987). As discussed previously, there appears to be a strong convergence among the different models of motion detection, suggesting that similar mechanisms may be used by both insects and primates.

In primates, the computation of speed and direction in V1 is evidenced by cells sensitive to direction, depth, velocity, and combinations of all three (Hubel and Wiesel, 1968). The speed responses of these cells fall into three classes, velocity low-pass (VLP), velocity band-pass (VBB) and velocity tuned (VT) (Orban et al., 1986). In these experiments, a slit of light was moved across the receptive field of the neuron of interest at varying speeds and directions. Despite the classifications, anywhere from 38-72% of these cells were not selective to direction making them speed rather than velocity sensitive. The tuning curves of the VT cells most closely resemble those of the NDM units of Higgins (2004), but it is not clear from the data whether they are tuned to a specific speed, or if their responses vary proportionally

with speed before dropping off. Speed responses of the NDS model better resemble the VBB neurons, with responses that first increase proportionally with speed and then level off at a constant level of activity (Rivera-Alvidrez, 2005). Although not tested rigorously, varying the width of the moving slit of light did not appear to change the velocity tuning curve, suggesting the response is independent of the spatial structure of the stimulus (Orban et al., 1986).

CHAPTER 3

Present Study

3.1 Introduction

The goal of this study was to investigate the suitability of non-directional motion detectors for modeling optic flow dependent behaviors in insects. To accomplish this, I characterized the speed dependent responses of different non-directional motion detectors, tested the efficacy of the models for reproducing optic flow dependent behaviors using a novel behavioral simulation framework, and designed and performed behavioral experiments with bumblebees to acquire a detailed spatial frequency tuning curve for the visual speed estimation system. The appended manuscripts describe the methods, results, and conclusions of my studies of the visual speed estimation system. The following is a summary of the most important findings in these documents.

3.2 Appendix A

The first attached manuscript examines the efficacy of two non-directional models of motion detection, the NDM and NDS models, for mimicking optic flow dependent behaviors. Their performance was benchmarked against that of the canonical model of motion detection in insects, the HR model (Hassenstein and Reichardt, 1956). The study was split into two parts. The first was the examination of the analytically derived responses of the three models to the moving sinusoidal stimuli. As part of this work, we reviewed the behavioral and neurobiological literature in order to determine appropriate model parameter values (e.g. filter time constants) and the relevant range of stimuli (e.g. pattern spatial frequencies used in behavioral

experiments). The analytically derived responses indicated that the responses of the NDS and NDM models were less dependent on the spatial frequency of the visual stimulus than the response of the HR model, and should therefore be better speed estimators.

The second part of this work was the development of a behavioral simulation framework for mimicking the centering response (Kirchner and Srinivasan, 1989; Srinivasan et al., 1991). As part of the simulation framework, we also developed a novel method for acquiring a global estimate of optic flow, while still maintaining sensitivity to small field motion. All of the models could be used to partially match real-world behaviors with different models better matching certain aspects of the behavior. While all of the models had difficulty with low spatial frequency patterns they still successfully navigated through the simulation environment.

The HR model was less dependent on spatial frequency than either of the non-directional models when using square wave stimuli. These results suggested that the HR model could effectively function as a speed estimator, but only when higher spatial frequencies are present in the visual image. However, while less dependent on spatial frequency, the HR model was much less accurate than the non-directional models for measuring the apparent speed of the tunnel walls. The NDS model was the most effective for this task, closely matching the predicted position of a bee by perfectly matching the apparent speed of the walls of a tunnel. In addition, when the NDS model deviated from the ideal case, the deviations were consistent with observations in honeybees (Baird et al., 2005).

The study concluded that all three models could potentially be used to mimic optic flow dependent behaviors, but that the NDS model was the most likely candidate. In addition to being the most accurate at estimating speed, the NDS model was the most easily implemented, matched many of the properties observed in optic flow dependent behaviors and had response characteristics consistent with known motion-sensitive cells in the insect optic lobes. Finally, the results suggested that

slight improvements in the spatial frequency tunings of the models could result in significantly better performance in behavioral simulations.

3.3 Appendix B

The work presented in this second manuscript logically extends from our previous modeling observations. In this study, we developed two methods for altering the spatial frequency tuning of the NDM and NDS models in order to better match previously published behavioral results. The two proposed modifications were the removal of the low-pass filters in the models and the inclusion of next nearest neighbor photoreceptors in the motion computation. We showed that these modifications can be used to alter the responses of the models so that they are speed-tuned at lower spatial frequencies, but with a concurrent decrease in the speed tuning of the models at higher spatial frequencies.

We then tested the modified non-directional models in an improved behavioral simulation framework in which we could present sinusoidal stimuli. As predicted, shifting the speed tunings of the models to lower spatial frequencies did improve model performance in behavioral simulations. However, all of the models retained at least some dependence on spatial frequency, although this was consistent with our behavioral results (Appendix C). We also noted the the speed-tuning of the models, and their subsequent performance in behavioral simulations, were very heavily dependent on the filter time constants used in the models.

We confirmed our previous simulation results by showing that all of the models were less sensitive to the spatial frequency of square wave gratings than to sinusoidal patterns. Furthermore, while the HR model could be used as a speed detector when square wave gratings were used in the behavioral simulations, it had a failure rate near 100% when sinusoidal gratings were used.

The proposed modifications to the original models did not significantly alter their biological plausibility and, in some cases, made the models easier to implement. We

concluded that one of these non-directional motion detectors may underlie optic flow dependent behaviors in insects, but that more electrophysiological and behavioral data was necessary to draw more specific conclusions.

3.4 Appendix C

The third attached manuscript presents behavioral studies aimed at acquiring a detailed spatial frequency tuning of the visual speed estimation system. In these studies, I video-recorded the flight paths of bumblebees *Bombus Impatiens* flying through a narrow tunnel whose walls were lined with various square wave and sinusoidal grating patterns.

The experiments showed that the estimate of optic flow is dependent on the spatial frequency of a stimulus, contrary to the general conclusions of previous studies (Srinivasan et al., 1991, 1996; Si et al., 2003; Baird et al., 2005), and that this dependence was not contrast dependent. In addition, a conservative estimate was acquired for the minimum spatial wavelength resolvable by the bumblebee optic flow system of 7 degrees.

These experiments demonstrated that square wave gratings are not perceived as narrowband stimuli by bumblebees, as shown by direct comparisons between the two types of patterns in centering experiments. Instead, the results suggest that the bees perceive square wave gratings as having higher spatial frequency content than sinusoidal patterns with the same spatial wavelength. Furthermore, while some dependence on the spatial frequency of square wave gratings was observed, the dependence was significantly less than that observed for sinusoidal stimuli. These results were consistent with simulation results using square wave stimuli.

These experiments provided a broad spatial frequency tuning curve with which to compare our modeling results. Although not explicitly detailed in the manuscript, these behavioral observations are consistent with our modeling results (Appendices A and B). In particular, the responses of the non-directional models tend to decrease

as spatial frequency increases, consistent with these behavioral results. In contrast, the HR model response increases with spatial frequency.

3.5 Relative Contributions

The experiments, simulations, derivations, software development and data analysis for the work presented in Appendices A, B, and C were all carried out by the author of this dissertation with the assistance of Dr. Charles M. Higgins, with three exceptions. The derivation of the NDS model response (Appendix A) was first performed by Zuley Rivera-Alvidrez (2005); the discovery and characterization of the simplified non-directional models (Appendix B) was the work of Dr. Vivek Pant (2007); and Dr. Higgins developed a significant portion of the graphics software used for the behavioral simulations in Appendices A and B. The author also wrote all of the manuscripts.

REFERENCES

Adelson, E. and J. Bergen (1985). Spatiotemporal energy models for the perception of motion. *Journal of the Optical Society of America A*, **2**(2), pp. 284–299.

Aubépart, F. and N. Franceschini (2007). Bio-inspired optic flow sensors based on FPGA: Application to Micro-Air-Vehicles. *Microprocessors and Microsystems*, **31**(6), pp. 408–419.

Baird, E., M. Srinivasan, S. Zhang, and A. Cowling (2005). Visual control of flight speed in honeybees. *Journal of Experimental Biology*, **208**(20), pp. 3895–3905.

Baird, E., M. Srinivasan, S. Zhang, R. Lamont, and A. Cowling (2006). Visual Control of Flight Speed and Height in the Honeybee. In *From Animals to Animats 9*, pp. 40–51. Springer, Berlin / Heidelberg.

Barlow, H. and W. Levick (1965). The mechanism of directionally selective units in rabbit's retina. *The Journal of Physiology*, **178**(3), pp. 477–504.

Barron, A. and M. Srinivasan (2006). Visual regulation of ground speed and headwind compensation in freely flying honey bees Apis mellifera L. *Journal of Experimental Biology*, **209**(5), pp. 978–984.

Blanes, C. (1986). Appareil visuel elementaire pour la navigation "á vue" dun robot mobile autonome. DEA Thesis, Universite D'Aix-Marseille II, pp. 57.

Borst, A. (2000). Models of motion detection. *Nature Neuroscience*, **3**(11), p. 1168.

Borst, A. and S. Bahde (1987). Comparison between the movement detection systems underlying the optomotor and the landing response in the housefly. *Biological Cybernetics*, **56**(4), pp. 217–224.

Borst, A. and M. Egelhaaf (1989). Principles of visual motion detection. *Trends in Neurosciences*, **12**(8), pp. 297–306.

Buchner, E. (1984). Behavioural analysis of spatial vision in insects. In Ali, M. (ed.) *Photoreception and vision in invertebrates*, pp. 561–622. Plenum, New York.

Buschbeck, E. and N. Strausfeld (1996). Visual Motion-Detection Circuits in Flies: Small-Field Retinotopic Elements Responding to Motion Are Evolutionarily Conserved across Taxa. *Journal of Neuroscience*, **16**(15), pp. 4563–4578.

Capaldi, E., A. Smith, J. Osborne, S. Fahrbach, S. Farris, D. Reynolds, A. Edwards, A. Martin, G. Robinson, G. Poppy, and J. Riley (2000). Ontogeny of orientation flight in the honeybee revealed by harmonic radar. *Nature*, **403**(6769), pp. 537–540.

Chittka, L. and J. Tautz (2003). The spectral input to honeybee visual odometry. *Journal of Experimental Biology*, **206**(14), pp. 2393–2397.

Clifford, C. and M. Ibbotson (2002). Fundamental mechanisms of visual motion detection: models, cells and functions. *Progress in Neurobiology*, **68**(6), pp. 409–437.

Coombe, P., M. Srinivasan, and R. Guy (1989). Are the large monopolar cells of the insect lamina on the optomotor pathway? *Journal of Comparative Physiology A: Neuroethology, Sensory, Neural, and Behavioral Physiology*, **166**(1), pp. 23–35.

Dacke, M. and M. Srinivasan (2007). Honeybee navigation: distance estimation in the third dimension. *Journal of Experimental Biology*, **210**(5), pp. 845–853.

David, C. T. (1982). Compensation for height in the control of groundspeed by-Drosophila in a new, barber's pole wind tunnel. *Journal of Comparative Physiology A: Neuroethology, Sensory, Neural, and Behavioral Physiology*, **147**(4), pp. 485–493.

de Voe, R., W. Kaiser, J. Ohm, and L. Stone (1982). Horizontal movement detectors of honeybees: Directionally-selective visual neurons in the lobula and brain. *Journal of Comparative Physiology A: Neuroethology, Sensory, Neural, and Behavioral Physiology*, **147**(2), pp. 155–170.

Douglass, J. and N. Strausfeld (1995). Visual motion detection circuits in flies: peripheral motion computation by identified small-field retinotopic neurons. *Journal of Neuroscience*, **15**(8), pp. 5596–5611.

Douglass, J. and N. Strausfeld (1996). Visual Motion-Detection Circuits in Flies: Parallel Direction- and Non-Direction-Sensitive Pathways between the Medulla and Lobula Plate. *Journal of Neuroscience*, **16**(15), pp. 4551–4562.

Dror, R., D. O'Carroll, and S. Laughlin (2001). Accuracy of velocity estimation by Reichardt correlators. *Journal of the Optical Society of America A*, **18**(2), pp. 241–252.

Egelhaaf, M. and A. Borst (1993). A look into the cockpit of the fly: visual orientation, algorithms, and identified neurons. *The Journal of Neuroscience*, **13**(11), pp. 4563–4574.

Esch, H. and J. Burns (1995). Honeybees use optic flow to measure the distance of a food source. *Naturwissenschaften*, **82**(1), pp. 38–40.

Esch, H. and J. Burns (1996). Distance estimation by foraging honeybees. *Journal of Experimental Biology*, **199**(1), pp. 155–162.

Esch, H., S. Zhang, M. Srinivasan, and J. Tautz (2001). Honeybee dances communicate distances measured by optic flow. *Nature*, **411**(6837), pp. 581–583.

Fennema, C. and W. Thompson (1979). Velocity determination in scenes containing several moving objects. *Computer Graphics and Image Processing*, **9**(4), pp. 301–315.

Fermi, G. and W. Reichardt (1963). Optomotorische Reaktionen der Fliege Musca domestica. *Kybernetik*, **2**(1), pp. 15–28.

Franceschini, N., A. Riehle, and A. Le Nestour (1989). Directionally selective motion detection by insect neurons. In Stavenga, D. and R. Hardie (eds.) *Facets of Vision*, pp. 360–390. Springer-Verlag, Heidelberg, New York.

Fry, S., N. Rohrseitz, A. Straw, and M. Dickinson (2009). Visual control of flight speed in Drosophila melanogaster. *Journal of Experimental Biology*, **212**(8), pp. 1120–1130.

Giurfa, M., M. Vorobyev, P. Kevan, and R. Menzel (1996). Detection of coloured stimuli by honeybees: minimum visual angles and receptor specific contrasts. *Journal of Comparative Physiology A: Neuroethology, Sensory, Neural, and Behavioral Physiology*, **178**(5), pp. 699–709.

Götz, K. (1964). Optomotorische Untersuchung des visuellen systems einiger Augenmutanten der Fruchtfliege Drosophila. *Biological Cybernetics*, **2**(2), pp. 77–92.

Götz, K. (1968). Flight control in Drosophila by visual perception of motion. *Biological Cybernetics*, **4**(6), pp. 199–208.

Götz, K. (1972). Principles of optomotor reactions in insects. In Bizzi, E. and J. Dichgans (eds.) *Cerebral Control of Eye Movements and Perception of Motion*, volume 82, pp. 411–417. J. Bibliotheca Ophthalmologica.

Götz, K. (1987). Course-Control, Metabolism and Wing Interference During Ultralong Tethered Flight in Drosophila Melanogaster. *Journal of Experimental Biology*, **128**(1), pp. 35–46.

Gribakin, F. (1969). Types of photoreceptor cells in the compound eye of the worker honey bee relative to their spectral sensitivity. *Cytologie (Tokyo)*, **11**, pp. 309–314.

Hassenstein, B. (1951). Ommatidienraster und afferente Bewegungsintegration. *Journal of Comparative Physiology A: Neuroethology, Sensory, Neural, and Behavioral Physiology*, **33**(4), pp. 301–326.

Hassenstein, B. and W. Reichardt (1956). Systemtheoretische Analyse der Zeit-, Reihenfolgen- und Vorzeichenauswertung bei der Bewegungsperzeption des Rsselkfers Chlorophanus. *Zeitschrift f ur Naturforschung B*, **11**(9), pp. 513–524.

Hausen, K. (1981). Monocular and binocular computation of motion in the lobula plate of the fly. *Verhandlungen der Deutschen Zoologischen Gesellschaft*, pp. 49–70.

Hausen, K. (1982). Motion sensitive interneurons in the optomotor system of the fly. *Biological Cybernetics*, **45**(2), pp. 143–156.

Hausen, K. and C. Wehrhahn (1983). Microsurgical Lesion of Horizontal Cells Changes Optomotor Yaw Responses in the Blowfly Calliphora erythrocephala. *Proceedings of the Royal Society of London. Series B, Biological Sciences*, **219**(1215), pp. 211–216.

Hecht, S. and E. Wolf (1929). The visual acuity of the honey bee. *Journal of General Physiology*, **12**(6), pp. 727–760.

Heran, H. (1956). Ein Beitrag zur Frage nach der Wahrnehmungsgrundlage der Entfernungsweisung der Bienen. *Zeitschrift fur Vergleichende Physiologie*, **38**, pp. 168–218.

Heran, H. and L. Wenke (1952). Beobachtungen ber die Entfernungsmeldung der Sammelbienen. *Zeitschrift fur Vergleichende Physiologie*, **34**, pp. 383–393.

Hertel, H. and U. Maronde (1987). Processing of Visual Information in the Honeybee Brain. In Menzel, R. and A. Mercer (eds.) *Neurobiology and Behavior of Honeybees*, pp. 141–157. Springer-Verlag, New York.

Higgins, C. (2004). Non-directional motion may underlie insect behavioral dependence on image speed. *Biological Cybernetics*, **91**(5), pp. 326–332.

Higgins, C., J. Douglass, and N. Strausfeld (2004). The Computational Basis of an Identified Neuronal Circuit for Elementary Motion Detection in Dipterous Insects. *Visual Neuroscience*, **21**(04), pp. 567–586.

Hildreth, E. and C. Koch (1987). The analysis of visual motion: from computational theory to neuronal mechanisms. *Annual Review of Neuroscience*, **10**, pp. 477–533.

Horn, B. and B. Schunck (1981). Determining optical flow. *Artificial Intelligence*, **17**(1-3), pp. 185–203.

Hrncir, M., S. Jarau, R. Zucchi, and F. Barth (2003). A stingless bee (*Melipona seminigra*) uses optic flow to estimate flight distances. *Journal of Comparative Physiology A: Neuroethology, Sensory, Neural, and Behavioral Physiology*, **189**(10), pp. 761–768.

Hubel, D. and M. Livingstone (1987). Segregation of form, color, and stereopsis in primate area 18. *Journal of Neuroscience*, **7**(11), pp. 3378–3415.

Hubel, D. and T. Wiesel (1968). Receptive fields and functional architecture of monkey striate cortex. *The Journal of Physiology*, **195**(1), pp. 215–243.

Ibbotson, M. (2001). Evidence for Velocity-Tuned Motion-Sensitive Descending Neurons in the Honeybee. *Proceedings of the Royal Society of London. Series B, Biological Sciences*, **268**(1482), pp. 2195–2201.

Kaiser, W. and E. Liske (1972). A preliminary report on the analysis of the optomotor system of the bee - behavioral studies with spectral lights. In Werner, R. (ed.) *Information Processing in the Visual Systems of Arthropods*, pp. 163–166. Springer-Verlag, Berlin-Heidelberg-New York.

Kaiser, W. and E. Liske (1974). Die optomotorischen Reaktionen von fixiert fliegenden Bienen bei Reizung mit Spektrallichtern. *Journal of Comparative Physiology A: Neuroethology, Sensory, Neural, and Behavioral Physiology*, **80**, p. 391408.

Katsov, A. and T. Clandinin (2008). Motion Processing Streams in Drosophila Are Behaviorally Specialized. *Neuron*, **59**(2), pp. 322–335. ISSN 0896-6273.

Kirchner, W. and M. Srinivasan (1989). Freely flying honeybees use image motion to estimate object distance. *Naturwissenschaften*, **76**(6), pp. 281–282.

Koch, C. (1999). *Biophysics of Computation: Information Processing in Single Neurons*. Oxford University Press, New York, NY, USA.

Kramer, J. and C. Koch (1997). Pulse-based analog VLSI velocity sensors. *Circuits and Systems II: Analog and Digital Signal Processing, IEEE Transactions on*, **44**(2), pp. 86–101.

Kunze, P. (1961). Untersuchung des Bewegungssehens fixiert fliegender Bienen. *Journal of Comparative Physiology A: Neuroethology, Sensory, Neural, and Behavioral Physiology*, **44**(6), pp. 656–684.

Land, M. (1999). Motion and vision: why animals move their eyes. *Journal of Comparative Physiology A: Neuroethology, Sensory, Neural, and Behavioral Physiology*, **185**(4), pp. 341–352.

Land, M. and T. Collett (1974). Chasing behaviour of houseflies (*Fannia canicularis*). *Journal of Comparative Physiology A: Neuroethology, Sensory, Neural, and Behavioral Physiology*, **89**(4), pp. 331–357.

Land, M. and D. Nilsson (2002). *Animal Eyes*. Oxford University Press, USA.

Laughlin, S. (1984). The roles of parallel channels in early visual processing by the arthropod compound eye. In Ali, M. (ed.) *Photoreception and vision in invertebrates*, pp. 457–482. Plenum, New York.

Laughlin, S. and G. Horridge (1971). Angular sensitivity of the retinula cells of dark-adapted worker bee. *Journal of Comparative Physiology A: Neuroethology, Sensory, Neural, and Behavioral Physiology*, **74**(3), pp. 329–335.

Lehmann, F. and M. Dickinson (1997). The changes in power requirements and muscle efficiency during elevated force production in the fruit fly Drosophila melanogaster. *Journal of Experimental Biology*, **200**(7), pp. 1133–1143.

Lehrer, M. (1998). Looking all around: honeybees use different cues in different eye regions. *Journal of Experimental Biology*, **201**(24), pp. 3275–3292.

Limb, J. and J. Murphy (1975). Estimating the Velocity of Moving Images in Television Signals. *Computer Graphics and Image Processing*, **4**(4), pp. 311–327.

Marr, D. and S. Ullman (1981). Directional Selectivity and its Use in Early Visual Processing. *Proceedings of the Royal Society of London. Series B, Biological Sciences*, **211**(1183), pp. 151–180.

Moore, D. and M. Rankin (1982). Direction-sensitive partitioning of the honeybee optomotor system. *Physiological Entomology*, **7**(1), pp. 25–36.

Moulden, B. and H. Begg (1986). Some tests of the Marr - Ullman model of movement detection. *Perception*, **15**(2), pp. 139–155.

Orban, G., H. Kennedy, and J. Bullier (1986). Velocity sensitivity and direction selectivity of neurons in areas V1 and V2 of the monkey: influence of eccentricity. *Journal of Neurophysiology*, **56**(2), pp. 462–480.

Osborne, J., S. Clark, R. Morris, I. Williams, J. Riley, A. Smith, D. Reynolds, and A. Edwards (1999). A Landscape-Scale Study of Bumble Bee Foraging Range and Constancy, Using Harmonic Radar. *Journal of Applied Ecology*, **36**(4), pp. 519–533.

Osorio, D. and J. Bacon (1994). A good eye for arthropod evolution. *BioEssays*, **16**(6), pp. 419–424.

Pant, V. (2007). *Biomimetic Visual Navigation Architectures for Autonomous Intelligent Systems*. Ph.D. thesis, University of Arizona, Tucson, Arizona.

Paulk, A., A. Dacks, J. Phillips-Portillo, J. Fellous, and W. Gronenberg (2009). Visual Processing in the Central Bee Brain. *Journal of Neuroscience*, **29**(32), pp. 9987–9999.

Paulk, A., J. Phillips-Portillo, A. Dacks, J. Fellous, and W. Gronenberg (2008). The Processing of Color, Motion, and Stimulus Timing Are Anatomically Segregated in the Bumblebee Brain. *Journal of Neuroscience*, **28**(25), pp. 6319–6332.

Paulk, A. C. and W. Gronenberg (2008). Higher order visual input to the mushroom bodies in the bee, Bombus impatiens. *Arthropod Structure & Development*, **37**(6), pp. 443–458.

Pinto, N., D. Cox, and J. DiCarlo (2008). Why is Real-World Visual Object Recognition Hard? *PLoS Computational Biology*, **4**(1), p. e27.

Reichardt, W., T. Poggio, and K. Hausen (1983). Figure-ground discrimination by relative movement in the visual system of the fly. *Biological Cybernetics*, **46**(0), pp. 1–30.

Reiser, M. and M. Dickinson (2008). A modular display system for insect behavioral neuroscience. *Journal of Neuroscience Methods*, **167**(2), pp. 127–139.

Riabinina, O. and A. Philippides (2009). A model of visual detection of angular speed for bees. *Journal of Theoretical Biology*, **257**(1), pp. 61–72.

Ribi, W. (1981). The first optic ganglion of the bee. *Cell and Tissue Research*, **215**(3), pp. 443–464.

Ribi, W. (1987). The structural basis of information processing in the visual system of the bee. In Menzel, R. and A. Mercer (eds.) *Neurobiology and Behavior of Honeybees*, pp. 130–140. Springer-Verlag, New York.

Ribi, W. and M. Scheel (1981). The second and third optic ganglia of the worker bee. *Cell and Tissue Research*, **221**(1), pp. 17–43.

Riehle, A. and N. Franceschini (1984). Motion detection in flies: Parametric control over ON-OFF pathways. *Experimental Brain Research*, **54**(2), pp. 390–394.

Riley, J., U. Greggers, A. Smith, D. Reynolds, and R. Menzel (2005). The flight paths of honeybees recruited by the waggle dance. *Nature*, **435**(7039), pp. 205–207.

Riley, J., D. Reynolds, A. Smith, A. Edwards, J. Osborne, I. Williams, and H. McCartney (1999). Compensation for wind drift by bumble-bees. *Nature*, **400**(6740), p. 126.

Rivera-Alvidrez, Z. (2005). *Computational Modeling of Neurons Involved in Fly Motion Detection*. Master's thesis, University of Arizona, Tucson, Arizona.

Ruffier, F. and N. Franceschini (2005). Optic flow regulation: the key to aircraft automatic guidance. *Robotics and Autonomous Systems*, **50**(4), pp. 177–194.

Schlieper, C. (1928). Über die Helligkeitsverteilung im Spektrum bei verschiedenen Insekten. *Journal of Comparative Physiology A: Neuroethology, Sensory, Neural, and Behavioral Physiology*, **8**(2), pp. 281–288.

Seidl, R. and W. Kaiser (1981). Visual field size, binocular domain and the ommatidial array of the compound eyes in worker honey bees. *Journal of Comparative Physiology A: Neuroethology, Sensory, Neural, and Behavioral Physiology*, **143**(1), pp. 17–26.

Serres, J., G. Masson, F. Ruffier, and N. Franceschini (2008). A bee in the corridor: centering and wall-following. *Naturwissenschaften*, **95**(12), pp. 1181–1187.

Serres, J., F. Ruffier, and N. Franceschini (2006). Two optic flow regulators for speed control and obstacle avoidance. In *Biomedical Robotics and Biomechatronics, 2006. BioRob 2006. The First IEEE/RAS-EMBS International Conference on*, pp. 750–757.

Si, A., M. Srinivasan, and S. Zhang (2003). Honeybee navigation: properties of the visually driven 'odometer'. *Journal of Experimental Biology*, **206**(8), pp. 1265–1273.

Souza, J., H. H., V. Ventura, and R. Menzel (1992). Response properties of stained monopolar cells in the honeybee lamina. *Journal of Comparative Physiology A: Neuroethology, Sensory, Neural, and Behavioral Physiology*, **170**(3), pp. 267–274.

Spaethe, J. and L. Chittka (2003). Interindividual variation of eye optics and single object resolution in bumblebees. *Journal of Experimental Biology*, **206**(19), pp. 3447–3453.

Srinivasan, M. (1994). An image-interpolation technique for the computation of optic flow and egomotion. *Biological Cybernetics*, **71**(5), pp. 401–415.

Srinivasan, M., M. Lehrer, W. Kirchner, and S. Zhang (1991). Range perception through apparent image speed in freely flying honeybees. *Visual Neuroscience*, **6**(5), pp. 519–535.

Srinivasan, M., M. Lehrer, S. Zhang, and G. Horridge (1989). How honeybees measure their distance from objects of unknown size. *Journal of Comparative Physiology A: Neuroethology, Sensory, Neural, and Behavioral Physiology*, **165**(5), pp. 605–613.

Srinivasan, M., R. Pinter, and D. Osorio (1990). Matched Filtering in the Visual System of the Fly: Large Monopolar Cells of the Lamina are Optimized to Detect Moving Edges and Blobs. *Proceedings of the Royal Society of London. Series B, Biological Sciences*, **240**(1298), pp. 279–293.

Srinivasan, M., M. Poteser, and K. Kral (1999a). Motion detection in insect orientation and navigation. *Vision Research*, **39**(16), pp. 2749–2766.

Srinivasan, M. and S. Zhang (1997). Visual control of honeybee flight. In Lehrer, M. (ed.) *Communication in Arthropods*, volume 84, pp. 95–113. Birkhäuser Basel, 1 edition.

Srinivasan, M. and S. Zhang (2004). Visual motor computations in insects. *Annual Review of Neuroscience*, **27**, pp. 679–696.

Srinivasan, M., S. Zhang, M. Altwein, and J. Tautz (2000a). Honeybee Navigation: Nature and Calibration of the "Odometer". *Science*, **287**(5454), pp. 851–853.

Srinivasan, M., S. Zhang, J. Berry, K. Cheng, and H. Zhu (1999b). Honeybee navigation: linear perception of short distances travelled. *Journal of Comparative Physiology A: Neuroethology, Sensory, Neural, and Behavioral Physiology*, **185**(3), pp. 239–245.

Srinivasan, M., S. Zhang, and N. Bidwell (1997). Visually mediated odometry in honeybees. *Journal of Experimental Biology*, **200**(19), pp. 2513–2522.

Srinivasan, M., S. Zhang, and J. Chahl (2001). Landing Strategies in Honeybees, and Possible Applications to Autonomous Airborne Vehicles. *Biological Bulletin*, **200**(2), pp. 216–221.

Srinivasan, M., S. Zhang, J. Chahl, E. Barth, and S. Venkatesh (2000b). How honeybees make grazing landings on flat surfaces. *Biological Cybernetics*, **83**(3), pp. 171–183.

Srinivasan, M., S. Zhang, and K. Chandrashekara (1993). Evidence for two distinct movement-detecting mechanisms in insect vision. *Naturwissenschaften*, **80**, pp. 38–41.

Srinivasan, M., S. Zhang, and M. Lehrer (1998). Honeybee navigation: odometry with monocular input. *Animal Behaviour*, **56**, pp. 1245–1259.

Srinivasan, M., S. Zhang, M. Lehrer, and T. Collett (1996). Honeybee navigation en route to the goal: visual flight control and odometry. *Journal of Experimental Biology*, **199**(1), pp. 237–244.

Strausfeld, N. (1976). *Atlas of an Insect Brain*. Springer, Berlin.

Strausfeld, N. and J. Campos-Ortega (1973). The L4 monopolar neurone: a substrate for lateral interaction in the visual system of the flymusca domestica (L). *Brain Research*, **59**, pp. 97–117.

Strausfeld, N. J. and V. Braitenberg (1970). The compound eye of the fly (*Musca domestica*): connections between the cartridges of the lamina ganglionaris. *Journal of Comparative Physiology A: Neuroethology, Sensory, Neural, and Behavioral Physiology*, **70**(2), pp. 95–104.

Strauss, R., S. Schuster, and K. Götz (1997). Processing of artificial visual feedback in the walking fruit fly Drosophila melanogaster. *Journal of Experimental Biology*, **200**(9), pp. 1281–1296.

Tammero, L., M. Frye, and M. Dickinson (2004). Spatial organization of visuomotor reflexes in Drosophila. *Journal of Experimental Biology*, **207**(1), pp. 113–122.

Tautz, J., S. Zhang, J. Spaethe, A. Brockmann, A. Si, and M. Srinivasan (2004). Honeybee Odometry: Performance in Varying Natural Terrain. *PLoS Biology*, **2**(7), p. e211.

Torre, V. and T. Poggio (1978). A Synaptic Mechanism Possibly Underlying Directional Selectivity to Motion. *Proceedings of the Royal Society of London. Series B, Biological Sciences*, **202**(1148), pp. 409–416.

Ugolini, A. (1987). Visual information acquired during displacement and initial orientation in Polistes gallicus (L.) (Hymenoptera, Vespidae). *Animal Behaviour*, **35**(2), pp. 590–595.

van der Schaaf, A. and J. van Hateren (1996). Modelling the power spectra of natural images: Statistics and information. *Vision Research*, **36**(17), pp. 2759–2770.

van Santen, J. and G. Sperling (1984). Temporal covariance model of human motion perception. *Journal of the Optical Society of America A*, **1**(5), pp. 451–473.

van Santen, J. and G. Sperling (1985). Elaborated Reichardt detectors. *Journal of the Optical Society of America A*, **2**(2), pp. 300–320.

von Frisch, K. (1993). *The Dance Language and Orientation of Bees*. Harvard Univesity Press, Cambridge, MA.

Wenner, A. (1963). The flight speed of honeybees: a quantitative approach. *Journal of Apicultural Research*, **2**, pp. 25–32.

Wolf, R. and M. Heisenberg (1986). Visual orientation in motion-blind flies is an operant behaviour. *Nature*, **323**(6084), pp. 154–156.

Zanker, J., M. Srinivasan, and M. Egelhaaf (1999). Speed tuning in elementary motion detectors of the correlation type. *Biological Cybernetics*, **80**(2), pp. 109–116.

APPENDIX A

Non-directional motion detectors can be used to mimic optic flow dependent behaviors

Jonathan P. Dyhr and Charles M. Higgins

In preparation for submission to

Biological Cybernetics

Biological Cybernetics manuscript No.
(will be inserted by the editor)

Non-directional motion detectors can be used to mimic optic flow dependent behaviors

Jonathan P. Dyhr[1] and Charles M. Higgins[2,3]

[1]Graduate Program in Neuroscience

[2]Department of Neuroscience

[3]Department of Electrical and Computer Engineering

The University of Arizona

1040 E. 4th Street

Tucson, Arizona 85721-0077

USA

The date of receipt and acceptance will be inserted by the editor

Abstract Insect navigational behaviors including obstacle avoidance, grazing landings and visual odometry are dependent on the ability to estimate flight speed based only on visual cues. In honeybees, this visual estimate of speed is largely independent of both the direction of motion and the spatial frequency content of the image. Electrophysiological recordings from the motion-sensitive cells believed to underlie these behaviors have long supported spatio-temporally tuned correlation-type models of visual motion detection whose speed tuning changes as the spatial frequency of a stimulus is varied. The result is an apparent conflict between behavioral experiments and the electrophysiological and modeling data. In this paper we demonstrate that conventional correlation-type models are sufficient to reproduce some of the speed dependent behaviors observed in honeybees when square wave gratings are used, contrary to the theoretical predictions. However, these models fail to match the behavioral observations for sinusoidal stimuli. Instead, we show that non-directional motion detectors, which underlie the correlation-based computation of directional motion, can be used to mimic these same behaviors even when narrowband gratings are used. The existence of such non-directional motion detectors is supported both anatomically and electrophysiologically, and they have been hypothesized to be critical in the Dipteran elementary motion detector (EMD) circuit.

Correspondence to: Jonathan P. Dyhr, jdyhr@email.arizona.edu

1 Introduction

The pioneering work of Karl von Frisch demonstrated that honeybees communicate the location of a distant food source to other honeybees in the hive via the 'waggle dance' (reviewed in von Frisch, 1993). The underlying estimate of distance was later shown to be the result of a visual 'odometer' that integrates the apparent speed of the visual scene during flight (Esch *et al.*, 2001). Since then, many other behaviors have been shown to be dependent on visual estimates of speed (reviewed in Srinivasan and Zhang, 2004). Among these behaviors is the *centering response*, in which a honeybee matches the apparent image speed on each eye to center its flight path through a tunnel lined with sinusoidal or square wave patterns on the left and right walls (Kirchner and Srinivasan, 1989). The reliability of the waggle dance and the centering response as behavioral measures have revealed a number of interesting properties of the underlying neural mechanisms.

Studies of the centering response by Srinivasan and Zhang (1993) suggested that the speed of the visual scene is estimated by a small field mechanism that is insensitive to the direction of visual motion. In these experiments, a small section of the tunnel walls was replaced on one side with a computer monitor displaying a moving grating pattern, and on the other side with a transparent cover to allow for the measurement of the vertical flight path. Because the transparent section of the wall was left empty, honeybees trained to fly through this tunnel demonstrated a characteristic 'movement avoidance' response away from the computer screen and towards the empty wall. The magnitude of the response was dependent on the speed of the moving pattern. The lateral component of this response could be modulated by motion in both the horizontal and vertical directions, suggesting that the mechanism responsible for the centering response was non-directional. The authors then presented a grating stimulus with interleaved rows moving in opposite directions such that the average speed of the entire pattern was zero. The magnitude of the movement avoidance response to this stimulus was equal to that of a single grating moving at the same speed, contrary to what one would expect from a wide-field, directionally selective mechanism, indicating an underlying small-field mechanism. Further work by Dacke and Srinivasan (2007) demonstrated that both the vertical and the horizontal speed of the visual image contribute to the distance estimates of honeybees during foraging flights, necessitating a sensor that can measure speed in multiple directions.

Additional studies have demonstrated that the estimate of speed is largely independent of both spatial frequency and contrast of the patterns lining the tunnel walls (Srinivasan *et al.*, 1996; Si *et al.*, 2003). Centering studies have demonstrated that honeybees will fly through the center of a tunnel despite four-fold differences between the walls in the spatial frequency of a square wave pattern and two-fold differences between sinusoidal patterns (Srinivasan *et al.*, 1991). These conclusions are supported by studies of the visual odometer, which have shown that honeybees will judge similar travel distances despite four-fold differences in the spatial frequency of square wave (Srinivasan *et al.*, 1996) or sinusoidal (Si *et al.*, 2003) patterns lining the tunnel walls.

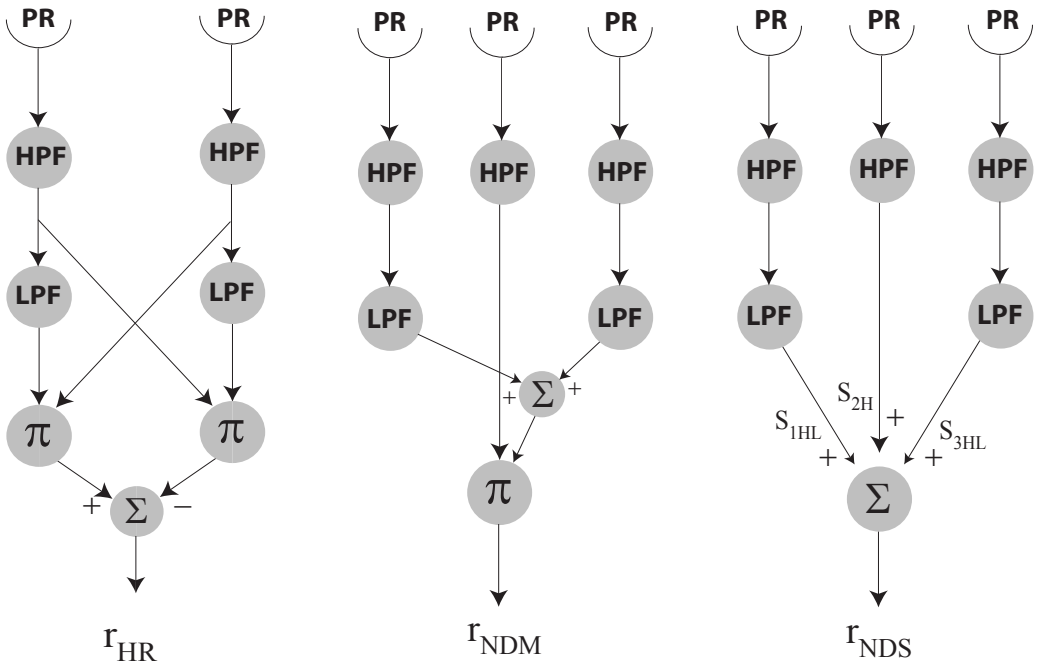

Fig. 1 Computational Models of Motion Detection. Photoreceptor outputs (PR) are operated on by high-pass (HPF) and low-pass (LPF) filters. Different combinations of the filtered outputs can then be summed (Σ) and/or multiplied (π) to yield motion sensitive outputs. (a) The Hassenstein-Reichardt (HR) model generates a directionally selective motion signal via the subtraction of two overlaid mirror-symmetrical subunits. Each subunit is composed of two spatially offset, high-pass filtered photoreceptor channels, one of which is also low-pass filtered. (b) The Non-Directional Multiplication (NDM) model is composed of three spatially offset, high-pass filtered photoreceptor channels. In addition, the lateral channels are low-pass filtered and summed. The outputs of the central channel and the summed channels are then multiplied to yield a motion sensitive output. (c) The Non-Directional Summation (NDS) model is identical to the NDM model except the that final multiplication step is replaced by a summation. As a consequence, the NDS model is completely linear.

Despite all this detailed behavioral information, we still have a poor understanding of how the brain processes visual information to yield an estimate of speed. Part of the problem lies in the apparent mechanism by which biological systems extract motion information from the intensity fluctuations detected by the photoreceptors. There is strong evidence that biological motion detectors function by correlating the time-delayed outputs of adjacent photoreceptors (reviewed in Borst and Egelhaaf, 1989). The outputs of these detectors, while motion sensitive, are generally dependent on the spatial and temporal frequency of the stimulus. This means that the speed tuning of these models to a narrowband (sinusoidal) stimulus will be different at each spatial frequency, making it difficult to estimate speed based solely on their outputs. Such

is the case for the canonical model of motion detection in insects, the Hassenstein-Reichardt (HR) model (Figure 1a; Hassenstein and Reichardt, 1956; van Santen and Sperling, 1985).

This conflict between modeling and behavior can be reconciled by analyzing the neuronal circuit that produces the HR-like outputs of cells in the insect brain. In the neuronally-based model of the fly elementary motion detector (EMD) developed by Higgins *et al.* (2004), whose final output is comparable to that of the HR model, the authors noted that 'non-directional motion' is computed prior to the final output of the putative dipteran EMD circuit. We define a non-directional motion detector as responding preferentially to motion over flicker but showing no preference for a direction of motion. One such non-directional motion detector was shown to have speed-tuned responses relatively independent of spatial frequency (Higgins, 2004). This model, which we will refer to as the non-directional multiplication (NDM) model (Figure 1b), exhibits a mean response proportional to the speed of an image and is relatively insensitive to the spatial frequency of a stimulus.

Further work by Rivera-Alvidrez (2005) investigating the EMD circuit yielded a more anatomically plausible non-directional model that we refer to as the non-directional summation (NDS) model (Figure 1c). The NDS model is completely linear and has an *amplitude* response that is proportional to speed. Support for such non-directional models comes from anatomical studies of the early visual pathways of the fly, electrophysiological recordings from the Tm1 cell (Douglass and Strausfeld, 1995), and modeling work on the EMD circuit (Higgins *et al.*, 2004).

In order to reconcile the hypothesized physiological mechanisms of motion detection with the behavioral properties of visual speed estimation, we demonstrate how the NDS and NDM models can be used to mimic the real world behaviors seen in honeybees using a relatively simple computational framework. Since it has not been previously presented in the literature, we also elaborate on the response properties of the NDS model.

2 Methods

All numerical calculations and simulations were carried out in the *Matlab* package (The Mathworks, Natick, MA). A one-dimensional time-varying sinusoidal input with contrast C, temporal frequency ω_t and spatial frequency ω_x was used for numerical evaluations of the models and can be written as

$$S(x,t) = \frac{1}{2} \cdot (1 + C \cdot \sin(\omega_x \cdot x + \omega_t \cdot t)) \tag{1}$$

Note that the speed of the sinusoidal stimulus, $v = \frac{\omega_t}{\omega_x}$, is dependent on both the temporal and spatial frequencies. To represent luminance, this sinusoid is offset such that it never reaches negative values.

A contrast-reversing sinusoid, used to investigate the flicker response of the NDS model, can be expressed as

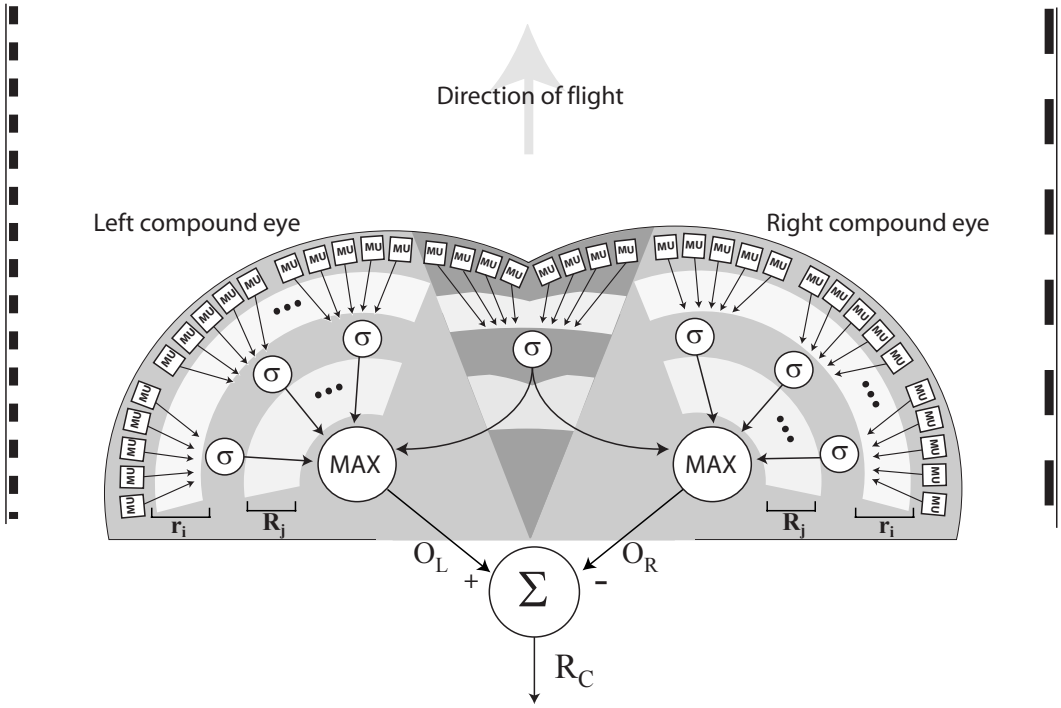

Fig. 2 Diagram of the behavioral simulation setup. The walls of the arena are denoted by the dashed lines. The eyes are composed of two slightly overlapping semicircular arrays of Motion Units (MU). The shaded region in the center delineates the binocular overlap zone, composed of eight overlapping photoreceptors. Adjacent MUs were grouped into subfields and their outputs, r_i, were averaged (σ). The maximal response from the subfield outputs (R_j) of each eye were used as the global speed estimates for each eye (O_L and O_R). The final outputs from each eye were then subtracted (Σ) to yield a turn command (R_C).

$$S_C(x,t) = \frac{1}{2} \cdot (1 + C \cdot \sin(\omega_x \cdot x) \cdot \sin(\omega_f \cdot t)) \tag{2}$$

where ω_f is the temporal frequency of the contrast reversals.

The temporal filters used were all first-order linear filters with time constants of $\tau_1 = 2\ ms$ for the high-pass filters, matching the physiological data for high-pass filtering in the early visual pathways (Juusola *et al.*, 1991), and $\tau_2 = 50\ ms$ for the low-pass filters matching the value used by Higgins (2004). The magnitude responses of the high-pass filters h_1 and low-pass filters h_2 can be expressed as

$$h_1(\omega_t) = \frac{\omega_t \cdot \tau_1}{\sqrt{1 + (\omega_t \cdot \tau_1)^2}} \tag{3}$$

$$h_2(\omega_t) = \frac{1}{\sqrt{1 + (\omega_t \cdot \tau_2)^2}} \tag{4}$$

The phase shift resulting from the application of the high-pass filters was identical for all pathways and can thus be ignored. In contrast, the selective application of the low-pass filter added a phase term ϕ_2 that can be expressed as

$$\phi_2(\omega_t) = -tan^{-1}(\omega_t \cdot \tau) \tag{5}$$

With no loss of generality, the spacing between photoreceptors was set to one. The relative phase between sinusoidal inputs at neighboring photoreceptors was then $\phi_x = \omega_x$.

For the behavioral simulations, the eyes of the honeybee were composed of two semicircular arrays containing a total of 90 photoreceptors (Figure 2). The visual field of the the bee, spanning 180°, was synthesized at high resolution and then downsampled by a factor of 10 to smooth the sharp edges in the image that would otherwise create discontinuities in the motion detector responses. The visual field was then divided into pixels such that each photoreceptor (PR) had an angular spacing of approximately 2° in agreement with studies in honeybees (Seidl and Kaiser, 1981). The outputs of the eight central photoreceptors were shared by both eyes in order to mimic the binocular overlap zone in both flies (Beersma *et al.*, 1977) and bees (Seidl and Kaiser, 1981). The PR outputs were processed by Motion Units (MU) with receptive fields either two (HR) or three (NDM and NDS) pixels wide. Sequential MUs were offset by a single pixel so that each eye contained either 48 (HR) or 47 (NDM and NDS) units. The angle of the head of the simulated bee was held fixed, looking in the forward direction to prevent rotation of the visual field in agreement with studies in flies showing that the head angle is held constant during translational flight (van Hateren and Schilstra, 1999).

Our method for deriving a global estimate of speed for each eye, the reasoning for which will be detailed in the Results section, was as follows. MUs were first subdivided into five non-overlapping subfields, such that each subfield spanned approximately 18° (Srinivasan and Zhang, 1993). With the exception of the two most central subfields, each contained nine adjacent MUs whose responses (r_i) were averaged (σ) to determine the subfield response (R_j). The maximal response from the subfield outputs of each eye were used as the global speed estimates for each eye (O_L and O_R). These outputs were subtracted to yield a turn command (R_C). The turn command was then multiplied by a gain scale factor (g) to specify an angular velocity ($\dot{\theta}$). The maximum magnitude of the angular velocity was limited to $45^o/s$; in addition to better mimicking gradual, real-world flight paths of honeybees, this limit also prevented the simulations from becoming unstable.

For a simulated bee traveling at fixed speed v_b, the x and y positions and angular orientation of the body θ at each time step t were specified by the equations:

$$\dot{\theta}(t) = g \cdot R_C(t) \tag{6}$$

$$\theta(t) = \theta(t-1) + \dot{\theta}(t) \cdot \Delta t \tag{7}$$

$$x(t) = x(t-1) + v_b \cdot \cos\theta(t) \cdot \Delta t \tag{8}$$

$$y(t) = y(t-1) + v_b \cdot \sin\theta(t) \cdot \Delta t \tag{9}$$

The simulated bee navigated through an arena of length 400 cm and width 12 cm (Figure 3) at speeds ranging from 30 - 50 cm/s to match real world experimental conditions (Srinivasan *et al.*, 1991). To avoid discontinuities at the beginning and end of the tunnel, simulation runs were limited to the middle 200 cm of the arena as denoted by the dashed black lines in Figure 3. During the first twenty time steps, the angular velocity of the bee was held at zero in order to ignore startup transients from the temporal filters. Simulations were stopped when the bee traveled 200 cm along the length of the tunnel or upon contact with one of the walls.

Two different types of arenas were used for the behavioral simulation experiments. The first arena was composed of rows of objects that were projected into the visual field of the simulated bee such that their size in the visual field varied inversely with their distance from the bee. Spatial frequency was varied by changing the number of objects on each wall. The brightness (or relative contrast) of each object in the visual field was equal to $1/(1 + d/d_{half})$ where d was the distance of the object from the center of the tunnel and d_{half} was the distance at half contrast. Because honeybees normally fly in bright sunlight we chose a relatively large value of 600 cm for d_{half}.

To better test the narrowband spatial frequency dependence of the models in behavioral simulations we used a second method to construct the visual field in which periodic sinusoidal or square wave patterns f with contrast $C = 1$ were projected onto the eye of the simulated bee using the following equation

$$I(\phi) = B \cdot (1 + C \cdot f(\frac{2\pi \cdot \omega_x \cdot (D + x)}{\tan(\phi)})) \tag{10}$$

Where B was a constant factor specifying the background illumination, x was the lateral position of the bee in the tunnel, D was the half-width of the tunnel and ϕ was the viewing angle of the photoreceptor.

Multiple simulations with different starting positions and flight speeds (v_b) were performed for each experimental condition. The starting position varied between x positions of 1.4-12.6 cm and the flight speed v_b between 30-50 cm/s. Trials in which the bee passed through one of the walls were counted as failures. For each successful simulation run, the mean distance of the bee from the center of the arena ($\overline{x}$) along the

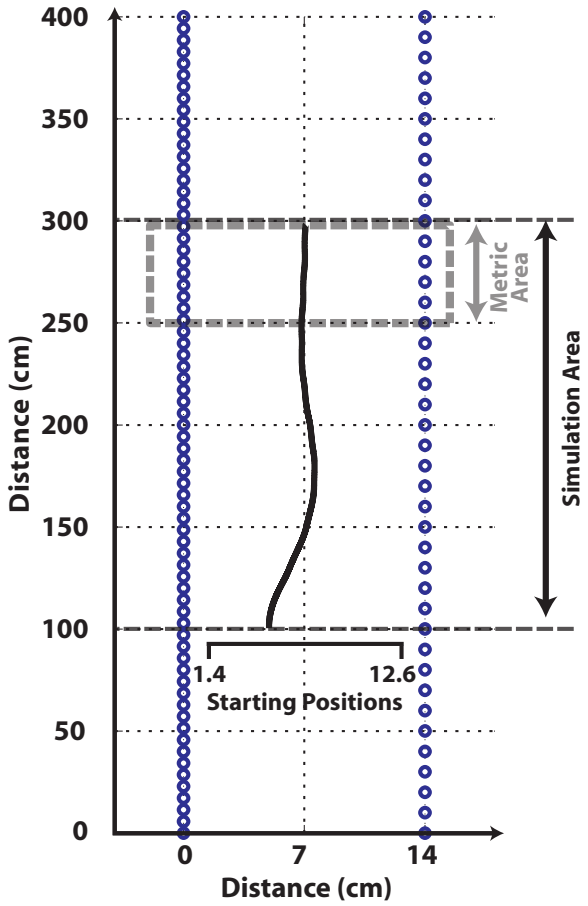

Fig. 3 Behavioral simulation arena. Black circles denote the 400 cm long tunnel walls that were composed of columns of equally spaced objects or the lateral distance of a grating pattern that was projected onto the eyes of the simulated bee. The width of the tunnel was 12 cm. The dashed black lines delineate the 200 cm long section of the arena in which simulations were run. The dashed gray box indicates the 50 cm length of the tunnel where the performance metric was calculated. The labeled bracket indicates the range of starting positions used for simulations runs. The solid black line is an example path of a simulated bee and is included for illustration.

final one quarter length of the tunnel (dashed gray box, Figure 3) was used as a performance metric. This metric was chosen because it measured the average lateral position of the bee during steady-state flight, providing information about any biases in the path while ignoring initial transient maneuvering. To measure the overall performance of the bee for each experimental condition, we calculated the mean and standard deviation of $\overline{x}$ across successful trials.

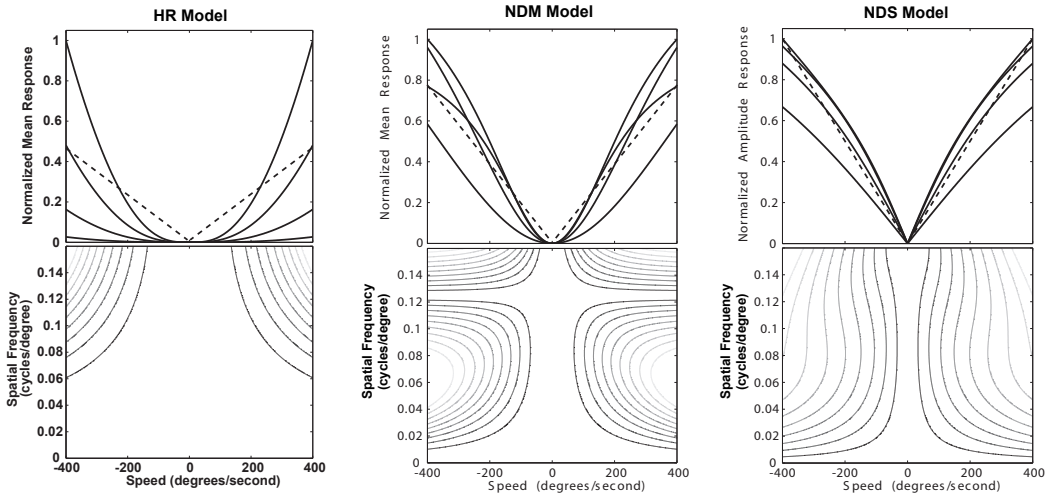

(a) (b) (c)

Fig. 4 Model speed tuning. (a) *Top*: The normalized, rectified response of the HR model (Equation 11). Solid lines indicate model responses to sinusoidal gratings of 0.03 (minimum peak response), 0.05, 0.07 and 0.09 (maximum peak response) cycles per degree. Centering experiments in honeybees have used sinusoidal gratings with frequencies of 0.017, 0.038 and 0.07 cycles per degree and square wave gratings ranging from 0.01 to 0.04 cycles per degree (Srinivasan *et al.*, 1991). The dashed line is representative of a linear speed response. *Bottom*: Contour plot demonstrating the variation of the rectified HR model response relative to speed and spatial frequency. Darker lines represent stronger model responses. Vertical lines would indicate spatial frequency independent response to speed. (b) *Top*: Normalized response of the NDM model (Equation 12) plotted against speed. Solid lines denote responses at spatial frequencies of 0.03 (maximum peak response), 0.05, 0.07 and 0.09 (minimum peak response) cycles per degree. Note the reversal of maximal and minimal peak responses relative to the rectified HR model. *Bottom*: Contour plot of NDM model response relative to speed and spatial frequency. (c) *Top*: Normalized and rectified NDS model response plotted against speed. Solid lines denote responses at spatial frequencies of 0.03 (maximum peak response), 0.05, 0.07 and 0.09 (minimum peak response) cycles per degree. *Bottom*: Contour plot of NDS model response relative to speed and spatial frequency.

3 Results

Speed responses of the three motion sensitive models shown in Figure 1, the HR, the NDM and the NDS models, were tested and compared in theoretical and behavioral simulation frameworks.

3.1 Theoretical Speed Tuning

The version of the HR model used for our simulations is shown in Figure 1a. The outputs of two spatially separated photoreceptors are first temporally high-pass filtered to removed sustained illumination compo-

nents. Next, one of the outputs is low-pass filtered, adding a differential phase delay, and multiplied with the undelayed output. This operation is repeated in a mirror-symmetrical fashion after which the processed outputs are subtracted from each other to yield a directionally-selective response. The time-averaged output of the HR model in response to a sinusoidal stimulus (Equation 1), as derived in Higgins (2004), is

$$\bar{O}_{HR} = \frac{C^2}{4} \cdot \frac{(\omega_t \cdot \tau_1)^2}{(1 + (\omega_t \cdot \tau_1)^2)} \cdot \frac{(\omega_t \cdot \tau_2)}{(1 + (\omega_t \cdot \tau_2)^2)} \cdot \sin(\omega_x) \tag{11}$$

Because of the ω_t^3 term in this expression, the sign of the HR response will change with the direction of motion. We were only interested in the speed estimate of the model so we used the absolute value of this mean response to represent the speed estimate of the model.

The mean responses of the HR model to sinusoidal gratings of different spatial frequencies moving at different speeds are plotted in Figure 4a (top). The mean response of the HR model increases hyperbolically with speed. The magnitude of the responses changes dramatically as the spatial frequency is varied. This dependence on spatial frequency can be seen more clearly in the contour plot (Figure 4a, bottom) where vertical contour lines would indicate a speed tuning independent of spatial frequency. The lack of vertical lines in the plot demonstrate that the HR model is not speed-tuned in the range of image speed typically seen during flight.

Using the mean response of the HR model as a benchmark, we can compare the motion responses of the two non-directional models beginning with the NDM model (Figure 1b). As derived by Higgins (2004), the time-averaged response of the NDM model to a sinusoidal input (Equation 1) is

$$\bar{O}_{NDM} = \frac{C^2}{4} \cdot \frac{(\omega_t \cdot \tau_1)^2}{(1 + (\omega_t \cdot \tau_1)^2) \cdot (1 + (\omega_t \cdot \tau_2)^2)} \cdot \cos(\omega_x) \tag{12}$$

A plot of NDM model mean responses to sinusoids of different spatial frequencies moving at different speeds is shown in Figure 4b (top). Unlike the HR model, the response of the NDM model increases approximately linearly with speed and shows much less spatial frequency dependence. The contour plot (Figure 4b, bottom) provides a better visualization of how this proportional response to speed changes with spatial frequency. Compared to the HR model, the NDM model is speed-tuned at a broader range of speeds and at lower spatial frequencies.

An alternative non-directional model, the NDS model, was proposed by Rivera-Alvidrez (2005) after working on a neuronally based model of elementary motion detection (Higgins *et al.*, 2004). The NDS and NDM models differ only in the final step: the final multiplication of the NDM model is replaced by a summation (Figure 1). The ramifications of the change are dramatic, both in terms of the ease of neuronal implementation and in the response properties of the model.

To show this, we begin with the same sinusoidal stimulus (Equation 1) used for the previous derivations. The overall model response is simply the sum of the filtered photoreceptor outputs marked S_{1HL}, S_{2H} and

S_{3HL} in Figure 1c. Assuming, without loss of generality, that the absolute phase difference between the stimulus and the left-most photoreceptor is zero, the filtered outputs can be written as follows:

$$S_{1HL} = \frac{C}{2} \cdot h_1 \cdot h_2 \cdot sin(\omega_t \cdot \tau + \phi_2) \tag{13}$$

$$S_{2H} = \frac{C}{2} \cdot h_1 \cdot sin(\omega_t \cdot \tau + \phi_x) \tag{14}$$

$$S_{3HL} = \frac{C}{2} \cdot h_1 \cdot h_2 \cdot sin(\omega_t \cdot \tau + \phi_2 + 2 \cdot \phi_x) \tag{15}$$

The amplitude response for the NDS model can then be expressed as

$$A_{NDS} = \frac{C}{2} \cdot h_1 \cdot \sqrt{4 \cdot h_2 \cdot [(h_2 \cdot cos^2(\omega_x) + cos(\omega_x) + cos(\phi_2)] + 1} \tag{16}$$

Substituting in equations 3, 4 and 5 then yields the equation:

$$A_{NDS} = \frac{C}{2} \cdot \frac{\omega_t \cdot \tau_1}{\sqrt{1 + (\omega_t \cdot \tau_1)} \cdot \sqrt{1 + (\omega_t \cdot \tau_2)}} \cdot \sqrt{[2 \cdot \cos(\omega_x) + 1]^2 + (\omega_t \cdot \tau)^2} \tag{17}$$

Note that this is the amplitude, as opposed to the mean, response of the model. Because it is linear, the mean response of the NDS model over one cycle of a sinusoid is equal to zero. The amplitude response of the NDS model increases proportionally to speed much like the mean response of the NDM model (Figure 4c). Combined with the weak spatial frequency tuning of the model at lower speeds (Figure 4c, bottom), the NDS model can be used as a very effective speed estimator.

The NDS model also responds more strongly to motion than to flicker. Using Equation 2 (counter phase flicker) as input, the response of the NDS model can be shown to be

$$A_{NDS_{CF}} = \frac{C}{2} \cdot h_1 \cdot \sin(\omega_x \cdot (p_0 + 1)) \sqrt{4 \cdot h_2 \cdot [(h_2 \cdot cos^2(\omega_x) + cos(\omega_x) + cos(\phi_2)] + 1} \tag{18}$$

where p_0 indicates the angular position, in degrees, of the leftmost photoreceptor relative a sinusoidal grating fixed in space. This is identical to Equation 16 except for the additional $\sin(\omega_x \cdot (p_0 + 1))$ term that has a maximum value of one. Thus, the average response to flicker is less than that to motion, but the responses can be equal depending on the spatial position of the grating.

3.2 Behavioral Simulations

Next, we wanted to test the extent to which the theoretical differences between the models would be reflected in a behavioral setting. To this end, we implemented all three models in a behavioral simulation framework (Figure 2) and compared their efficacy for mimicking centering behaviors.

As derived previously, the raw outputs from the individual models are not themselves speed-tuned, but rather are speed dependent in either their mean or amplitude responses. Rather than taking an explicit temporal mean of model outputs, we approximate a temporal mean by averaging spatially (discussed further below). Since we use the absolute mean response of the HR model to represent its speed estimate, we take the absolute value of the spatially averaged HR outputs. The NDM model, which represents speed in its mean response with a strictly positive signal, requires only spatial averaging. To extract a speed estimate from the NDS model, which represents speed in its *amplitude*, we took the absolute value of individual NDS model outputs prior to spatial averaging. Because the temporal mean of a rectified sinusoid with amplitude A is $\frac{2 \cdot A}{\pi}$, this makes the signal linearly proportional to the amplitude of NDS outputs, and thus proportional to speed.

A key component of the behavioral simulation setup was acquiring a global estimate of speed from the arrays of small field MUs making up each eye. We tested a number of different methods for spatial collation of the individual model responses including: straight and weighted averages of the model responses; taking the maximal response from each eye; taking a weighted average of the maximal responses from each eye; and finally, taking the maximum subfield response as described in the Methods section.

The maximal subfield collation proved advantageous for a number of reasons. First, the straight and weighted averaging functions consistently failed because they were inherently dependent on the overall illumination; whichever wall had more objects naturally provided a stronger average signal. On the other hand, methods using the maximal MU response from each eye had dramatic fluctuations in value at each time step. The fluctuation in the responses between the eyes resulted in very jittery, oscillatory paths unless the gain scale factor was set extremely low. However, lowering the gain scale factor hampered the ability of the simulated bee to respond to high speeds and increased the number of failed simulation runs. Taking a weighted average of the maximal responses addressed this problem, but did not improve the performance beyond that of the maximal subfield method.

A major advantage of the maximal subfield method was that it approximated a temporal average. If the same periodic stimulus is seen by all the MUs then a spatial average is the same as a temporal average as long as multiple periods are present within a fixed subfield. Thus, averaging within the same periodic by taking the spatial average of adjacent MUs we approximated a temporal average. Assuming a constant speed, the approximation holds in the limit of higher spatial frequencies or increasing subfield size. As the spatial frequency of a sinusoid increases, a larger number of cycles will be averaged within each visual subfield,

giving a more accurate estimate of the mean response. As the spatial frequency decreases, the spatial period will eventually exceed the size of the subfield, giving a partial average. In our simulations each subfield covered approximately 18 ° so that this only became a problem when the bee was extremely close to a wall, thereby greatly decreasing the apparent spatial frequency of the wall. However, one faces a similar challenge in using a temporal average. As the spatial frequency increases, one needs to average over a longer period of time in order to get an accurate estimate of the mean response. While spatially averaging the MU responses was an imperfect approximation of the mean response, it was generally accurate and had the advantage of giving an instantaneous estimate of speed.

We were most interested in testing the spatial frequency dependence of the different models in centering simulations. Behavioral experiments have shown that bees are capable of visually estimating speed despite four-fold differences in the spatial frequency of square wave grating patterns (Srinivasan *et al.*, 1991). Our first set of simulation experiments used evenly spaced point objects to approximate square wave gratings. The number of objects on one wall was varied such that the approximate spatial frequencies ranged from 0.1 to 0.4 cycles/cm. The spatial frequency of the opposite wall was held constant at either 0.2 or 0.1 cycles/cm. Multiple trials at different speeds and starting positions were run for each set of spatial frequencies and the results are presented in Figure 5a.

As can be seen, all of the models showed some dependence on spatial frequency by tending towards the lower spatial frequency wall. This dependence was small when the spatial frequency of one wall was held constant at 0.2 cycles/cm, with the largest deviation being 1.5 cm from the center of the tunnel. The simulated bee displayed significantly larger deviations from the center of the tunnel when a constant spatial frequency of 0.1 cycles/cm was used. However, even in this case the bee did not range more that 2.5 cm from the center of the tunnel. On average the HR model displayed the least dependence on spatial frequency while the NDM model outperformed the other two models when the average spatial frequency was high. The NDS model was the most dependent on spatial frequency, the opposite of what one would have predicted based on the analytically derived responses. None of the results changed significantly with flight speed.

Because of these unexpected results we modified our simulations so that we could present narrowband stimuli. Using this second method, we performed the same set of experiments with true square wave gratings (Figure 5b). The most notable difference is the inversion of the path bias for the NDM model. While in the previous simulations the NDM model caused the bee to fly closer to the low frequency wall, the bee instead approached the higher frequency wall. In addition, the NDM model deviated further from the center of the tunnel, especially at high spatial frequencies. While the polarity of the HR and NDS model responses remained the same the relative efficacy of the two models was reversed, with the NDS performing better than the HR model. All of the models showed significantly less variability between trials when true square wave gratings were used.

When sinusoidal patterns were used to line the tunnel walls (Figure 5c) there were again dramatic changes in model performance. The HR model proved incapable of successfully navigating the tunnel except when the spatial frequencies of the sinusoidal gratings were the same, and even then only when the simulations were started from the center of the tunnel (data not shown). In contrast, the non-directional models successfully navigated the length of the tunnel, although they showed larger deviations from the center than observed previously. The direction of the NDM model response reverted to that observed when point objects were used, with the simulated bee approaching the lower frequency wall. When the NDS model was used the lateral position of the bee changed approximately linearly with spatial frequency and the variation across trials was much larger than with square wave gratings. These results qualitatively match those of Srinivasan *et al.* (1991) who found that the lateral flight paths of honeybees are more sensitive to narrowband stimuli, such that they are biased by two-fold differences in the spatial frequency of sinusoidal patterns versus four-fold differences between square wave gratings.

Our second set of simulation experiments tested the efficacy of each model for accurately measuring the speed of a moving wall. These experiments were based on those of Srinivasan *et al.* (1991) in which the lateral position of the honeybees' flight path through a tunnel was biased by moving one of the tunnel walls. Moving the wall in the direction of flight (positive wall speed) reduced the apparent speed of the wall, and resulted in the honeybee flying closer to the moving wall. The opposite was also true; moving one wall opposite the direction of flight (negative) caused the bee to fly further from that wall.

In our moving wall simulation experiments, the spatial frequency of each wall was held constant at 0.2 cycles/cm and the speed of the left wall was varied between -30 and 30 cm/s. The change in the mean lateral positions a function of wall speed is plotted for a simulated bee flying at 40 cm/s using the three different types of gratings (Figure 6). These results are compared to the expected distance from the center d_c of a bee perfectly balancing the apparent image motion on each eye, adapted from Srinivasan *et al.* (1991), which can be expressed as

$$d_c = 120 \cdot \frac{1 - v_r}{2 - v_r} - 60 \tag{19}$$

where v_r is the speed of the left wall relative to the speed of the bee.

When point objects were used for the visual stimulus (Figure 6a) all three models fit the general shape of the scaled prediction. The HR and NDM models did not fully compensate for the changes in the apparent speed of the walls, while the NDS model displayed a much better match to the theoretical prediction.

Replacing the rows of objects with true square wave gratings (Figure 6b) improved the performance of both the HR and NDS models. The NDM model once again responded very differently to true square wave grating stimuli and failed to compensate for the moving wall at speeds below 10 cm/s. Even at higher wall

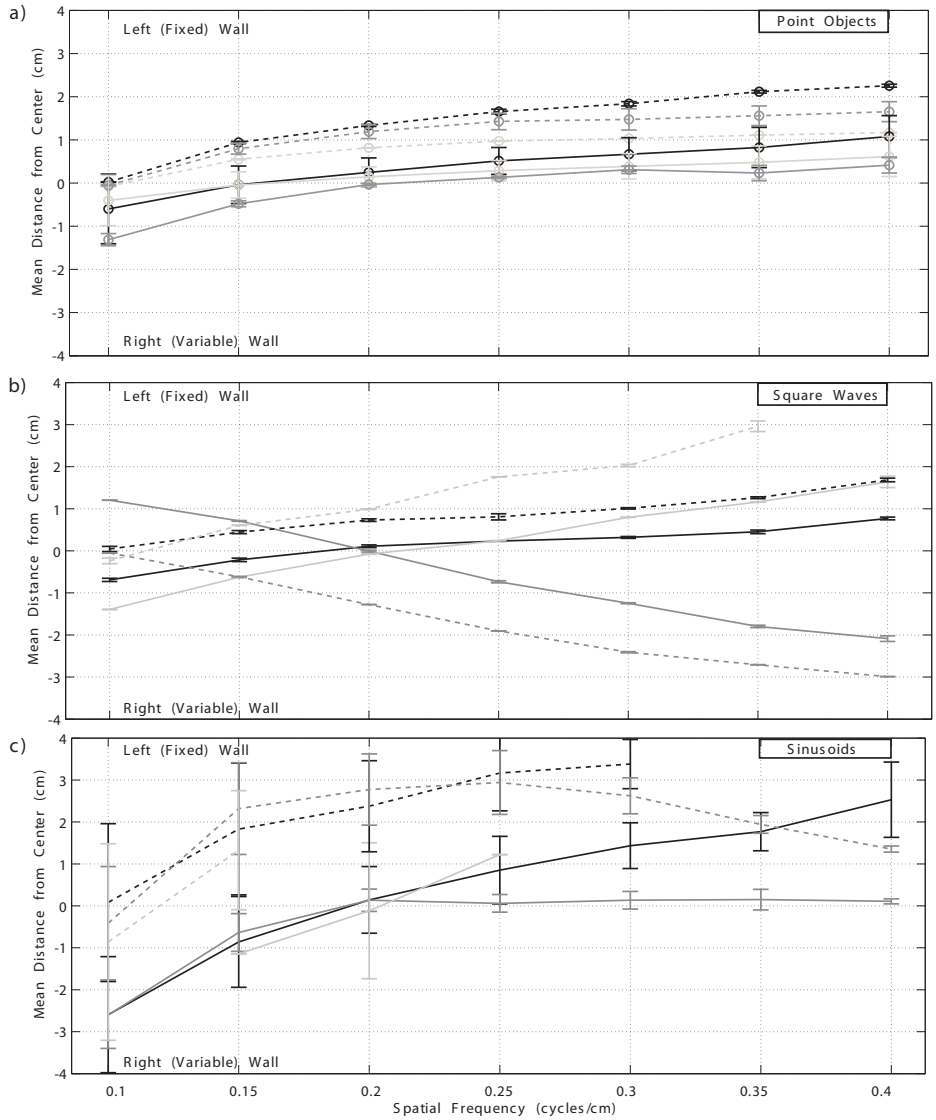

Fig. 5 The effect of spatial frequency on model performance. The mean lateral position of the bee along the last quarter of the tunnel is plotted versus the spatial frequency of the right (variable) wall while the spatial frequency of the left (fixed) wall was held constant at either 0.1 cycles/cm (dashed lines) or 0.2 cycles/cm (solid lines). The results are show for three different types of stimuli: (a) evenly spaced point objects, (b) square wave gratings and (c) sinusoidal gratings. The mean and standard deviation of the mean positions of the bee for each trial were calculated and are plotted for the HR (light gray), NDM (dark gray) and NDS (black) models. For each condition, the starting position and speed of the bee were varied across trials.

speeds the NDM model still showed much smaller deviations than would be predicted by an ideal speed estimator.

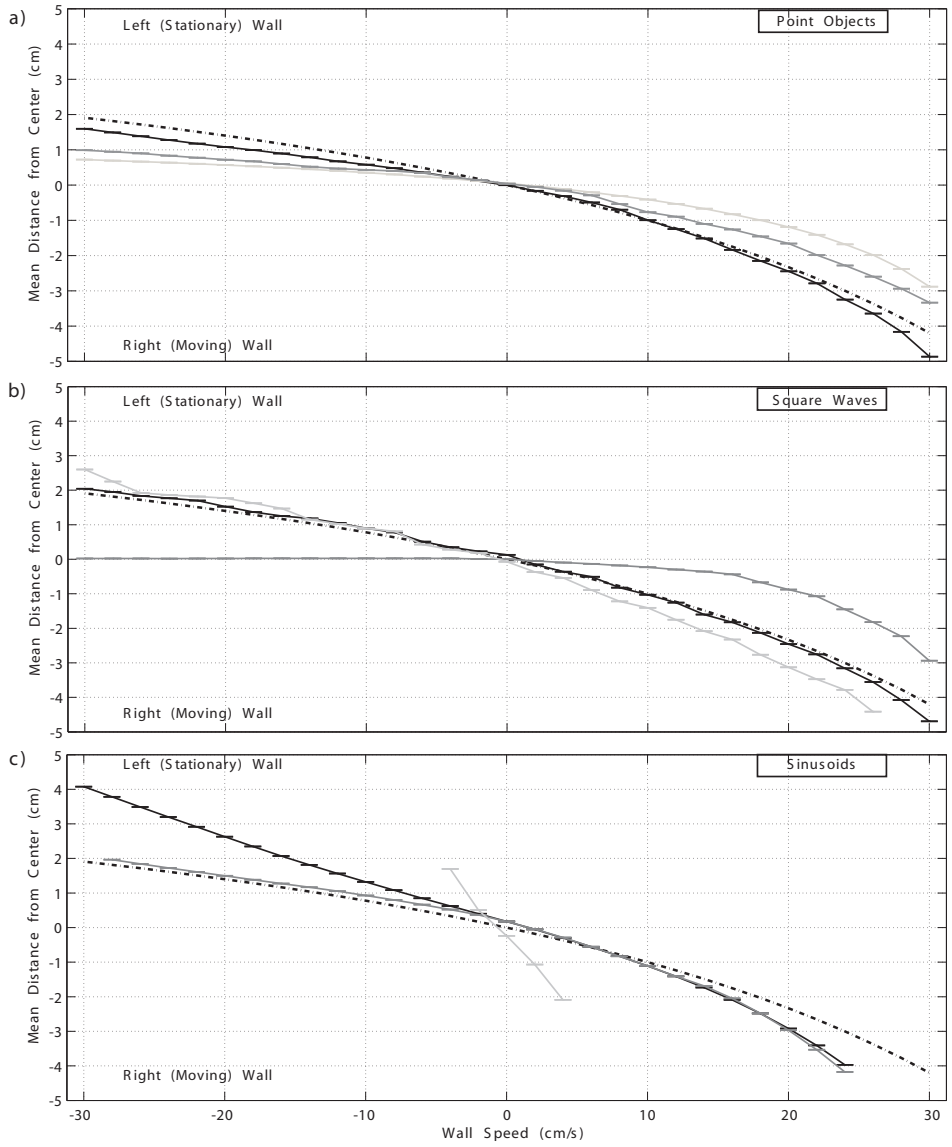

Fig. 6 The effect of moving one of the walls on centering simulations. The mean distance from the center of the tunnel for a simulated bee flying at 40 cm/s is plotted versus the speed of the left wall for the HR (light gray), NDM (dark gray) and NDS (black) models. The spatial frequency of the (a) point objects, (b) square wave gratings or (c) sinusoidal gratings was the same for both walls (0.2 cycles/cm). The black dashed line is the predicted position of a bee perfectly matching the apparent speed of the walls d_c (Equation 19). Each point represents the mean paths for trials run at starting positions between of -5.6 to 5.6 cm. Negative speeds indicate the right wall moving opposite the direction of flight and negative mean values indicate proximity to the right (moving) wall.

Switching to narrowband gratings (Figure 6c) greatly improved the NDM model performance and greatly diminished the effectiveness of the HR model. This was in agreement with our previous narrowband experi-

ments, in which the HR model consistently failed to navigate the tunnel when sinusoids of different spatial frequency lined the walls of the tunnel. The NDS model performance also decreased, with the mean lateral position deviating from the ideal fit at negative wall speeds approximately linearly as the wall speed decreased below zero.

4 Discussion

In the present study, we compared the speed tunings of three models of motion detection: the HR, NDM and NDS models. We developed a simulation framework to acquire small-field, non-directional estimates of the apparent image speed during flight, in accordance with behavioral experiments in honeybees. In particular, we were interested in the efficacy of the two non-directional models and benchmarked their performance versus that of the HR model. Our results suggests that while all three models can partially mimic speed dependent behaviors given specific visual stimuli, only the NDS model was sufficiently robust to match the behaviors observed in honeybees over a range of conditions.

Surprisingly, the analytically derived model responses were not entirely predictive of our behavioral simulations results. While the NDS model was on average the most effective of the three models for mimicking centering behaviors independent of spatial frequency, it was outperformed by the NDM model when narrowband patterns were used in the behavioral simulations. Furthermore, the fact that the HR model could be used for mimicking centering behaviors when square wave gratings were used was contrary to what we expected based on the derived model responses (Figure 5).

The reasons for the success of the HR model are not entirely clear. One possibility is that the higher spatial frequency harmonics present in the spectrum of the square wave gratings dominated the HR model response. The responses at speeds below 200 degrees/second and spatial frequencies below 0.06 cycles/degree are so small that they are not even present in the contour plot in Figure 4a. This suggests that even moderately high spatial frequency inputs will have much larger contributions to the overall HR model response. This hypothesis is consistent with previous observations that the HR model has speed-tuned responses to images with broad spatial frequency compositions, such as natural scenes (Dror *et al.*, 2001). This may also explain some of the differences in the performance of the NDM model.

The NDM model was more robust than the HR model, but showed a very strong dependence on spatial frequency when true square wave gratings were used. The multiplication operation present in the NDM model will magnify the model responses to higher spatial frequencies, increasing the relative contributions of the high spatial frequency harmonics of the square wave gratings. As can be seen in Figure 4b the response of the NDM model contains a notable trough at 0.13 cycles/degree and subsequently increases with increasing spatial frequency. This complicated response profile, with certain higher spatial frequencies having large

contributions to the overall model response, is likely responsible for the perplexing behavior of the model to different grating stimuli.

For all three models, the largest deviations from the center of the tunnel occurred when the lowest spatial frequency tested (0.1 cycles/cm) was compared to a higher spatial frequency pattern. Two reasons for this deviation are the smaller number of edges, hence fewer motion cues, provided by the lower frequency wall and the decrease in the model responses at low spatial frequencies. These problems are unlikely to be experienced by a honeybee in a real world environment where the bee would have a wide field view with other potential motion cues and would not necessarily perceive very low frequency gratings as periodic patterns.

In contrast to the spatial frequency variation experiments, the moving wall simulations better matched the predictions of the analytically derived model responses. The NDS model closely matched the predicted position of a bee perfectly matching the apparent speed of the walls (d_c, Equation 19) and previous behavioral experiments (Srinivasan *et al.*, 1991) for both square wave stimuli. In the case of narrowband patterns, the NDS model matched the shape of the ideal curve, but tended to overestimate the speed of the moving wall. Unfortunately, we lack any behavioral data from moving wall centering experiments using narrowband patterns so we cannot directly compare these simulation results with actual behavioral data. Simulations using the NDM and HR models using rows of objects matched the general shape of the curve, but the models were less effective when true square wave (NDM) or sinusoidal gratings (HR) were used.

In our simulation setup the head of the bee was always facing forward in order to eliminate rotational motion artifacts. This condition is consistent with observations in flies suggesting that the head remains fixed during forward flight and is quickly rotated when the insect is turning (van Hateren and Schilstra, 1999). Our initial experiments included head rotation, but the additional motion caused a number of difficulties. The rotational motion signal would often outweigh that of translational motion, greatly altering the motion differential between the eyes. In addition, turning the head of the bee caused asymmetries in the relative input to each eye, often resulting in a failed simulations. Finally, in initial trials in which the directionality HR model was preserved, rotational motion often caused one of the eyes to produce a negative speed output, creating a positive feedback loop in which the simulated bee would continue to turn further in the same direction resulting in a failed simulation run.

We also developed a novel method for using small-field motion to guide global behaviors. Our solution to this problem was to average responses from small collections of cells and then select the largest response among these subfields. Although there is no specific biological evidence supporting such a mechanism, it could be implemented by a biological system using a network of cells that receive inputs from neighboring speed-sensitive cells. The collator cell with the largest response could then inhibit the neighboring cells, thereby implementing a winner-take-all function among these neurons.

While the HR model was surprisingly effective for mimicking optic flow dependent behaviors in our simulations, it is important to note that this required a number of additional processing steps. Many of these steps are inconsistent with the properties of HR-like computations performed by biological systems. Much of the biological support for the HR model comes from recordings of the wide-field, directionally-selective lobula plate tangential cells of the fly (reviewed in Borst and Egelhaaf, 1989). The responses of these cells peak at temporal frequencies between 30 and 40 Hz and almost completely disappears at 100 Hz. In contrast, optic flow dependent behaviors necessitate the detection of temporal frequencies at or above 100 Hz (Srinivasan *et al.*, 1999). While our results suggest that the HR model can be used to explain some speed dependent behaviors, the outputs of the lobula plate tangential cells cannot. Instead, this would require a separate pathway that is small-field, eliminates directional motion information and sensitive to high temporal frequencies. This would require significant additional processing and eliminates the main argument for the relevance of the HR model. It also begs the question of why the brain would compute the direction of motion only to later discard that information.

Alternative models have been proposed to explain optic flow behaviors, the most notable being the gradient based scheme of Srinivasan *et al.* (1991) and the Angular Speed Detector (ASD) of Riabinina and Philippides (2009) and the 'token-matching scheme' used by Serres *et al.* (2008). One major disadvantage of these models is that they require sharp edges in order to function necessitating a preprocessing step in which the visual image is converted to a binary image via a thresholding operation before the models can be used as optic flow sensors (Srinivasan *et al.*, 1991; Riabinina and Philippides, 2009). While such a mechanism has been proposed for the Lamina Monopolar Cells (Srinivasan *et al.*, 1991), none of these proposed mechanisms have biological comaparable to correlation-type schemes.

A parallel non-directional pathway for visual speed estimation provides a much simpler explanation for the biological basis of visual speed estimation. Optic flow dependent behaviors have been shown to be small-field, non-directional and sensitive to flicker, all properties matched by the non-directional models. Non-directionally sensitive cells have been electrophysiologically identified in the early visual pathways of the fly (Douglass and Strausfeld, 1995), the most notable being the the Tm1 cell, and appear to precede the computation of directional motion (Higgins *et al.*, 2004). Modeling work on the EMD in the fly suggest that the computation performed by the Tm1 cell is identical to that of the NDS model presented in this paper. Additional processing of the Tm1 cell output, in parallel to the directional motion computation, could easily extract optic flow information with minimal additional processing. More detailed electrophysiological recordings from these non-directional cells could shed further light onto this problem.

One component necessary to achieve the full range of optic flow dependent behaviors is a speed control mechanism. Other studies have specifically investigated potential control systems for using optic flow for centering and flight speed control, but have used very basic speed detectors (Serres *et al.*, 2008). Our study

was focused on the biological mechanism underlying visual speed estimation, but adding a more sophisticated navigational algorithm to our simulations may improve our results and subsequent predictions. However, the qualitative performance of the models is unlikely to change.

Finally, while both the non-directional models displayed some dependence on spatial frequency in our behavioral experiments, it may be possible to alter the models in order to broaden their spatial frequency tuning. The effectiveness of all of the models was heavily dependent on the filter time constants (data not shown). Unlike other modeling studies (Higgins *et al.*, 2004; Higgins, 2004; Riabinina and Philippides, 2009) we used a much smaller high-pass filter time constant of $\tau_1 = 2\ ms$ to match the apparent high-pass filtering between the photoreceptor-L2 synapse. Increasing the time constant up to 50 ms significantly reduces the range of speeds that the models can respond to, suggesting that it may be possible to modify the time constants to optimize the speed tuning of the models. Even a slight shift in the spatial frequency tuning of the NDS model towards lower frequencies will likely to improve the effectiveness of the model for mimicking centering behaviors.

In conclusion, we believe that the computation of non-directional motion in the visual motion pathway serves multiple functions, including the visual speed estimation and as a precursor to the computation of directional motion. The NDS model is the most likely candidate for this role, having already been implicated in the EMD circuit in the fly. Our results show that the NDS model can be used to mimic some of the optic flow dependent behaviors observed in insects. In addition, the evidence of non-directional cells in early motion detecting pathways (Douglass and Strausfeld, 1995), the fact that they precede the computation of directional motion (Higgins *et al.*, 2004), and the behavioral evidence for non-directional motion (Srinivasan and Zhang, 1993) all support this hypothesis.

Acknowledgements This work was supported by individual fellowships from the NSF IGERT program and the BIO5 institute awarded by the Biology, Math and Physics Initiative at the University of Arizona. Support was also provided by the NIH through an NINDS NRSA pre-doctoral fellowship (1F31NS053433) and by the NCRR (grant number 5R01RR008688-21).

References

Baird, E., M. V. Srinivasan, S. W. Zhang and A. Cowling (2005). Visual control of flight speed in honeybees. *Journal of Experimental Biology* 208(20): 3895-3905.

Barlow, H. B. and W. R. Levick (1965). The mechanism of directionally selective units in rabbit's retina. *Journal of Physiology (London)* 178: 477–504.

Beersma, D. G. M., D. G. Stavenga and J. W. Kuiper (1977). Retinal Lattice, Visual Field and Binocularities in Flies. *Journal of Comparative Physiology A* 119: 207-220.

Borst, A. and M. Egelhaaf (1989). Principles of Visual Motion Detection. *Trends in Neuroscience* 12: 297-306.

Buschbeck, E. K. and N. J. Strausfeld (1996). Visual motion-detection circuits in flies: small field retinotopic elements responding to motion are evolutionarily conserved across taxa. *Journal of Neuroscience* 16: 4563–4578.

Dacke, M. and M. V. Srinivasan (2007) Honeybee navigation: distance estimation in the third dimension. *The Journal of Experimental Biology* 210: 845-853.

Douglass, J. K. and N. J. Strausfeld (1995). Visual motion detection circuits in flies: Peripheral motion computation by identified small field retinotopic neurons. *Journal of Neuroscience* 15: 5596–5611.

Douglass, J. K. and N. J. Strausfeld (1996). Visual motion detection circuits in flies: Parallel direction- and non-direction sensitive pathways between the medulla and lobula plate. *Journal of Neuroscience* 16: 4551–4562.

Dror, R. O., D. C. O'Carroll, and S. B. Laughlin (2001). Accuracy of velocity estimation by Reichardt correlators. *Journal of the Optical Society of America A* 18(2): 241–252.

Egelhaaf, M. and A. Borst (1989). Transient and steady-state response properties of movement detectors. *Journal of the Optical Society of America A* 6: 116–127.

Esch, H.E., S. W. Zhang, M. V. Srinivasan and J. Tautz (2001) Honeybee dances communicate distances measured by optic flow. *Nature* 411: 581-583.

Hassenstein, B. and W. Reichardt (1956). Systemtheorische analyse der Zeit-, Reihenfolgen- und Vorzeichenauswertung bei der Bewegungsperzeption des Rüsselkäfers *Chlorophanus*. *Zeitschrift für Naturforschung* 11b: 513–524.

Higgins, C. M. (2004) Non-directional motion may underlie insect behavioral dependence on image speed. *Biological Cybernetics* 91(5): 326-332.

Higgins, C. M., J. K. Douglass, and N. J. Strausfeld (2004). The computational basis of an identified neuronal circuit for elementary motion detection in dipterous insects. *Visual Neuroscience* 21(4): 567-586.

Ibbotson, M.R. (2001) Evidence for velocity-tuned motion-sensitive descending neurons in the honeybee. *Proceedings of the Royal Society London B* 268: 2195-2201.

Juusola, M., M. Weckstrom, R. O. Uusitalo, M. J. Korenberg and A. S. French (1995). Nonlinear models of the first synapse in the light-adapted fly retina *Journal of Neurophysiology* 74(6): 2538–2547.

Seidl, R. and W. Kaiser (1981). Visual Field Size, Binocular Domain and the Ommatidial Array of the Compound Eyes in the Worker Honey Bees. *Journal of Comparative Physiology A* 143: 17-24.

Kirchner, W. H. and M. V. Srinivasan (1989). Freely flying honeybees use image motion to estimate object distance. *Naturwissenschaften* 76: 281–282.

Riabinina, O. and A. O. Philippides (2009). A model of visual detection of angular speed for bees. Journal of Theoretical Biology 257(1): 61–72.

Rivera-Alvidrez, Z. (2005). Computational Modeling of Neurons Involved in Fly Motion Detection. Masters Thesis (Advisor: C.M. Higgins), University of Arizona.

Serres, J., D. Dray, F. Ruffier, N.Franceschini (2008). A vision-based autopilot for a miniature air vehicle: joint speed control and lateral obstacle avoidance. *Auton. Robots* 25(1-2): 103–122.

Si, A., M. V. Srinivasan and S. W. Zhang (2003) Honeybee navigation: properties of the visually driven 'odometer'. *The Journal of Experimental Biology* 206: 1265-1273.

Srinivasan, M. V., M. Lehrer, W. H. Kirchner and S. W. Zhang (1991). Range perception through apparent image speed in freely flying honeybees. *Visual Neuroscience* 6(5): 519–535.

Srinivasan, M. V. and S. W. Zhang (1993). Evidence for two distinct movement-detecting mechanisms in insect vision. *Naturwissenschaften* 80: 38–41.

Srinivasan, M. V., S. W. Zhang, M. Lehrer, and T. S. Collett (1996). Honeybee navigation en route to the goal: visual flight control and odometry. *Journal of Experimental Biology* 199: 237–244.

Srinivasan, M. V., M. Poteser, and K. Kral (1999). Motion detection in insect orientation and navigation. *Vision Research* 39(19): 2749–2766.

Srinivasan, M. V. and S. W. Zhang (2004) Visual motor computations in insects. *Annual Review of Neuroscience* 27: 679-696.

van Hateren, J. H. and C. Schilstra (1999). Blowfly flight and optic flow. II. Head movements during flight. *Journal of Experimental Biology* 202(11): 1491–1500.

van Santen, J. P. H. and G. Sperling (1985). Elaborated Reichardt detectors. *Journal of the Optical Society of America A* 2: 300–320.

von Frisch, K. (1993) *The dance language and orientation of bees.* Cambridge, MA: Harvard University Press

APPENDIX B

Non-directional models for visually estimating image speed

Jonathan P. Dyhr, Vivek Pant and Charles M. Higgins

In preparation for submission to

Biological Cybernetics

Biological Cybernetics manuscript No.
(will be inserted by the editor)

Non-directional models for visually estimating image speed

Jonathan P. Dyhr[1], Vivek Pant[3] and Charles M. Higgins[2,3]

[1]Graduate Program in Neuroscience

[2]Department of Neuroscience

[3]Department of Electrical and Computer Engineering

The University of Arizona

1040 E. 4th Street

Tucson, Arizona 85721-0077

USA

The date of receipt and acceptance will be inserted by the editor

Abstract Many insect behaviors have been shown to be dependent on estimates of the angular speed of the visual image, termed optic flow. Behavioral evidence suggests that optic flow is detected via a small-field, non-directional mechanism that is sensitive to speed independent of the spatial frequency of a stimulus. Because most biologically-based motion detectors are tuned to the spatio-temporal frequency of a stimulus, the mechanisms by which optic flow is extracted from the visual image remain unknown. One proposal is that non-directional motion detectors, sensitive to motion independent of direction, may underlie the visual speed estimate. In this paper we present two different modifications to previously presented non-directional models that can be used to alter their speed tuning to better match behavioral observations.

1 Introduction

The detection of the angular speed of the visual image, termed *optic flow*, has been studied in many different organisms and plays a key role in many navigational behaviors. In honeybees these include visual odometry (Esch and Burns, 1995; Si *et al.*, 2003), visual flight speed control (Baird *et al.*, 2005; Barron and Srinivasan, 2006), and distance estimation (Lehrer *et al.*, 1988; Kirchner and Srinivasan, 1989). Extensive studies of these behaviors have revealed that many of the properties of the visual speed estimation system are inconsistent with our current models of motion detection. The problem is further complicated by the fact that while there

Correspondence to: Jonathan P. Dyhr, jdyhr@email.arizona.edu

are reports of velocity-sensitive descending neurons in the ventral nerve cord of the honeybee (Ibbotson, 2001), we have not identified any speed-tuned cells in the early visual processing pathways of the insect brain.

Behavioral studies in honeybees have shown that the visual speed estimate is relatively independent of the spatial frequency (Srinivasan *et al.*, 1991, 1997; Si *et al.*, 2003; Baird *et al.*, 2005) and the contrast (Srinivasan *et al.*, 1991, 1997; Si *et al.*, 2003; Baird *et al.*, 2005) of a visual stimulus. The optic flow estimate also appears to be insensitive to the direction of motion (Srinivasan *et al.*, 1993; Dacke and Srinivasan, 2007) and is acquired by a small-field mechanism (Srinivasan *et al.*, 1993) with a receptive field that does not exceed 20 degrees (Srinivasan and Zhang, 1997). Motion in the both the lateral and ventral visual fields contribute to the visual speed estimate (Srinivasan *et al.*, 1997; Si *et al.*, 2003; Baird *et al.*, 2006), with motion in the lateral visual fields directly perpendicular to the direction of flight having the largest contribution to the estimate (Srinivasan *et al.*, 1991). As with other motion systems, optic flow is processed using information only from the green spectral channel (Chittka and Tautz, 2003). The optic flow detection mechanism also appears to be sensitive to flicker, but the magnitude of the flicker response is approximately half of that to motion (Srinivasan *et al.*, 1993).

Honeybees have been shown to hold the rate of optic flow constant between 230 and 320 degrees/second when flying through tunnels (Srinivasan *et al.*, 1991, 1996; Baird *et al.*, 2005; Barron and Srinivasan, 2006; Serres *et al.*, 2008) and in open, outdoor environments (Capaldi *et al.*, 2000). While the optic flow estimate increases approximately linearly with speed, visual flight speed control studies have suggested that honeybees may underestimate optic flow when the image speed is very high and to overestimate optic flow when image speed is very low.

Many of these properties are in strict contrast to the those observed for other motion dependent behaviors, particularly those modeled by the canonical model of motion detection for insects, the Hassenstein-Reichardt (HR) model (1956). The HR model responds selectively to the direction of motion, is sensitive to the spatio-temporal frequency of a stimulus (as opposed to speed), and is relatively insensitive to flicker (Buchner, 1984). Furthermore, the behaviors and cellular responses described by the HR model are wide-field (Hausen, 1981, 1982), dependent on contrast (Buchner, 1984), respond maximally at low temporal frequencies (between 30-40 Hz) and do not respond to temporal frequencies above 100 Hz (Srinivasan *et al.*, 1999).

All of this has suggested that a separate neuronal pathway is responsible for the detection of optic flow (Srinivasan *et al.*, 1993), but no clearly speed-tuned cells have been identified in the early visual pathways. However, some recordings have shown that motion-sensitive neurons that respond preferentially to motion over flicker and are insensitive to the direction of motion are present in the insect optic lobes (Gilbert *et al.*, 1991; Douglass and Strausfeld, 1995, 1996), but the difficulty of recording from these cells has prevented thorough characterization of their speed responses.

Higgins (2004) proposed that non-directional motion detectors, sensitive to motion in any direction while responding more strongly to motion than to flicker, could be used to explain the various behavioral results from studies of the visual speed estimation system. His detector, which we term the NDM model, combined two mirror symmetric subunits of the HR model, each sensitive to motion in a single direction, to create a non-directional motion detector. The response of the NDM model increases proportionally to speed over a range, is less dependent on the spatial frequency of a stimulus, and has a reduced response to flicker compared to motion. Two advantage of the NDM model are that it uses biologically supported, correlation-like computations and displays improved speed sensitivity over similar models. Higgins (2004) also suggested that the non-directionally sensitive Tm1 could be a potential neuronal candidate for performing an NDM-like computation.

A second non-directional model, also based on the Tm1 cell, was proposed by Rivera-Alvidrez (2005) based on its role in a putative elementary motion detection circuit (Higgins *et al.*, 2004). The non-directional summation (NDS) model (Rivera-Alvidrez, 2005) is identical to the NDM model except that the final multiplication step is replaced by a summation. It is also a completely linear model that is speed-tuned in its amplitude response.

Studies by Dyhr and Higgins (unpublished) investigated the effectiveness of these two non-directional models for mimicking optic flow dependent behaviors and found that while they were effective, they were not sufficiently robust to fully match the behavioral results from honeybees. In particular, the models had difficultly when very low spatial frequency stimuli were used. They suggested that slightly improving the speed tuning of the models at low spatial frequencies could cause significant improvements in the performance of the models in behavioral simulations of the centering response.

In the current study we present two modifications to the non-directional models, the removal of the low-pass filters and the inclusion of next-nearest neighbor photoreceptors, that can be used to alter their spatio-temporal frequency tunings and make them more sensitive to speed. We then perform basic behavioral simulations to show that the alterations can improve their utility for mimicking optic flow dependent behaviors. Some of this work has been previously presented by Pant (2007) in dissertation form.

2 Methods

All simulations were performed using the Matlab software package (The Mathworks, Natick, MA).

2.1 Model parameters

The input used for all of the models was a simple time-varying sinusoidal stimulus with contrast C, temporal frequency ω_t and spatial frequency ω_x

$$S(x,t) = \frac{1}{2} \cdot (1 + C \cdot \sin(\omega_x \cdot x + \omega_t \cdot t)) \tag{1}$$

The speed of the sinusoid can be expressed as $v = \frac{\omega_t}{\omega_x}$. The amplitude modulation due to first-order linear high-pass filters h_1 and low-pass filters h_2 can be expressed as

$$h_1(\omega_t) = \frac{\omega_t \cdot \tau_1}{\sqrt{1 + (\omega_t \cdot \tau_1)^2}} \tag{2}$$

$$h_2(\omega_t) = \frac{1}{\sqrt{1 + (\omega_t \cdot \tau_2)^2}} \tag{3}$$

Where τ_1 and τ_2 are the filter time constants in seconds. For this study we assumed the high-pass filtering operation occurred at the synapse between the photoreceptor and the L2 lamina monopolar cell (Higgins *et al.*, 2004) and was assigned a value of $\tau_1 = 0.002\ s$ in accordance with the available physiological data (Juusola *et al.*, 1995). Since there was no conclusive physiological data by which to estimate the low-pass filter time constant, we chose a value of $\tau_2 = 0.05\ s$ to match previous studies (Higgins, 2004; Higgins *et al.*, 2004; Riabinina and Philippides, 2009).

Both filters introduced phase delays, but the phase term from the high-pass filter was identical for all pathways and was ignored. The phase delay introduced by the low-pass filter ϕ_2 can be expressed as

$$\phi_2(\omega_t) = -tan^{-1}(\omega_t \cdot \tau_2) \tag{4}$$

The relative phase between sinusoidal inputs at neighboring photoreceptors ϕ_x can be expressed as then $\phi_x = \omega_x$.

$$\phi_x = \omega_x \cdot \Delta x \tag{5}$$

where the spacing between photoreceptors Δx is set to 2 degrees in accordance with data from honeybees (Seidl and Kaiser, 1981).

2.2 Simulation environment

In addition to investigating the theoretical speed tuning of the various non-directional models, we also implemented them in a behavioral simulation framework. The simulated bee flew through a 2 meter long tunnel of with width of 0.12 meters. The walls were lined with periodic sinusoidal or square wave patterns f with contrast C that were projected onto the eye of the simulated bee using the following equation

$$I(\theta) = B \cdot (1 + C \cdot f(\frac{2\pi \cdot \omega_x \cdot (D + y)}{\tan(\theta)})) \tag{6}$$

Where B was a constant factor specifying the background illumination, y was the lateral position of the bee in the tunnel, D was the half-width of the tunnel and θ was the angle of the photoreceptor. The image was then Gaussian blurred and the acceptance angle of each photoreceptor was set to 2 degrees (Seidl and Kaiser, 1981).

The processing of the intensity signals to yield a global estimate of speed was identical to the method of Dyhr and Higgins (unpublished). In short, photoreceptors outputs were processed by cascaded motion detectors covering an 180 degree field of view split between two eyes. The central 18 degrees, corresponding to the binocular overlap zone (Seidl and Kaiser, 1981), was shared by both eyes such that they individually had 99 degree fields of view. The head angle of the simulated bee was held fixed such that it was always looking in the forward direction. This prevent rotational motion artifacts and matched studies showing that flies keep their head angle constant during translational flight (van Hateren and Schilstra, 1999).

To derive a global speed estimate from small-field motion detectors we subdivided each eye into five non-overlapping subfields (Dyhr and Higgins, unpublished), each spanning approximately 18° (Srinivasan and Zhang, 1997). The motion detector outputs within each subfield were averaged and the maximal subfield response for each eye was used as the global estimate for each eye (v_{LE} and v_{RE}). The simulated bee traveled at a fixed forward flight speed v_f of 0.4 meters/second along the length of the tunnel. The lateral velocity v_l was determined at each time step ($t = 0.002$ seconds) by the low-pass filtering the difference between the speed estimates of each eye

$$v_l(t) = g \cdot (v_{LE}(t) - v_{RE}(t)) \tag{7}$$

Where g was a gain scale factor that was determined empirically for each model. The x and y positions of the bee were then specified by the following equations

$$x(t) = x(t-1) + v_f \cdot t \tag{8}$$

$$y(t) = y(t-1) + (\alpha \cdot v_l(t-1) - (1-\alpha) \cdot v_l(t)) \cdot t \tag{9}$$

Where $\alpha = e^{\frac{-t}{\tau_y}}$ is a low-pass filter term, with a time constant τ_y of 0.1 seconds, used to smooth the changes in v_l.

3 Results

We divide our discussions of the models into two sections, one each for the effects of the modifications on the speed responses of the NDM and NDS models. In each section we first analytically derive the responses of the different models to sinusoidal stimuli in order to investigate their speed tuning and spatial frequency

dependence. We then test the efficacy of the models for mimicking speed dependent behaviors using behavioral simulations of the *centering response*, in which the simulated bee flew through the center of a tunnel by balancing the apparent speed of two walls. Behavioral experiments have shown that, in honeybees, the centering response is insensitive to four-fold variations in the spatial frequency of square wave gratings, and is insensitive to two-fold differences between sinusoidal stimuli (Srinivasan *et al.*, 1991).

3.1 NDM models

The original NDM model (Figure 1a) consists of three photoreceptors whose outputs are all temporally high-pass filtered. The high-pass filtered outputs from the two distal channels are then temporally low-pass filtered (time delayed) and summed. This sum is multiplied by the high-pass filtered output of the central photoreceptor channel. The average response of the NDM model to a drifting sinusoidal gratings (Equation 1) as derived by Higgins (2004) can be shown to be

$$\bar{R}_{NDM} = \frac{C^2}{4} \cdot \frac{(\omega_t \cdot \tau_1)^2}{(1 + (\omega_t \cdot \tau_1)^2) \cdot (1 + (\omega_t \cdot \tau_2)^2)} \cdot \cos(\phi_x) \tag{10}$$

The average responses of the NDM model to sinusoidal gratings moving at different speeds are plotted in Figure 2a (top). As can be seen, the average response of the NDM model increases approximately linearly with speed. The contour plot (Figure 2a, bottom) shows how the response of the NDM model varies with spatial frequency and speed. The relatively vertical contour lines for speeds between 150 and 400 degrees/second and for spatial frequencies between 0.04 and 0.08 show that the NDM model is speed-tuned within this range.

Pant (2007) proposed that a simplified version of the NDM model (NDMs, Figure 1b) had an improved speed tuning over the original model. The average response of the NDMs model can be shown to be

$$\bar{R}_{NDMs} = \frac{C^2}{4} \cdot {h_1}^2 \cdot \cos(\phi_x) \tag{11}$$

and substituting in the amplitude expressions for the filters

$$\bar{R}_{NDMs} = \frac{C^2}{4} \cdot \frac{(\omega_t \cdot \tau_1)^2}{1 + (\omega_t \cdot \tau_1)^2} \cdot \cos(\phi_x) \tag{12}$$

The absence of the amplitude term from the low-pass filter in the NDMs model, compared to the original, greatly effects the speed responses (Figure 2b, top) and the spatial frequency tuning (Figure 2b, bottom) of the NDMs model. The reason for these differences is largely due to the choice of filter time constants. If the high-pass filter time constant of the NDMs models is increased to 0.05 seconds, the contour plots of the models are almost identical (data not shown). The NDMs model also responds proportionally to speed

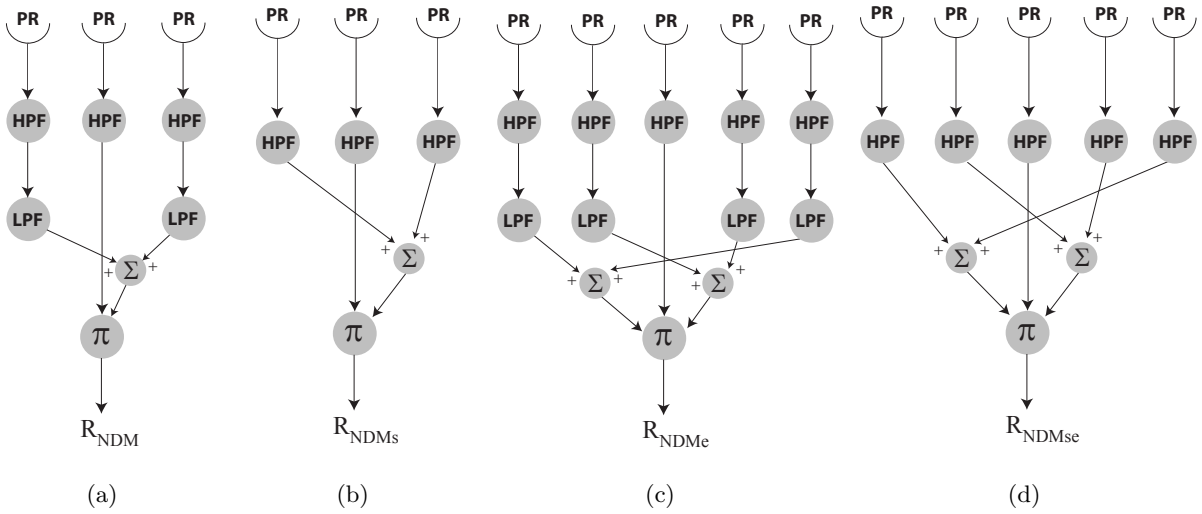

Fig. 1 Non-directional multiplication (NDM) models. Outputs from the photoreceptors (PR) are filtered by different combinations of high-pass (HPF) and low-pass (LPF) filters. The filtered outputs are then summed (Σ) and multiplied (π) to yield motion sensitive outputs. (a) The original non-directional multiplication (NDM) model consists of three spatially offset, high-pass filtered photoreceptor channels. The outputs from the two lateral channels are also low-pass filtered, summed and then multiplied by the output of the central channel to yield a motion sensitive output. (b) A simplified non-directional multiplication (NDMs) model in which the low-pass filters of the original model are removed. (c) The expanded non-directional multiplication (NDMe) model includes outputs from the next nearest neighbor photoreceptors. With the exception of the central channel, all the photoreceptor outputs are high-pass and low-pass filtered and then summed. This summed output is then multiplied by the high-pass filtered output of the central channel. (d) The simplified and expanded non-directional multiplication model (NDMse) in which the lateral channels are all high-pass filtered, summed and then multiplied by the high-pass filtered output of the central channel.

for small ranges of spatial, but the response at high spatial frequencies increases so dramatically that it dominates the other responses in both the speed and contour plots in Figure 2b.

We also wanted to investigate the effects of including next nearest neighbor photoreceptors on the original NDM model. The response of the expanded NDM model (NDMe, Figure 1b) can be shown to be

$$\bar{R}_{NDMe} = \frac{C^2}{4} \cdot {h_1}^2 \cdot {h_2}^2 \cdot (\cos(2 \cdot \phi_x) + \cos(\phi_x)) \tag{13}$$

and substituting in the filter magnitude expressions

$$\bar{R}_{NDMe} = \frac{C^2}{4} \cdot \frac{(\omega_t \cdot \tau_1)^2}{(1 + (\omega_t \cdot \tau_1)^2)} \cdot (\cos(2 \cdot \phi_x) + \cos(\phi_x)) \tag{14}$$

The NDMe model response is similar to that of the original, but with an additional $\cos(2 \cdot \phi_x)$ term. The speed response of the NDM model increase proportionally with speed until it reaches a saturation point

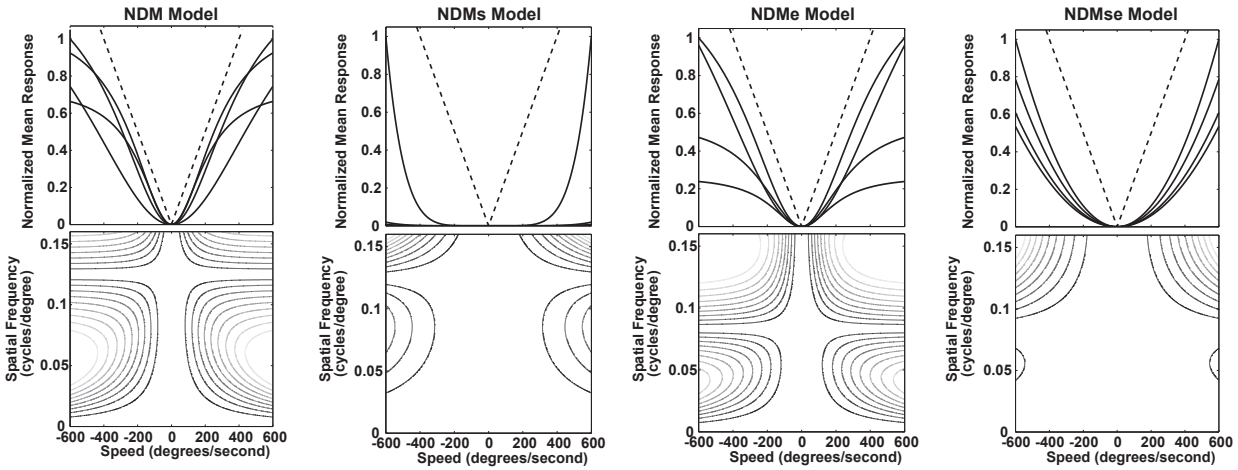

Fig. 2 NDM model responses. *Top*: The average responses of the (a) NDM, (b) NDMs, (c) NDMe and (d) NDMse models to sinusoidal gratings moving at different speeds are plotted for spatial frequencies of 0.03, 0.05, 0.07 and 0.09 cycles/degree. The dashed line represents a response proportional to speed. *Bottom*: Contour plots of the NDM models responses as the speed and spatial frequency of a sinusoidal pattern is varied. Darker contours represent weaker responses. Vertical lines indicated speed-tuned, spatial frequency independent responses.

and the response levels off (Figure 2c, top). The location of the saturation point and the maximum response size vary with spatial frequency. The contour plot (Figure 2b, top) shows that the dip in the contour plot of the NDM model at 0.13 cycles/degree (Figure 2a, bottom) is shifted down below 0.1 cycles/degree for the NDMe model. This increases the spatial frequency dependence of the model for low spatial frequencies, but decreases it at high spatial frequencies.

Finally, we wanted to determine the effects of adding both modifications to the NDM model. The response of the simplified, expanded NDM model (NDSse, Figure 1d) can be shown to be

$$\bar{R}_{NDMse} = \frac{C^2}{4} \cdot {h_1}^2 \cdot (\cos(2 \cdot \phi_x) + \cos(\phi_x)) \tag{15}$$

and, with the filter magnitudes substituted into the equation

$$\bar{R}_{NDMse} = \frac{C^2}{4} \cdot \frac{(\omega_t \cdot \tau_1)^2}{1 + (\omega_t \cdot \tau_1)^2} \cdot (\cos(2 \cdot \phi_x) + \cos(\phi_x)) \tag{16}$$

The speed responses of the NDMse increase approximately hyperbolically with speed (Figure 2d, top). There is also a spatial frequency dependent shift in the slope, but it is relatively minor compared to the NDMs model. The contour plot (Figure 2d, bottom) is very similar to the NDMs model, with the contours shifted down towards lower spatial frequencies and laterally towards higher speeds. It does not appear that

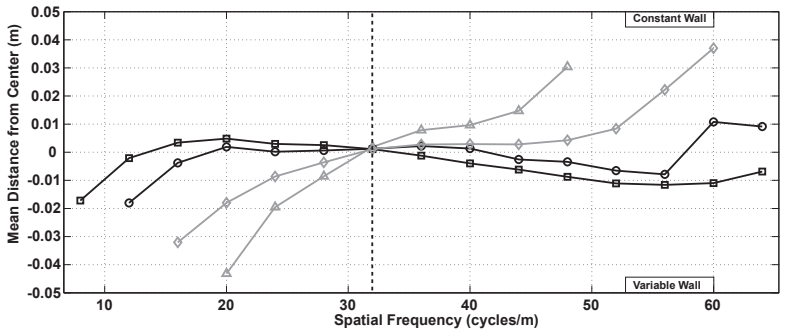

(a)

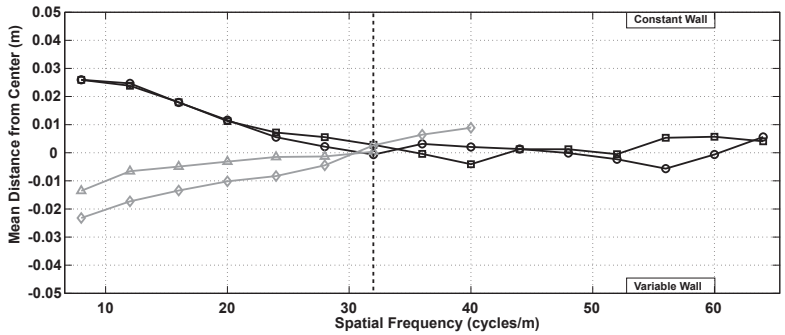

(b)

Fig. 3 NDM model variable spatial frequency simulations. The mean distance of the simulated bee from the center of the tunnel is plotted versus the spatial frequency on the variable wall for the NDM (black circle), NDMs (gray triangle), NDMe (black square) and NDMse (gray diamond) models. The spatial frequency of the constant wall was 32 cycles/meter and the vertical dashed line indicates when the two wall patterns are identical. The performance of the models is show when either (a) sinusoidal patterns or (b) square wave patterns are used to line the walls.

the NDMse model could be used as an effective speed estimator, but it is important to note that one reasons for lack of speed tuning due to our choice of the high-pass filter time constant (as discussed previously).

3.2 NDM model behavioral simulations

After deriving the responses to the models and predicting their usefulness as speed estimators, we wanted to test these predictions using behavioral simulations. It has been previously noted by Dyhr and Higgins (unpublished) that predictions based on the derived responses of the HR, NDM and NDS models were not entirely predictive of the performance of the models in behavioral simulations. Furthermore, the models appeared to behave very differently when square wave patterns were used (Dyhr and Higgins, unpublished).

Our first set of simulations were based of the work of Srinivasan *et al.* (1991) who noted that the centering response was relatively insensitive to two-fold differences in the spatial frequencies of sinusoidal gratings, between linear spatial frequencies of approximately 16 and 30 cycles/meter. However, they did note a significant deviation in the path towards the high frequency wall when they compared sinusoids of approximately 16 and 60 cycles/meter. In our simulations we held the spatial frequency of a sinusoidal pattern on one wall constant at 32 cycles/meter while the spatial frequency of the sinusoidal grating on the opposite wall was varied between 8 to 64 cycles/meter. The results for all of the NDM models are shown in Figure 3a.

The NDM and NDMe models show the least dependence on the spatial frequency of the pattern, with the NDMe performing better at low spatial frequencies and the NDM model centering more effectively at high spatial frequencies. When the spatial frequency on the variable wall is 16 cycles/meter neither of these models deviates more the 0.005 meters from the center of the tunnel. When the variable wall has a spatial frequency of 64 cycles/meter both the NDM and NDMe models show significant deviations towards the high spatial frequency walls, matching the observations of Srinivasan *et al.* (1991).

Both of the NDMs and NDMse showed significant dependence on the narrowband spatial frequency of the patterns. In fact, both the models often failed to center and exited the tunnel when the differences between the spatial frequency of the walls was more than approximately 20 cycles/meter, in which case no data was plotted.

Next, we wanted to see if we could match the observations of Srinivasan *et al.* (1991) when they used square wave gratings to line the tunnel walls. The results plotted in Figure 3b show that the models have significantly different behavior when using square wave gratings. Both the NDM and NDMe models deviate significantly from the center of the tunnel when the spatial frequency on the variable wall is lower than 32 cycles/meter and in the opposite direction as that observed for sinusoidal patterns. The dependence disappears as spatial frequency is increased above 32 cycles/meter.

The NDMs and NDMse models show the opposite behavior at low spatial frequencies and tend to deviate away from the higher frequency constant wall. When the spatial frequency is increased above 32 cycles/meter the models completely fail at centering. These results are not in agreement with the behavioral results from honeybees, in which there was no exhibited spatial frequency dependence for square wave gratings.

3.3 NDS models

The NDS model (Figure 4a) was first investigated by Rivera-Alvidrez (2005). The NDS model is identical to the NDM model except that the final multiplication is replaced by a summation. Because it consists of only addition operations and temporal filters, the NDS model response is linear and its average response to

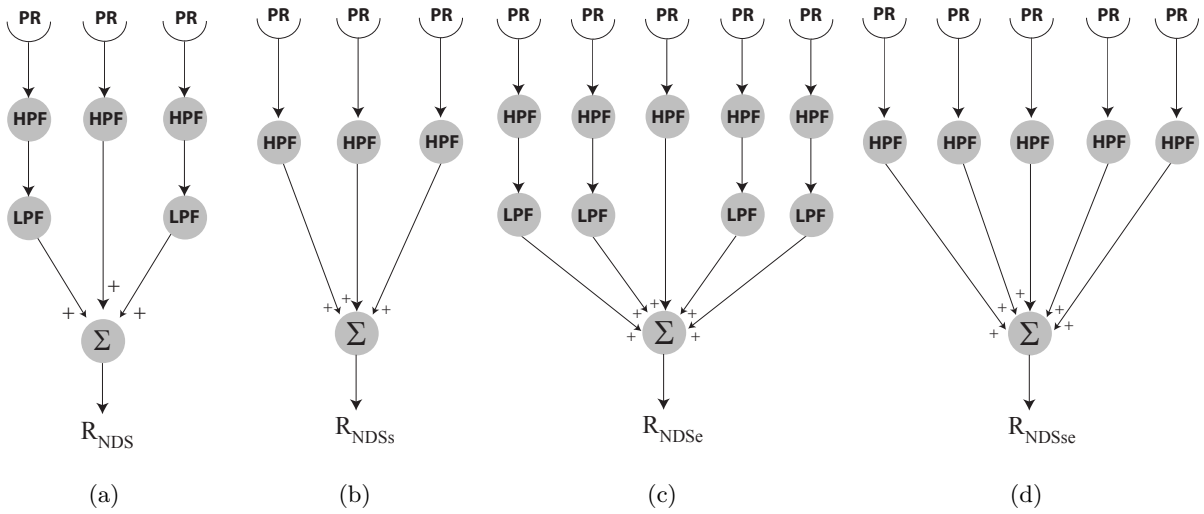

Fig. 4 Non-directional summation (NDS) models. Outputs from the photoreceptors (PR) are filtered by different combinations of high-pass (HPF) and low-pass (LPF) filters. The filtered outputs are then summed (Σ) to yield motion sensitive outputs. (a) The original non-directional summation (NDS) model consists of three spatially offset, high-pass filtered photoreceptor channels. The outputs from the two lateral channels are also low-pass filtered, and summed with the output of the central channel to yield a motion sensitive output. (b) A simplified non-directional summation (NDSs) model in which the low-pass filters of the original model are removed. (c) The expanded non-directional summation (NDSe) model includes outputs from the next nearest neighbor photoreceptors. With the exception of the central channel, all the photoreceptor outputs are high-pass and low-pass filtered, after which all of the outputs are summed. (d) The simplified and expanded non-directional summation (NDSse) in which the lateral channels are all high-pass filtered and summed.

a moving sinusoidal grating is zero. Instead, we are interested in the amplitude responses of the model which has previously been shown to be

$$A_{NDS} = \frac{C}{2} \cdot \frac{\omega_t \cdot \tau_1}{\sqrt{1+(\omega_t \cdot \tau_1)^2} \cdot \sqrt{1+(\omega_t \cdot \tau_2)^2}} \cdot \sqrt{[2 \cdot \cos(\omega_x)+1]^2 + (\omega_t \cdot \tau)^2} \tag{17}$$

One can see in Figure 5a (top) that the amplitude response of the model increases approximately linearly with speed. The model also appears to be much less dependent on spatial frequency that any of the NDM models (Figure 5a, bottom).

The simplified NDS model (NDSs, Figure 4b) requires only the summation of the high-pass filtered photoreceptors. The amplitude of the model is as follows

$$A_{NDSs} = \frac{C}{2} \cdot {h_1}^2 (2 \cdot \cos(\phi_x) + 1) \tag{18}$$

and, after substituting in the filter magnitudes, one gets the following expression

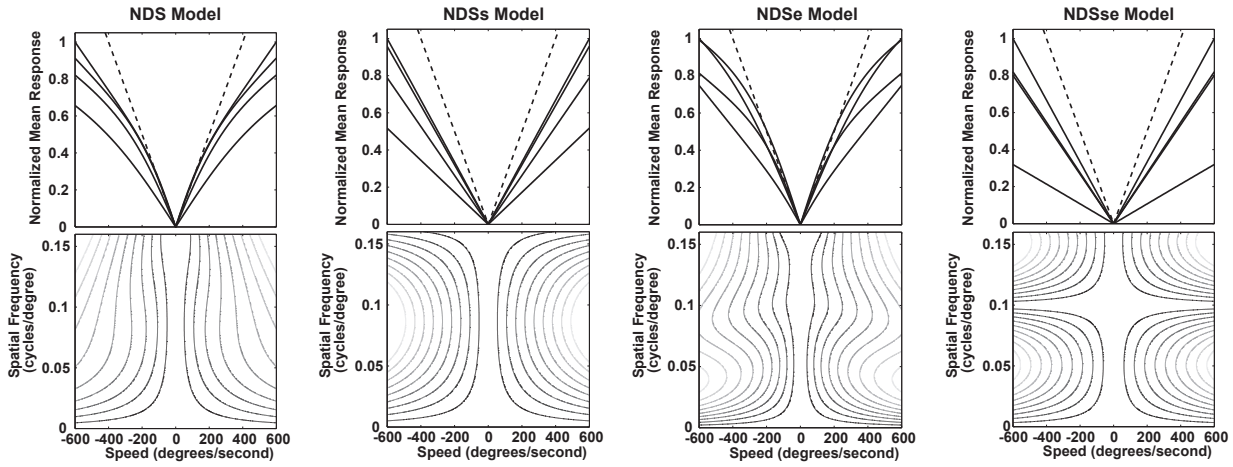

Fig. 5 NDS model responses. *Top*: The average responses of the (a) NDS, (b) NDSs, (c) NDSe and (d) NDSse models to sinusoidal gratings moving at different speeds are plotted for spatial frequencies of 0.03, 0.05, 0.07 and 0.09 cycles/degree. *Bottom*: Contour plots of the NDM models responses as the speed and spatial frequency of a sinusoidal pattern is varied. Vertical lines indicated speed-tuned, spatial frequency independent responses.

$$A_{NDSs} = \frac{C}{2} \cdot \frac{(\omega_t \cdot \tau_1)^2}{1 + (\omega_t \cdot \tau_1)^2} \cdot (2 \cdot \cos(\phi_x) + 1) \tag{19}$$

The NDSs model amplitude response increases linearly with speed (Figure 5b, top), but the slope of the response is spatial frequency dependent. This can be better visualized in the contour plot in Figure 5b (bottom). Compared to the original NDS model, the spatial frequency tuning of NDSs model is shifted towards lower spatial frequencies, suggesting it may have improved performance in behavioral simulations (Dyhr and Higgins, unpublished). However, the shift also decreases the speed tuning of the model at high spatial frequencies.

Including next nearest neighbor photoreceptors also shift the speed tuning of the model to lower frequencies, but has less of an effect on the model response at higher spatial frequencies. The amplitude response of the NDSe model (Figure 4c) can be expressed as

$$A_{NDSe} = \frac{C}{2} \cdot h_1 \cdot \sqrt{4 \cdot {h_2}^2 \cdot (\cos(4 \cdot \phi_x) + \cos(3 \cdot \phi_x) + 3 \cdot \cos(2 \cdot \phi_x) + 3 \cdot \cos(\phi_x) + 2) + 1} \tag{20}$$

and substituting in the filter values

$$A_{NDSe} = \frac{C}{2} \cdot \frac{\omega_t \cdot \tau_1}{\sqrt{1 + (\omega_t \cdot \tau_1)^2}} \cdot \sqrt{4 \cdot \frac{1}{1 + (\omega_t \cdot \tau_2)^2} \cdot (\cos(4 \cdot \phi_x) + \cos(3 \cdot \phi_x) + 3 \cdot \cos(2 \cdot \phi_x) + 3 \cdot \cos(\phi_x) + 2) + 1} \tag{21}$$

As with the other models, the amplitude response of the NDSe model increases proportionally with speed (Figure 5c, top) However, the spatial frequency tuning of the NDSe model is much different (Figure 5c, bottom). The contour lines of the NDSe model remain relatively vertical even at very high speeds, although there are some spatial frequency dependent fluctuations in the response. The speed tuning of the NDSe model also extends to lower spatial frequencies, similar to the NDSs model.

Combining the two modifications yields the simplified, expanded NDS model (NDSse, Figure 4c). The response of the model is relatively simple to derive and can be show to be

$$A_{NDSse} = \frac{C}{4} \cdot h_1 \cdot (\cos(2 \cdot \phi_x) + \cos(\phi_x)) \tag{22}$$

and with the substitution of the filter values

$$A_{NDSse} = \frac{C}{4} \cdot \frac{\omega_t \cdot \tau_1}{\sqrt{1 + (\omega_t \cdot \tau_1)^2}} \cdot (\cos(2 \cdot \phi_x) + \cos(\phi_x) + 1) \tag{23}$$

The amplitude responses of the NDSse (Figure 5d, top) increase linearly with speed, but shows the same spatial frequency dependent change in slope as the NDSs model. The spatial frequency tuning of the model is compressed, such that the contour lines in Figure 5d (bottom) are vertical at low speeds with the exception of the notch in the response at 0.1 cycles/degree. Compared to the other three versions of the model, the NDSse model appears to be the least speed tuned.

3.4 NDS behavioral simulations

Because the average response of the NDS model to a sinusoidal grating is zero, we first extracted the amplitude of the model by taking the absolute value of its output. The rectified and spatially averaged outputs are then proportional to the amplitude of the NDS model (Dyhr and Higgins, unpublished). Otherwise, we used the same simulation procedure to test the NDS models as used for the NDM models (Section 3.2). The results from the first set of simulations, investigating the narrowband spatial frequency dependence of NDS models, are plotted in Figure 6a. All of the NDS models, with the exception of the original, display little dependence on high spatial frequencies. However, only the NDSe model remains centered when the spatial frequency drops below 28 cycles/meter. Thus, only the NDSe model is sufficiently robust to match the behavioral results of Srinivasan *et al.* (1991).

When square wave gratings are used to line the tunnel walls, the spatial frequency dependence of all of the models is significantly reduced (Figure 6b). In addition, the NDS model response reverses such that it approaches the constant wall at low spatial frequencies and the variable wall at high spatial frequencies. The response of the NDSe model also flips, but in this case it approaches the variable wall at low spatial frequencies. Unlike any of the other models tested in this study, the NDSe model response remains relatively

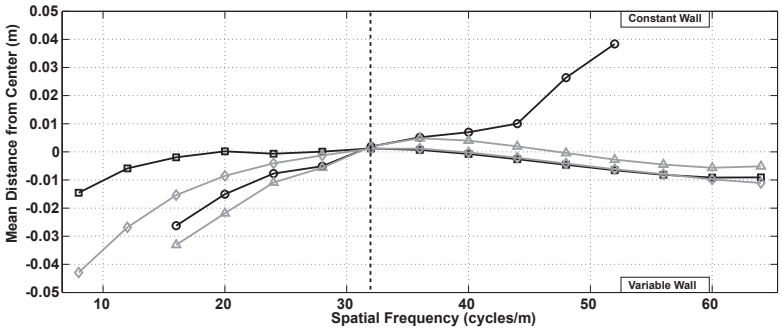

(a)

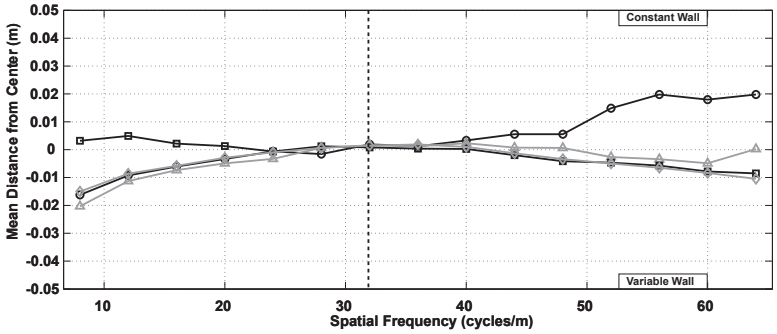

(b)

Fig. 6 NDS model variable spatial frequency simulations. The mean distance of the simulated bee from the center of the tunnel is plotted versus the spatial frequency on the variable wall for the NDS (black circle), NDSs (gray triangle), NDSe (black square) and NDSse (gray diamond) models. The spatial frequency of the constant wall was 32 cycles/meter and the vertical dashed line indicates when the two wall patterns are identical. The performance of the models is show when either (a) sinusoidal patterns or (b) square wave patterns are used to line the walls.

flat when the spatial frequency of a square wave grating varies between 8 to 40 cycles/meter, matching the results of Srinivasan *et al.* (1991).

Overall, the NDS model responses are much more robust than those of the NDM models, showing significantly less dependence on spatial frequency and less variability in centering performance compared to the NDM models.

4 Discussion

In the present study we have shown that the speed tuning of two non-directional models, the NDM and NDS models, can be improved by either simplifying the models by removing the low-pass filters, expanding the models by including next nearest neighbor photoreceptors, or both. The apparent improvement in the

speed-tuning is reflected in behavioral simulations, where in most cases the models are better able to mimic optic flow dependent behaviors.

The expanded models performed the best in behavioral simulations, matching the results of behavioral experiments in honeybees. The NDSe model in particular was consistent with all of the findings of Srinivasan *et al.* (1991) and appears to be the most likely candidate for a biological speed detectors. There are a number of cells in the known visual motion detection pathways that could accomplish such a basic computation. The Tm1 cell has previously been proposed as a putative speed detector (Higgins, 2004; Rivera-Alvidrez, 2005) both because of its proposed role in the elementary motion detection (EMD) circuit in the fly (Higgins *et al.*, 2004) and its non-directional responses to motion. In the EMD model, the low-pass filtered inputs to the Tm1 cell originate from amacrine cells in the lamina, and reach the Tm1 cell via the intermediary T1 cells. Amacrine cells are laterally connected across optic cartridges (Campos-Ortega and Strausfeld, 1973) and could provide additional low-pass filtered input from nearest neighbor photoreceptors to the T1 cell. In this scenario the Tm1 cell would then be performing an equivalent computation to the NDSe model.

Another model that displayed robust responses in behavioral simulations was the NDMe model. Higgins (2004) noted a weak frequency doubling in the response in a recording from the Tm1 cell (Douglass and Strausfeld, 1995) and suggested that it could be indicative of a multiplication-like operation somewhere in the neuronal pathways providing input to the Tm1 cell. Thus, the Tm1 cell could alternatively be performing an NDMe-like.

Although not as robust, the simplified NDS models also show improved responses over the original model. Simplified non-directional models could be very easily implemented, requiring only high-pass filtering and spatial summation of the photoreceptor outputs. Two potential candidates are the L2 and L4 cells. Although not true for flies, in the honeybee the L2 lamina monopolar cell has collaterals that extend into neighboring optic cartridges Hertel and Maronde (1987). Given the high-pass filtering between the photoreceptor-L2 synapse observed in the fly (Juusola *et al.*, 1995), the honeybee L2 cell may very likely perform an NDSs-like computation. However, if the computation does take place it is not clear that the visual system would use that information for the detection of optic flow. Another lamina cell has the necessary lateral connections to perform such a computation is the L4 cell, present in both flies (Strausfeld and Campos-Ortega, 1973) and honeybees (Hertel and Maronde, 1987).

Previous studies of the NDS models have compared their performance to the HR model (Higgins, 2004, Dyhr and Higgins, unpublished), noting that the HR model could function as a speed estimator when square wave patterns are used in simulations. We were able to verify that the HR model functions as a reasonable speed estimator in response to square wave gratings, but simulations with the HR model using narrowband stimuli showed that the model consistently failed to even stay within the tunnel (data not shown). Therefore

we did not explicitly compare it with the other models. It is also worth noting that none of these proposed modifications will act to improve the speed tuning of the HR model.

The difference between the model responses to square wave versus sinusoidal stimuli raises an important issue for both modeling and behavioral studies. Our experiments demonstrate that they are not identical and can, in some case, yield the opposite result. It also suggests that real world optic flow dependent behaviors may be more dependent on narrowband spatial frequency than previously believed, as past experiment have made general conclusions about the narrowband spatial frequency tuning based on the behavioral responses to square waves. This conclusion is supported by the studies of Srinivasan *et al.* (1991) who found that the centering response was more dependent on the spatial frequency of sinusoidal compared to square wave gratings. Si *et al.* (2003) have also noted that the visual odometry system yields different values between sinusoidal gratings, but that these differences are not apparent when compared to control experiments using checkerboard patterns.

One very important parameter for all of the models were the filter time constants. We used the same high-pass filter time constant of 0.002 seconds based on physiological data from the synapse between the photoreceptor and L2 cell in the fly (Juusola *et al.*, 1995). However, in his original studies of the simplified models, Pant (2007) used a time constant of 0.05 seconds based on previous modeling studies. In this case, the responses of the simplified models, particularly the NDMs and NDMse, are much different from those is presented in this paper, but still not as robust as some of the other models we have discussed.

Finally, we were most interested in the spatial frequency tuning and speed sensitivity of the models and so we performed behavioral simulations of the centering response. Further simulations of the non-directional models to mimic other behaviors, such as flight speed control (Baird *et al.*, 2005) and visual odometry (Srinivasan *et al.*, 1997) may lend further support to the biological relevance of the non-directional models. Previous modeling studies have already suggested algorithms by which to mimic both of these behaviors using other speed sensitive models (Serres *et al.*, 2006; Riabinina and Philippides, 2009).

Acknowledgements Support for this work was provided by the NIH through an NRSA fellowship (1F31NS053433) granted through the NINDS, and by the NCRR. Further support was also provided by the NSF IGERT program and the BIO5 institute through the Biology, Math and Physics Initiative at the University of Arizona.

References

Baird, E., M.V. Srinivasan, S.W. Zhang, and A. Cowling (2005). Visual control of flight speed in honeybees. *J Exp Biol* 208(20): 3895–3905.

Baird, E., M.V. Srinivasan, S.W. Zhang, R. Lamont, and A. Cowling (2006). Visual Control of Flight Speed and Height in the Honeybee. In *From Animals to Animats 9*, pp. 40–51. Springer, Berlin / Heidelberg.

Barron, A. and M.V. Srinivasan (2006). Visual regulation of ground speed and headwind compensation in freely flying honey bees Apis mellifera L. *Journal of Experimental Biology* 209(5): 978–984.

Buchner, E. (1984). Behavioural analysis of spatial vision in insects. In Ali, M.A., editor, *Photoreception and vision in invertebrates*, pp. 561–622. Plenum, New York.

Campos-Ortega, J.A. and N.J. Strausfeld (1973). Synaptic connections of intrinsic cells and basket arborizations in the external plexiform layer of the fly's eye. *Brain Research* 59: 119–136.

Capaldi, E.A., A.D. Smith, J.L. Osborne, S.E. Fahrbach, S.M. Farris, D.R. Reynolds, A.S. Edwards, A. Martin, G.E. Robinson, G.M. Poppy, and J.R. Riley (2000). Ontogeny of orientation flight in the honeybee revealed by harmonic radar. *Nature* 403(6769): 537–540.

Chittka, L. and J. Tautz (2003). The spectral input to honeybee visual odometry. *J Exp Biol* 206(14): 2393–2397.

Dacke, M. and M.V. Srinivasan (2007). Honeybee navigation: distance estimation in the third dimension. *Journal of Experimental Biology* 210(5): 845–853.

Douglass, J.K. and N.J. Strausfeld (1995). Visual motion detection circuits in flies: peripheral motion computation by identified small-field retinotopic neurons. *J. Neurosci.* 15(8): 5596–5611.

Douglass, J.K. and N.J. Strausfeld (1996). Visual Motion-Detection Circuits in Flies: Parallel Direction- and Non-Direction-Sensitive Pathways between the Medulla and Lobula Plate. *J. Neurosci.* 16(15): 4551–4562.

Esch, H.E. and J.E. Burns (1995). Honeybees use optic flow to measure the distance of a food source. *Naturwissenschaften* 82(1): 38–40.

Gilbert, C., D.K. Penisten, and DeVoe. R.D. (1991). Discrimination of visual motion from flicker by identified neurons in the medulla of the fleshfly sarcophaga bullata. *Journal of Comparative Physiology A: Neuroethology, Sensory, Neural, and Behavioral Physiology* 168(6): 653–673.

Hausen, K. (1981). Monocular and binocular computation of motion in the lobula plate of the fly. *Verhandlungen der Deutschen Zoologischen Gesellschaft* pp. 49–70.

Hausen, K. (1982). Motion sensitive interneurons in the optomotor system of the fly. *Biological Cybernetics* 45(2): 143–156.

Hertel, H. and U. Maronde (1987). The structural basis of information processing in the visual system of the bee. In Menzel, R. and A. Mercer, editors, *Neurobiology and Behavior of Honeybees*, pp. 130–140. Springer-Verlag, New York.

Higgins, C.M. (2004). Non-directional motion may underlie insect behavioral dependence on image speed. *Biological Cybernetics* 91(5): 326–332.

Higgins, C.M., J.K. Douglass, and N.J. Strausfeld (2004). The Computational Basis of an Identified Neuronal Circuit for Elementary Motion Detection in Dipterous Insects. *Visual Neuroscience* 21(04): 567–586.

Ibbotson, M.R. (2001). Evidence for Velocity-Tuned Motion-Sensitive Descending Neurons in the Honeybee.

Proceedings: Biological Sciences 268(1482): 2195–2201.

Juusola, M., M. Weckstrom, R.O. Uusitalo, M.J. Korenberg, and A.S. French (1995). Nonlinear models of the first synapse in the light-adapted fly retina. *Journal of Neurophysiology* 74(6): 2538–2547.

Kirchner, W.H. and M.V. Srinivasan (1989). Freely flying honeybees use image motion to estimate object distance. *Naturwissenschaften* 76(6): 281–282.

Lehrer, M., M.V. Srinivasan, S.W. Zhang, and G.A. Horridge (1988). Motion cues provide the bee's visual world with a third dimension. *Nature* 332(6162): 356–357.

Pant, V. (2007). Biomimetic Visual Navigation Architectures for Autonomous Intelligent Systems. Ph.D. diss., University of Arizona, Tucson, Arizona.

Riabinina, O. and A.O. Philippides (2009). A model of visual detection of angular speed for bees. *Journal of Theoretical Biology* 257(1): 61–72.

Rivera-Alvidrez, Z. (2005). Computational Modeling of Neurons Involved in Fly Motion Detection. Master's thesis, University of Arizona, Tucson, Arizona.

Seidl, R. and W. Kaiser (1981). Visual field size, binocular domain and the ommatidial array of the compound eyes in worker honey bees. *Journal of Comparative Physiology A: Neuroethology, Sensory, Neural, and Behavioral Physiology* 143(1): 17–26.

Serres, J., G. Masson, F. Ruffier, and N. Franceschini (2008). A bee in the corridor: centering and wall-following. *Naturwissenschaften* 95(12): 1181–1187.

Serres, J., F. Ruffier, and N. Franceschini (2006). Two optic flow regulators for speed control and obstacle avoidance. In *Biomedical Robotics and Biomechatronics, 2006. BioRob 2006. The First IEEE/RAS-EMBS International Conference on*, pp. 750–757.

Si, A., M.V. Srinivasan, and S.W. Zhang (2003). Honeybee navigation: properties of the visually driven 'odometer'. *J Exp Biol* 206(8): 1265–1273.

Srinivasan, M.V., M. Lehrer, W.H. Kirchner, and S.W. Zhang (1991). Range perception through apparent image speed in freely flying honeybees. *Visual Neuroscience* 6(5): 519–535.

Srinivasan, M.V., M. Poteser, and K. Kral (1999). Motion detection in insect orientation and navigation. *Vision Research* 39(16): 2749–2766.

Srinivasan, M.V. and S.W. Zhang (1997). Visual control of honeybee flight. In Lehrer, M., editor, *Communication in Arthropods*, Vol. 84, pp. 95–113. Birkhäuser Basel, 1 edition.

Srinivasan, M.V., S.W. Zhang, and N. Bidwell (1997). Visually mediated odometry in honeybees. *J Exp Biol* 200(19): 2513–2522.

Srinivasan, M.V., S.W. Zhang, and K. Chandrashekara (1993). Evidence for two distinct movement-detecting mechanisms in insect vision. *Naturwissenschaften* 80: 38–41.

Srinivasan, M.V., S.W. Zhang, M. Lehrer, and T. Collett (1996). Honeybee navigation en route to the goal:

visual flight control and odometry. *J Exp Biol* 199(1): 237–244.

Strausfeld, N.J. and J.A. Campos-Ortega (1973). The l4 monopolar neurone: a substrate for lateral interaction in the visual system of the flymusca domestica (L). *Brain Research* 59: 97–117.

van Hateren, J.H. and C. Schilstra (1999). Blowfly flight and optic flow. II. head movements during flight. *J Exp Biol* 202(11): 1491–1500.

APPENDIX C

The Spatial Frequency Tuning of Optic Flow Dependent Behaviors in the Bumblebee *Bombus impatiens*

Jonathan P. Dyhr and Charles M. Higgins

preparation for submission to

The Journal of Experimental Biology

Journal of Experimental Biology manuscript No.
(will be inserted by the editor)

The spatial frequency tuning of optic flow dependent behaviors in the bumblebee *Bombus impatiens*

Jonathan P. Dyhr[1] and Charles M. Higgins[2,3]

[1]Graduate Program in Neuroscience

[2]Department of Neuroscience

[3]Department of Electrical and Computer Engineering

The University of Arizona

1040 E. 4th Street

Tucson, Arizona 85721-0077

USA

The date of receipt and acceptance will be inserted by the editor

Abstract Insects use visual estimates of flight speed for a variety of behaviors, including visual navigation, odometry, grazing landings, and flight speed control, but the neuronal mechanisms underlying speed detection remain unknown. While many models and theories have been proposed for how the brain extracts the angular speed of the retinal image, termed *optic flow*, we lack the detailed electrophysiological and behavioral data necessary to conclusively support any one model. One key property by which different models of motion detection can be differentiated is their spatio-temporal frequency tuning. Numerous studies have suggested that optic flow dependent behaviors are largely insensitive to the spatial frequency of a visual stimulus, but they have sampled only a narrow range of spatial frequencies, have not always used narrowband stimuli, and have yielded slightly different results between studies based on the behaviors being investigated. In this study, we present a detailed analysis of the spatial frequency dependence of the centering response in the bumblebee *Bombus impatiens* (Cresson, 1863) using sinusoidal and square wave patterns.

1 Introduction

The ability to visually estimate the angular speed of an image on the eye (termed *optic flow*) plays a critical role in many important insect behaviors. In honeybees (*Apis mellifera* L.), these behaviors include: flight

Correspondence to: Jonathan P. Dyhr, jdyhr@email.arizona.edu

speed control, in which the bee will vary its flight speed so as to maintain a constant rate of optic flow (Baird *et al.*, 2005); the *centering response*, in which a bee will fly through the center of a narrow tunnel by matching the apparent speed of the walls (Kirchner and Srinivasan, 1989); depth perception, in which honeybees will use the relative speed of objects in the environment to judge their distance (Srinivasan *et al.*, 1989); and visual odometry, in which a honeybee will integrate the apparent image speed experienced during flight to estimate the distance traveled (Esch and Burns, 1995; Srinivasan *et al.*, 1996). Given the importance of visual speed estimation to insect behavior, it is surprising that we know little of the underlying neuronal mechanisms. While many different models have been proposed, both correlation-type (Higgins, 2004; Riabinina and Philippides, 2009) and gradient-based (Srinivasan *et al.*, 1991), none possesses strong electrophysiological and anatomical support while still being sufficiently robust to match the results from behavioral experiments.

David (1982) provided the first evidence of a speed-tuned motion detection system in insects. In his studies, *Drosophila virilis* (Sturtevant, 1916) flew through a horizontally oriented cylindrical wind tunnel. The walls of the tunnel held a 'barber's pole' pattern that, when rotated, created the illusion of moving bars. He found that flies would 'hover' against a headwind when the surrounding pattern was moved at a specific speed, regardless of whether the striped pattern had a wavelength of 40 or 72 degrees. Studies in honeybees provided conclusive evidence for the existence of a small field optic flow detection system that is relatively insensitive to direction (Srinivasan *et al.*, 1993; Dacke and Srinivasan, 2007) and spatial frequency (Srinivasan *et al.*, 1991, 1997; Si *et al.*, 2003; Baird *et al.*, 2005). These properties clearly differentiated the visual speed estimation system from the wide-field, directionally-selective mechanism underlying the optomotor response described by the Hassenstein-Reichardt (HR) model (1956).

The sensitivity of these behaviors to speed has created difficulty in identifying the mechanisms underlying visual speed estimation because overwhelming biological evidence supports the use of correlation-type detectors that are not generally speed-tuned (Buchner, 1984; Borst, 2007). This has led to many competing theories as to how the insect brain computes optic flow, including gradient-based detectors (Srinivasan *et al.*, 1991), modified correlation detectors (Zanker *et al.*, 1999; Higgins, 2004; Riabinina and Philippides, 2009), combinations of multiple correlators with different spatio-temporal optima (Srinivasan *et al.*, 1999), the adaptation of correlation model time constants in response to motion (O'Carroll *et al.*, 1996), 'token-matching' algorithms measuring the time delay between two subsequent photoreceptor activations (Blanes, 1986; Aubépart and Franceschini, 2007) and arguments for the sufficiency of the HR model in real world scenarios (Dror *et al.*, 2001).

One key response property that can be used to distinguish between many of these models is their spatio-temporal frequency tuning. Gradient models, token-matching schemes, and population codes all encode the angular speed of the image independent of the spatial frequency, whereas the modified correlation detectors

retain some spatial frequency dependence. Behavioral studies generally suggest that optic flow dependent behaviors are not dependent on the spatial frequency of a stimulus, but there has been some evidence from honeybees and *Drosophila* that this may not be entirely correct (Srinivasan *et al.*, 1991; Fry *et al.*, 2009).

Further compounding the problem is the lack of electrophysiological data from the early visual pathways. While velocity-sensitive descending neurons have been reported in the ventral nerve cord of honeybees (Ibbotson, 2001), the spatial frequency dependence of potentially speed-tuned neurons in the optic lobes has not been comprehensively investigated. Most of our understanding of motion detection in insects has come from studies of lobula plate tangential cells (LPTCs, Hausen, 1981, 1982) that are believed to underlie optomotor behaviors (Borst and Bahde, 1987; Egelhaaf and Borst, 1993).

The goal of the present work was to acquire a detailed spatial frequency tuning of the optic flow system using the centering response of the bumblebee, *Bombus impatiens* (Cresson, 1863). We chose the centering response because it depends on the difference between the optic flow estimates of each eye, enabling the direct comparison of speed estimates from two different patterns. Furthermore, it is not dependent on cues from the dorsal or ventral visual fields and is an easily measured behavior that requires little subjective interpretation from the observer.

Although the bulk of behavioral experiments have been performed using honeybees, bumblebees are closely related and display a rich visual ecology and complicated foraging behaviors (Osborne *et al.*, 1999). In addition, bumblebees have larger eyes and better visual acuity than honeybees (Spaethe and Chittka, 2003), allowing us to acquire a broader spatial frequency tuning curve of the underlying speed estimation mechanism. They are also well suited for the electrophysiological investigations that will be necessary in order to undercover the neuronal circuitry responsible for the visual estimation of speed (Riveros and Gronenberg, 2009; Paulk and Gronenberg, 2008; Paulk *et al.*, 2008). Finally, the large size variations in bumblebees provide opportunities to explore the effects of optical variation on motion related behaviors (Spaethe and Chittka, 2003) and their larger size makes them more amenable to remote tracking (Riley *et al.*, 1999; Osborne *et al.*, 1999).

2 Methods

Experiments were performed in a 120 cm long, 20 cm wide, 30 cm high tunnel constructed of transparent acrylic sheets (Figure 1). Holes were cut in the acrylic walls at both ends of the tunnel so that a bumblebee colony (*Bombus impatiens*; Biobest, Leamington, Ontario, CA) and a feeder box could be connected at opposite ends. The feeder and colony were connected to the tunnel via gated, clear plastic tubes. These entrances were marked by cork perches from which the bees could take off and land. The bottom of the tunnel was lined with white paper in order to maximize the contrast between the bees and the floor of the tunnel for an overhead camera. The only available food was in the feeder box and consisted of two containers

full of BIOGLUC® sugar solution (Biobest, CA). The entire experimental setup was housed inside a climate controlled room with an average temperature of 24°C. The lighting in the room was provided by multiple incandescent lights, which were on for eight hours each day. Two different colonies were used over the course of the experiments.

The inside walls of the tunnel were lined with sinusoidal or square wave gratings of different spatial frequencies and contrasts, or with a uniform gray pattern. Each pattern was printed onto a single length of photo paper using a high quality inkjet poster printer (Hewelett Packard Designjet) and cut to a length of 120 cm and width of 30 cm. We tested sinusoidal patterns of spatial frequency 0.05, 0.1, 0.15, 0.17, 0.2, 0.3, 0.4, 0.6, 0.8, 1.2 and 1.6 cycles/cm with apparent spatial frequencies of 0.016, 0.023, 0.03, 0.032, 0.037, 0.053, 0.08, 0.11, 0.14, 0.21 and 0.28 cycles/degree when viewed from the center of the tunnel. We convert spatial frequency into angular units as measured from the center of the tunnel when comparing our results to those of previous studies. In data plots, the uniform gray pattern is labeled as having a spatial frequency of zero. We also printed square wave gratings at two sample frequencies of 0.15 and 0.6 cycles/cm (0.03 and 0.11 cycles/degree respectively) and low contrast sinusoidal patterns with a spatial frequency of 0.15 cycles/cm (0.03 cycles/degree). These sample frequencies were chosen because they were well within the resolvable range, but still different enough to potentially yield response differences. All gratings were printed at the maximum achievable Michelson contrast of 0.6 (limited by the printer) unless otherwise noted, where the Michelson contrast C is defined as follows

$$C = \frac{I_{max} - I_{min}}{I_{max} + I_{min}} \tag{1}$$

where I_{max} and I_{min} are the maximum and minimum luminance of the pattern. The average luminance in the tunnel was approximately 380 lux. Patterns were taped to the inside walls of the tunnel and the bees were allowed to forage through the tunnel when experiments were not being run.

A high definition digital video camera (Canon Vixia HG20) was situated 140.5 cm above the tunnel and captured a one meter section of the tunnel. Video was recorded at 30 frames per second with a resolution of 1440 x 1080. For each experimental trial, video was recorded continuously for 30-120 minutes.

Video sequences were first edited to include only sections in which bees were flying through the tunnel. The edited video clips were then analyzed frame-by-frame in Matlab (The Mathworks, Natick, MA) using the image processing toolbox. Due to their exceedingly large size, the images were converted to grayscale and downsampled in size by a factor of two, yielding a resolution of approximately 1.3 mm/pixel at the middle heights of the tunnel. Because the floor was covered in white paper, the bee created a high contrast black object against a white background. To pick out the bumblebees as bright features against a black background, the contrast in each frame was first inverted, then the image was spatially band-pass filtered to eliminate any noise. The image was then passed through a simple threshold operation, leaving only the

clear, high contrast objects (bumblebees). The centroid, major axis, orientation angle and size of each bee for each frame was calculated and time-stamped.

Once we had the positions of the bees at each time point, we reconstructed the paths of individual bees using freely available tracking software (Crocker and Grier, 1996; Blair and Dufresne, 2007). For each flight path we calculated the mean lateral position, speed and size of the bee. Because we were only interested in paths in which the bees flew directly and continuously across the length of the tunnel, we selected only the paths from bees moving at a minimum speed of 26 cm/s whose body angle relative to the center of tunnel never exceeded 60°.

The automated tracking of the bees did not allow us to identify the number of individual bees recorded during experiments. In order to ensure that we were not simply recording the paths from only one or two individual bees, we tagged individual bees for a small subset of experiments and counted the number of individual bees recorded during single trials. These tests indicated that the minimum number of individuals recorded over a single trial was no less than six, but generally ranged between 10 to 14 individuals.

Statistical analyses of the mean lateral flight paths and speeds of the bees for each experimental condition were performed in Matlab. One-way ANOVA comparisons were used to determine the significance of the results and the Tukey-Kramer method (Kramer, 1956) was used when performing multiple comparisons between the trials.

3 Results

Before testing the narrowband spatial frequency tuning of the centering response, we first attempted to identify the range of perceptible and behaviorally relevant spatial frequencies. The perception of high spatial frequencies is limited by the spatial resolution of the eye (Land and Nilsson, 2002), while very low spatial frequencies change so gradually as the bees fly that they are unlikely to be perceived as periodic patterns and may be removed by high-pass temporal filtering in the visual processing pathways. In order to test the upper resolution limits, we lined one wall of the tunnel with a sinusoidal grating and the opposite wall with a uniform gray pattern. If the bees were unable to resolve the grating pattern, therefore perceiving two gray walls of equal intensity, then we would expect them to fly through the center of the tunnel on average. If, however, they were able to resolve the gratings one would expect them to fly closer to the gray wall because it would provide fewer motion cues and therefore appear to be moving slower.

The results plotted in Figure 2a show the mean lateral positions of the bees as a function of the spatial frequency of one wall. Two control trials in which the walls were lined with the same sinusoidal patterns are provided for comparison. At low spatial frequencies the flight paths of the bees are strongly biased towards the gray wall. This lateral path bias gradually decreases with increasing spatial frequency until it eventually disappears, presumably because the bees are no longer able to resolve the pattern.

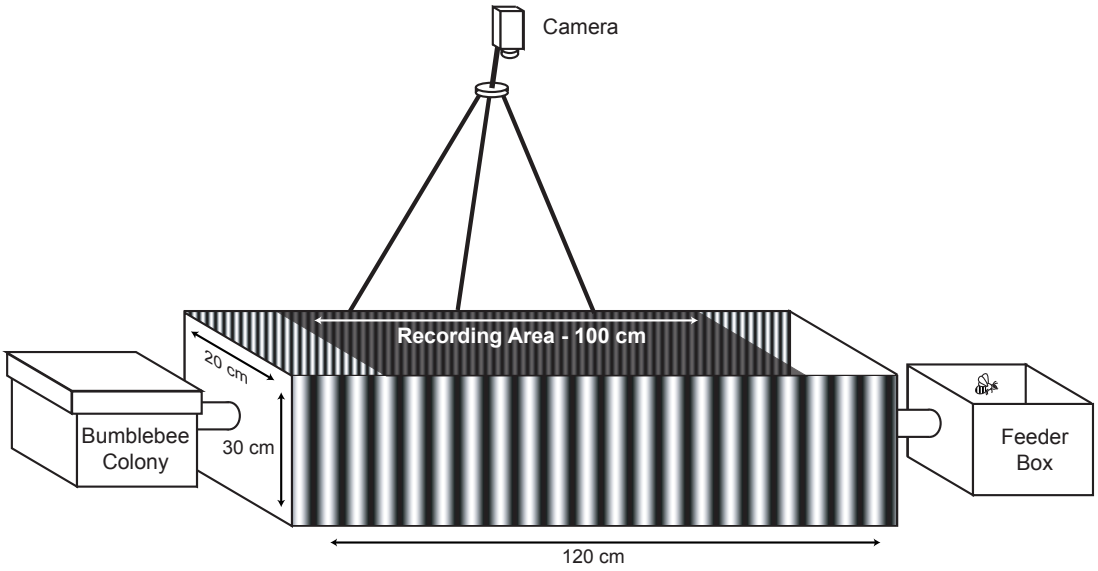

Fig. 1 A bumblebee colony was connected directly to a clear acrylic tunnel through which the bees navigated to reach the sugar solution housed inside of the feeder box. Bees traveling through the shaded region of the tunnel were recorded using a tripod-mounted video camera situated above the tunnel. The inside of the walls of the tunnel were lined with different patterns; in the case illustrated, two sinusoidal gratings of different spatial frequencies.

In addition to the changes in the mean lateral position, the average flight speed increases with the spatial frequency of one wall (Figure 2b). The changes in the flight speed are much smaller and less significantly different than the lateral path deviations. The relatively weak effects of spatial frequency on flight speed may be due to the fact that motion signals from the ventral visual field remains constant across trials. Thus, while the bees are seeing fewer motion cues from the walls, the variations in the global optic flow estimate are lower than the differences in the optic flow estimates between eyes. Honeybees are known to use cues from the ventral visual field for both flight speed control (Baird *et al.*, 2006) and visual odometry (Si *et al.*, 2003).

The bees fly at much higher speeds when one wall holds a high spatial frequency pattern as opposed to both walls holding gray patterns (zero spatial frequency). Similar results have been reported previously (Srinivasan *et al.*, 1991; Baird *et al.*, 2005) and it has been proposed that adaptation to the low contrast gray pattern may enable the bees to use otherwise invisible motion cues. This can also help explain why the bees appeared to be acquiring motion cues from the floor despite it being lined with blank white paper. Baird *et al.* (2006) previously noted the same contrast adaptation when the floor of a tunnel is lined with a blank white pattern. When replaced with a high contrast axially striped pattern the honeybees will actually

fly through a tunnel faster, suggesting they are detecting fewer motion cues from the axial stripes than from the blank floor.

Also of note is that bees were less likely to fly through the entire length of the tunnel when one wall held a uniform gray pattern. Instead they would repeatedly fly through a small section of the tunnel, orient themselves, and loop back. This behavior would be repeated, with the bee flying progressively farther into the tunnel each time, until it would finally fly to the opposite end of the tunnel. The lateral variation in the flight paths was much greater in these experiments compared to trials with grating patterns on both walls.

Next, we tested the spatial frequency tuning of the centering response by lining the tunnel walls with sinusoidal (narrowband) patterns of different spatial frequencies. We used only spatial frequencies that appeared to be resolvable from the gray wall experiments, such that the mean lateral position of the bee was significantly different from the control trials. Representative data of the results of these experiments for two sample spatial frequencies of 0.15 and 0.6 cycles/cm are shown in Figure 3. These two frequencies were chosen because they were comfortably within the resolvable range of the insect optics and allowed for direct comparison between the behavioral responses at high and low frequencies.

All comparisons between different patterns were made over a five-fold range of spatial frequencies between 0.15 and 0.8 cycles/cm. We observed no significant deviations in the lateral flight paths when any combination of 0.15 to 0.4 cycles/cm gratings were compared, such that the centering response was insensitive to narrowband spatial frequency varying by a factor of 2.5. For spatial frequencies outside this range we observed consistent average path deviations towards the wall with the higher spatial frequency.

As can be seen in Figure 3a, the two tuning curves have a similar shape but the 0.6 cycle/cm curve is shifted in the positive direction. The fact that the bees are flying closer to the high spatial frequency wall suggests that the bees are acquiring a lower speed estimate from the higher frequency patterns. Even when the spatial frequency of one wall is relatively high (0.6 cycles/cm), the curve still remains relatively flat between 0.15 - 0.6 cycles/cm. This shift is also apparent in the plot of average flight speed (Figure 3), although the flight speeds are much more variable and the differences are not always significant.

The optics of the bee's eye attenuate the contrast of high spatial frequency patterns on the bee's retina (Land and Nilsson, 2002). We wanted to determine whether the spatial frequencies used in our centering experiments were close to the high spatial frequency cutoff. To accomplish this, we lined one wall of the tunnel with a high frequency sinusoidal grating (0.6 cycles/cm) with a contrast of 0.6 and the other wall with low frequency sinusoidal gratings (0.15 cycles/cm) with contrasts of 0.6, 0.3, 0.2, 0.1 and 0.05 (Figure 4). If the 0.6 cycles/cm grating was close to the cutoff frequency we would expect the previously observed flight path bias of the bee to disappear as a result of contrast attenuation. The results demonstrate that the path bias is decreased, but not eliminated, at extremely low contrast making it unlikely that the flight path differences seen at high spatial frequencies are due to attenuation by the optics.

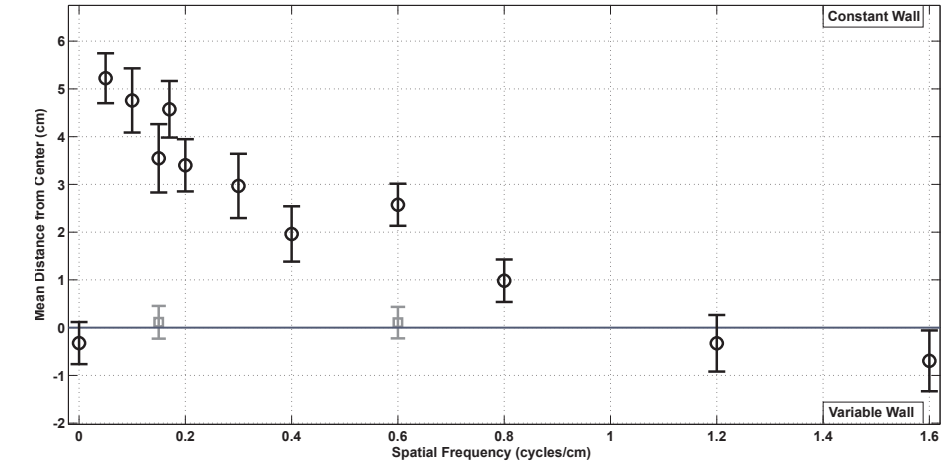

(a)

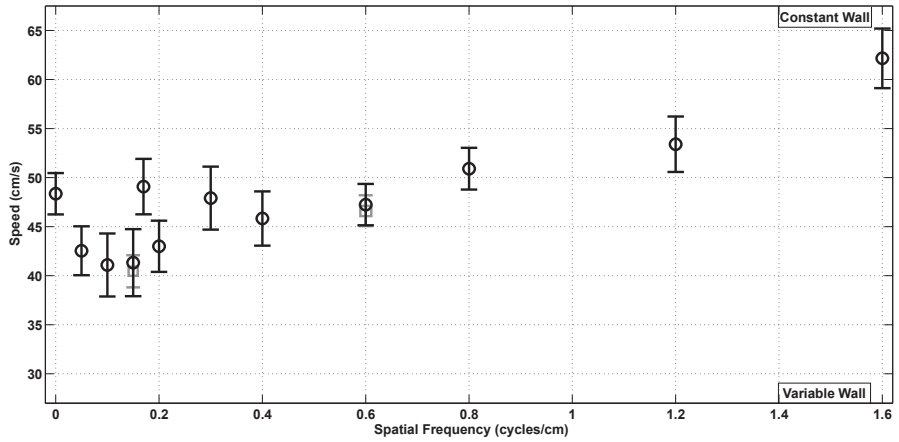

(b)

Fig. 2 Gray wall experiments. (a) The mean lateral distance from the center of the tunnel (black circles) is plotted for bees flying through a tunnel lined with a uniform gray pattern on one wall (constant wall) and a sinusoidal pattern of varying spatial frequency on the opposite wall (variable wall). For comparison, two control trials in which both walls carried the same sinusoidal grating (dark gray squares) are also plotted. (b) The average flight speed is plotted versus spatial frequency (black circles) and compared to control trials (black squares). Error bars denote the 95% confidence intervals between groups derived from a Tukey-Kramer multiple comparison test on the one-way ANOVA results. The number of paths analyzed was $n = 1139$. Zero spatial frequency represents a uniform gray pattern.

The large number of experiments in the present work required that half of the contrast experiments be run with a second colony of bees that were individually much larger in size. The results for the two colonies are qualitatively the same, but the magnitude of the lateral path deviations were significantly larger for the second colony. The largest path deflections were seen for contrasts of 0.2 and 0.3, which used bees from the

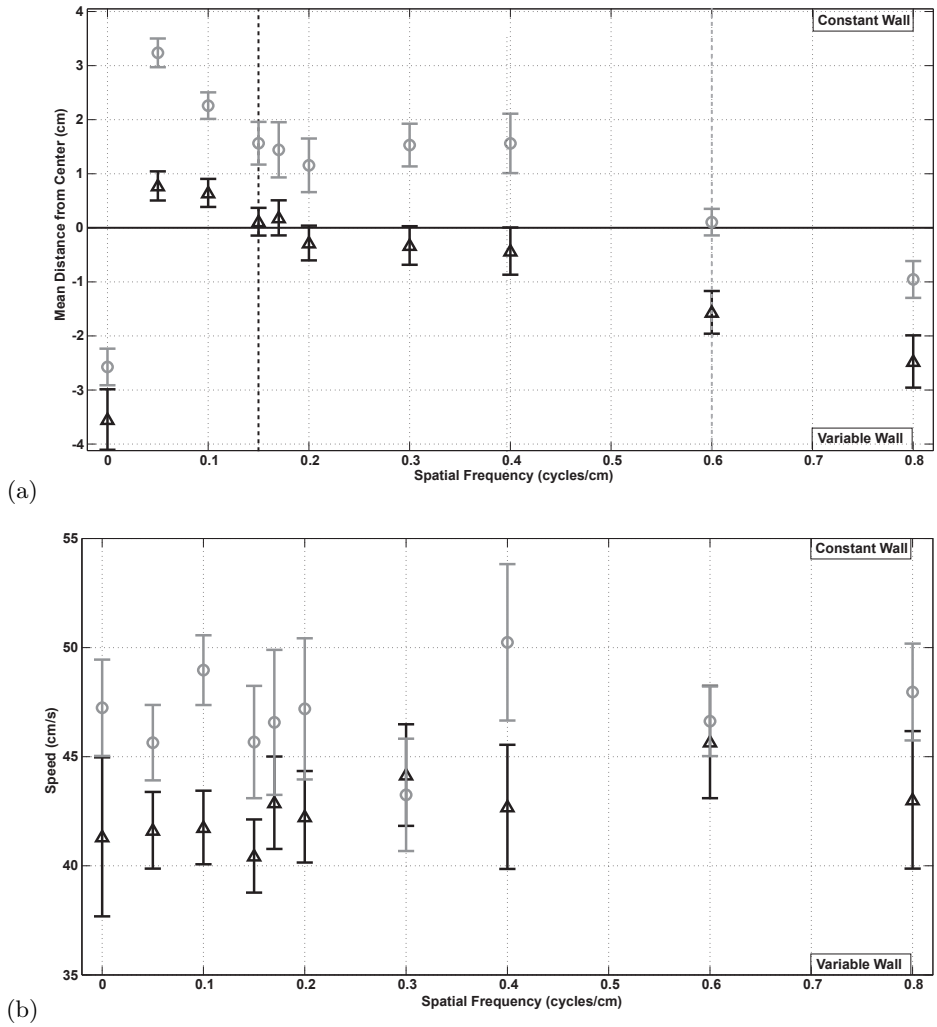

Fig. 3 Spatial frequency tuning curves of the centering response. (a) The dependence of the mean lateral flight position on spatial frequency is compared for experiments in which one pattern was held constant (constant wall) at either 0.15 cycles/cm (black triangles) or 0.6 cycles/cm (gray circles) while the spatial frequency of the opposite wall was varied. The dashed lines indicate the predicted zero crossings for when both walls hold the same pattern of either 0.15 cycles/cm (black) or 0.6 cycles/cm (gray). (b) The average speed of the bees is plotted versus the spatial frequency of the variable wall. Error bars represent the 95% confidence intervals for $n = 1961$ unique paths.

second larger colony. Because of this observation, we reanalyzed the data from the first colony by calculating the average size of all of the bees and splitting them into two groups based on whether they were larger or smaller than average. Bees from the larger group did not show contrast-dependent path variations, even when the contrast was 0.05 (data not shown). In contrast, the mean distance from the center of the tunnel was significantly reduced for the smaller bees. However, there was still a significant difference between the mean

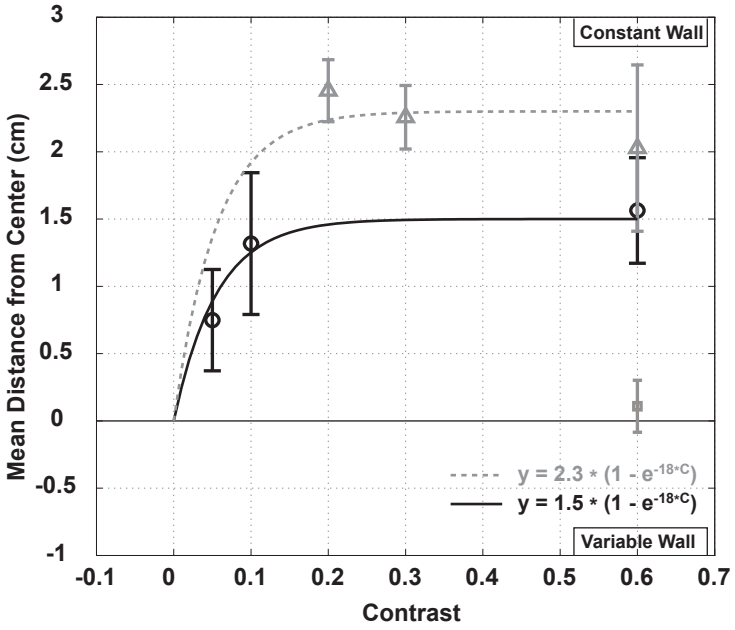

Fig. 4 Contrast sensitivity of the centering response. The mean distance from the center of the tunnel when one wall was lined with a 0.6 cycles/cm sinusoidal, 0.06 contrast pattern (constant wall) and the other wall was lined with a 0.15 cycle/cm gratings with varying contrast. The black circles and dark gray triangles are data collected from the first and second colonies, respectively. The single black square denotes the combined mean lateral positions for control in which both walls held either 0.6 cycles/cm or0.15 cycles/cm patterns. The lines denote two exponential functions fit to the data of either the first (black solid line) or the second (dashed gray line) colony. The Error bars represent the 95% confidence intervals for $n = 942$ paths.

lateral positions of the bees in the second colony when compared to the larger bees from the first colony, suggesting that there is genetic variability between the bees in the magnitude of the centering response.

Finally, previous experiments using square wave gratings failed to uncover the spatial frequency dependence of the centering response, although a weak dependence was observed for sinusoidal gratings (Srinivasan *et al.*, 1991). In order to determine if bees respond differently to square wave versus sinusoidal stimuli, we lined the walls of the tunnel with different combinations of sinusoidal and square wave patterns with spatial frequencies of 0.15 and 0.6 cycles/cm. As can be seen in Figure 5, the previously observed spatial frequency dependence is still present when the walls are lined with square wave gratings, but it is significantly reduced. The bees uniformly perceive the square wave patterns as moving slower as evidenced by the path biases towards the wall carrying the square wave grating. Based on our previous results, this suggests that the bees perceive the square wave patterns as having higher spatial frequency content than a sinusoidal grating of the same spatial frequency. Paradoxically, the path bias between two square wave patterns is lower than that

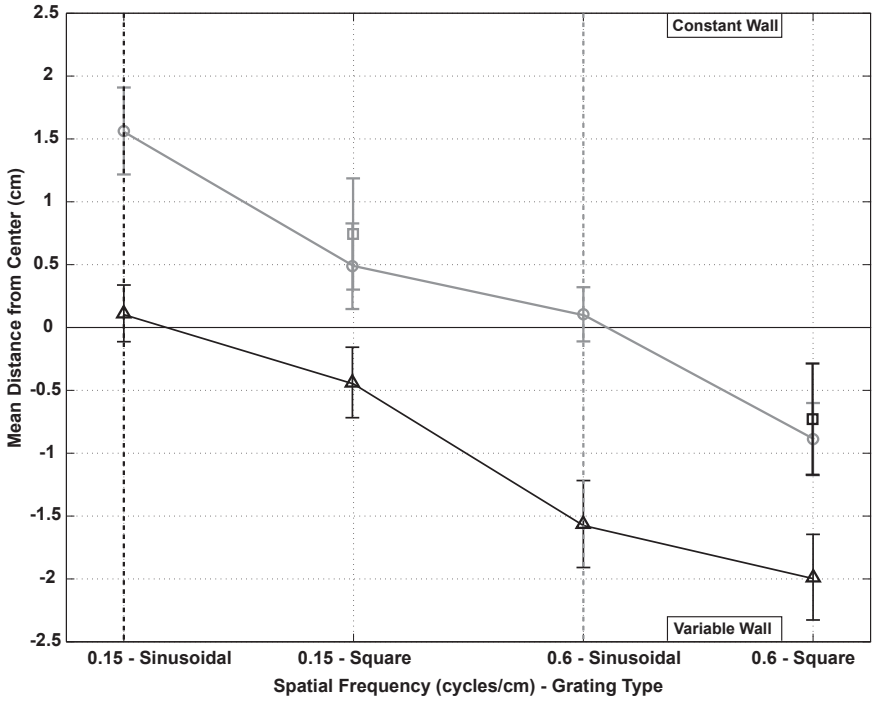

Fig. 5 Response differences between square wave and sinusoidal stimuli. The mean distance from the center of the tunnel is plotted when the constant wall holds a sinusoidal pattern with a spatial frequency of 0.15 cycles/cm (black triangles, solid line) or 0.6 cycles/degree (dark gray circles, solid line) while the variable wall is lined with square wave and sine wave gratings of different spatial frequencies. The squares represent the mean distance from the center when the constant wall holds either a 0.15 cycles/cm (black) or a 0.6 cycles/cm (gray) square grating. Vertical dashed lines indicate the predicted zero crossing when the constant wall holds a 0.15 cycles/cm (black) or 0.6 cycles/cm (gray) sinusoidal pattern. Error bars represent the 95% confidence intervals for $n = 1091$ paths.

between two sinusoidal gratings the opposite of what we observe for sinusoidal gratings. The trend from the narrowband spatial frequency comparisons was that the magnitude of the path deviations increased with spatial frequency. These results suggest that, despite the high-pass filtering inherent in the insect compound eye, square wave patterns are not perceived as narrowband stimuli by insects. Similar results have been observed in more controlled studies of the optomotor response (McCann and MacGinitie, 1965).

4 Discussion

Our experiments indicate that the centering response, and by extension the underlying optic flow system, are dependent on the spatial frequency of a stimulus. Although these results appear to contradict the conclusions of previous studies, the apparent discrepancies can be explained by differences in the behavioral measures and visual stimuli between studies.

Previously, the most comprehensive studies of the narrowband spatial frequency sensitivity of the optic flow system were those of Baird *et al.* (2005). They trained honeybees to forage within a narrow tunnel and measured their flight speed when the tunnels walls were moved with or against the direction of flight. They did not observe any significant variation in flight speed when both walls were lined with sinusoidal gratings of frequencies of either 0.03, 0.06 or 0.11 cycles/degree.

Our results indicate that changes in flight speed provide a much weaker measure of the perceived optic flow than the centering response. It has been previously observed that bees use optic flow information from both the lateral and ventral visual fields (Srinivasan *et al.*, 1997; Si *et al.*, 2003), even when the floor is lined with a blank white pattern (Baird *et al.*, 2006). Hence, the bee's flight speed likely depends on the optic flow information from the entire visual field, making it difficult to make definitive conclusions about the spatial frequency sensitivity based only on flight speed. In contrast, the centering response relies on a direct comparison of the optic flow from each eye providing a more accurate measure of the perceived differences. Furthermore, Baird *et al.* (2005) noted that honeybees do not adjust their flight speed until the optic flow deviates by 10-15 degrees/s from a preferred rate, raising the possibility that spatial frequency dependent changes in the optic flow estimate may be too subtle to significantly impact flight speed.

Past studies of the centering response by Srinivasan *et al.* (1991) suggested that the optic flow estimate depended weakly on spatial frequency. They tested square wave and sinusoidal gratings with angular spatial frequencies of 0.017, 0.025 or 0.044 cycles/degree and 0.022, 0.038 or 0.07 cycles/degree, respectively. They found a significant change in the lateral flight path only for mismatched sinusoidal gratings of 0.022 and 0.07 cycles/degree, but they did not compare square wave gratings to sinusoidal patterns. This is in general agreement with our results in which we found that the spatial frequency dependence of the centering response only becomes apparent for frequencies outside of the 0.03 - 0.08 cycles/degree range.

Two studies have tested the spatial frequency sensitivity of the visual odometer. Srinivasan *et al.* (1997) trained honeybees to collect a sugar reward from a tunnel holding a square wave grating with a spatial frequency of 0.05 cycles/degree. In test trials in a tunnel with no feeder, they found that the bees searched at the former location of the feeder regardless of whether the spatial period was halved or doubled, resulting in spatial frequencies of 0.1 and 0.03 cycles/degree respectively. We did not observe a significant difference in the centering response when a sinusoidal grating of 0.053 cycles/deg was compared to gratings either 0.03 or 0.08 cycles/deg. Because we observed smaller path deviations when using square wave gratings, we believe our observations are consistent with these results.

Si *et al.* (2003) measured the distance estimates of bees, as measured by the duration of the waggle dance, foraging in narrow tunnels. They lined both walls of the tunnel with sinusoidal gratings of either 0.02, 0.03 or 0.06 cycles/degree and noted a significant *decrease* in the mean waggle duration for the 0.02 cycles/degree pattern versus the other higher frequency sinusoids. However, none of these estimates were significantly

different from the checkerboard control, leading them to conclude that the visual odometer was insensitive to spatial frequency. The relative decrease in the distance estimate for the low spatial frequency grating is the opposite of what would be predicted by both our results and those of Srinivasan *et al.* (1991), in which the apparent speed of the stimulus appeared to increase with decreasing spatial frequency. We are unable to reconcile these results with ours aside from the statement by Si *et al.* (2003) that the distances interpreted from the waggle dance appeared to be less accurate than the actual odometer. It is therefore possible that the human interpretation of the waggle dance was not precise enough to measure differences in the speed estimates.

Fry *et al.* (2009) have used 'one parameter open-loop' experiments to probe the spatio-temporal tuning of the speed estimation system in *Drosophila*. In their experimental setup, they induced a fly to hover against a headwind by modulating the speed of the a visual stimulus projected onto the walls of a wind tunnel. Once the fly was stationary, they would move the pattern at fixed spatial and temporal frequencies and measure the fly's acceleration response. They observed a plateaued spatio-temporal frequency tuning such that, for stimuli moving at a set speed, the acceleration responses were relatively constant for the midrange spatial frequencies, but dropped off at both higher and lower ends. Our results are qualitatively similar, but cannot be directly compared due to the lower resolution of the *Drosophila* compound eye.

We also attempted to identify the resolution limit of the optic flow system by comparing different sinusoidal gratings to a uniform gray pattern. Our results suggest that spatial frequencies greater than 0.14 cycles/degree are not resolved by the optic flow system, corresponding to a minimum spatial wavelength of 7 degrees. Other studies have reported that the minimum angular separation at which bumblebees (*Bombus terrestris* L.) can still resolve two points is 3.5 degrees for large bees and 7 degrees for small bees (Spaethe and Chittka, 2003). Studies in honeybees have reported a minimum angular separation of 5 degrees (Giurfa *et al.*, 1996), while the minimum resolvable spatial wavelength of a moving grating is 2.6 degrees (Hecht and Wolf, 1929).

Our estimate of the minimum resolvable spatial wavelength for the centering response is much higher than would be predicted from these previous studies. In free flight experiments, the apparent spatial frequency of a grating changes with the bee's distance from the wall. From our data, the bees fly closer to a high spatial frequency pattern, thus lowering the apparent spatial frequency because the optic flow estimate varies inversely with spatial frequency. This would result in an overestimate of the minimum resolvable wavelength, supporting our conclusion that the bees were resolving the gratings in our spatial frequency comparison experiments.

The sensitivity and spatial resolution of the eye has previously been shown to vary with size in bumblebees (Spaethe and Chittka, 2003). We observed a similar result in our contrast experiments, in which there was a size-dependent change in behavior when the pattern contrast of one wall was decreased to 0.05. We concluded

that the contrast of the high spatial frequency pattern was being attenuated because it was close to the high spatial frequency cutoff of the optics for the smaller honeybees. However, we did not observe any size related differences in any of our other spatial frequency comparison experiments, some of which used higher spatial frequencies (data not shown). This raises the possibility that the decreased sensitivity to light of the smaller honeybees may be partially responsible for these behavioral differences.

Another interesting result was that the bumblebees perceived square wave as moving slower than sinusoidal gratings of the same wavelength. Our results suggest that there is a subtle but significant difference between the bees' perception of square and sine wave gratings indicating that the higher harmonics present in square-wave patterns are not entirely filtered out by the optics of the visual system.

Although many of the experiments with which we compared data were conducted on honeybees, we performed our experiments on bumblebees. While some differences between our results and previous studies may be due to species-specific variation, we believe that these differences are minimal. Both organisms rely on visual estimates of distance traveled while foraging, fly at similar heights and speeds when foraging (Osborne *et al.*, 1999; Capaldi *et al.*, 2000), and have similar optic capabilities (Spaethe and Chittka, 2003). Optic flow related behaviors have been observed in a wide range of insects, including flies (David, 1982; Fry *et al.*, 2009), wasps (Ugolini, 1987) and stingless bees (Hrncir *et al.*, 2003), such that the estimation of optic flow appears to be an elementary operation of the visual system.

Finally, our in-depth analysis of the spatial frequency dependence of the visual speed estimation system provides ample evidence with which to improve future modeling studies. Our results show that while the optic flow system is speed-tuned for certain ranges of spatial frequencies, the estimate varies inversely with spatial frequency outside of this range. These results are consistent with the non-directional speed estimation models of Higgins (2004), Rivera-Alvidrez (2005), Pant (2007) and Dyhr and Higgins (unpublished) all of which have speed estimates that drop off at high spatial frequencies. These also match other properties of the visual speed estimation system, such as being small-field models and sensitive to motion regardless of direction.

Acknowledgements The authors would like to thank Wulfila Gronenberg and Andre Riveros for their invaluable assistance, guidance and suggestions. Support for this work was provided by the NIH primarily through an NRSA predoctoral fellowship (1F31NS053433) granted by the NINDS with additional support coming from the NCRR (grant number 5R01RR008688-21).

References

Aubépart, F. and N. Franceschini (2007). Bio-inspired optic flow sensors based on FPGA: application to Micro-Air-Vehicles. *Microprocessors and Microsystems* 31(6): 408–419.

Baird, E., M.V. Srinivasan, S.W. Zhang, and A. Cowling (2005). Visual control of flight speed in honeybees. *Journal of Experimental Biology* 208(20): 3895–3905.

Baird, E., M.V. Srinivasan, S.W. Zhang, R. Lamont, and A. Cowling (2006). Visual Control of Flight Speed and Height in the Honeybee. In *From Animals to Animats 9*, pp. 40–51. Springer, Berlin / Heidelberg.

Blair, D. and E. Dufresne (2007). *http://physics.georgetown.edu/matlab/* .

Blanes, C. (1986). Appareil visuel elementaire pour la navigation "á vue" dun robot mobile autonome. DEA Thesis, Universite D'Aix-Marseille II, pp. 57.

Borst, A. (2007). Correlation versus gradient type motion detectors: the pros and cons. *Philosophical Transactions of the Royal Society B: Biological Sciences* 362(1479): 369–374.

Borst, A. and S. Bahde (1987). Comparison between the movement detection systems underlying the optomotor and the landing response in the housefly. *Biological Cybernetics* 56(4): 217–224.

Buchner, E. (1984). Behavioural analysis of spatial vision in insects. In Ali, M.A., editor, *Photoreception and vision in invertebrates*, pp. 561–622. Plenum, New York.

Capaldi, E.A., A.D. Smith, J.L. Osborne, S.E. Fahrbach, S.M. Farris, D.R. Reynolds, A.S. Edwards, A. Martin, G.E. Robinson, G.M. Poppy, and J.R. Riley (2000). Ontogeny of orientation flight in the honeybee revealed by harmonic radar. *Nature* 403(6769): 537–540.

Crocker, J.C. and D.G. Grier (1996). Methods of digital video microscopy for colloidal studies. *Journal of Colloid and Interface Science* 179(1): 298–310.

Dacke, M. and M.V. Srinivasan (2007). Honeybee navigation: distance estimation in the third dimension. *Journal of Experimental Biology* 210(5): 845–853.

David, C. T. (1982). Compensation for height in the control of groundspeed byDrosophila in a new, barber's pole wind tunnel. *Journal of Comparative Physiology A: Neuroethology, Sensory, Neural, and Behavioral Physiology* 147(4): 485–493.

Dror, R.O., D.C. O'Carroll, and S.B. Laughlin (2001). Accuracy of velocity estimation by Reichardt correlators. *Journal of the Optical Society of America A* 18(2): 241–252.

Egelhaaf, M. and A. Borst (1993). A look into the cockpit of the fly: visual orientation, algorithms, and identified neurons. *The Journal of Neuroscience* 13(11): 4563–4574.

Esch, H.E. and J.E. Burns (1995). Honeybees use optic flow to measure the distance of a food source. *Naturwissenschaften* 82(1): 38–40.

Fry, S.N., N. Rohrseitz, A.D. Straw, and M.H. Dickinson (2009). Visual control of flight speed in Drosophila melanogaster. *Journal of Experimental Biology* 212(8): 1120–1130.

Giurfa, M., M. Vorobyev, P. Kevan, and R. Menzel (1996). Detection of coloured stimuli by honeybees: minimum visual angles and receptor specific contrasts. *Journal of Comparative Physiology A: Neuroethology, Sensory, Neural, and Behavioral Physiology* 178(5): 699–709.

Hausen, K. (1981). Monocular and binocular computation of motion in the lobula plate of the fly. *Verhandlungen der Deutschen Zoologischen Gesellschaft* pp. 49–70.

Hausen, K. (1982). Motion sensitive interneurons in the optomotor system of the fly. *Biological Cybernetics* 45(2): 143–156.

Hecht, S. and E. Wolf (1929). The visual acuity of the honey bee. *Journal of General Physiology* 12(6): 727–760.

Higgins, C.M. (2004). Non-directional motion may underlie insect behavioral dependence on image speed. *Biological Cybernetics* 91(5): 326–332.

Hrncir, M., S. Jarau, R. Zucchi, and F.G. Barth (2003). A stingless bee (textitMelipona seminigra) uses optic flow to estimate flight distances. *Journal of Comparative Physiology A: Neuroethology, Sensory, Neural, and Behavioral Physiology* 189(10): 761–768.

Ibbotson, M.R. (2001). Evidence for Velocity-Tuned Motion-Sensitive Descending Neurons in the Honeybee. *Proceedings of the Royal Society of London. Series B, Biological Sciences* 268(1482): 2195–2201.

Kirchner, W.H. and M.V. Srinivasan (1989). Freely flying honeybees use image motion to estimate object distance. *Naturwissenschaften* 76(6): 281–282.

Kramer, C.Y. (1956). Extension of multiple range tests to group means with unequal numbers of replications. *Biometrics* 12(3): 307–310.

Land, M.F. and D.E. Nilsson (2002). *Animal Eyes*. Oxford University Press, USA.

McCann, G.D. and G.F. MacGinitie (1965). Optomotor response studies of insect vision. *Proceedings of the Royal Society of London. Series B, Biological Sciences* 163(992): 369–401.

O'Carroll, D.C., N.J. Bidwell, S.B. Laughlin, and E.J. Warrant (1996). Insect motion detectors matched to visual ecology. *Nature* 382(6586): 63–66.

Osborne, J.L., S.J. Clark, R.J. Morris, I.H. Williams, J.R. Riley, A.D. Smith, D.R. Reynolds, and A.S. Edwards (1999). A Landscape-Scale Study of Bumble Bee Foraging Range and Constancy, Using Harmonic Radar. *Journal of Applied Ecology* 36(4): 519–533.

Pant, V. (2007). Biomimetic Visual Navigation Architectures for Autonomous Intelligent Systems. Ph.D. diss., University of Arizona, Tucson, Arizona.

Paulk, A.C., J. Phillips-Portillo, A.M. Dacks, J.M. Fellous, and W. Gronenberg (2008). The Processing of Color, Motion, and Stimulus Timing Are Anatomically Segregated in the Bumblebee Brain. *Journal of Neuroscience* 28(25): 6319–6332.

Paulk, Angelique C. and Wulfila Gronenberg (2008). Higher order visual input to the mushroom bodies in the bee, Bombus impatiens. *Arthropod Structure & Development* 37(6): 443–458.

Riabinina, O. and A.O. Philippides (2009). A model of visual detection of angular speed for bees. *Journal of Theoretical Biology* 257(1): 61–72.

Riley, J.R., D.R. Reynolds, A.D. Smith, A.S. Edwards, J.L. Osborne, I.H. Williams, and H.A. McCartney (1999). Compensation for wind drift by bumble-bees. *Nature* 400(6740): 126.

Rivera-Alvidrez, Z. (2005). Computational Modeling of Neurons Involved in Fly Motion Detection. Master's thesis, University of Arizona, Tucson, Arizona.

Riveros, A.J. and W. Gronenberg (2009). Learning from learning and memory in bumblebees. *Communicative and Integrative Biology* 5(2).

Si, A., M.V. Srinivasan, and S.W. Zhang (2003). Honeybee navigation: properties of the visually driven 'odometer'. *Journal of Experimental Biology* 206(8): 1265–1273.

Spaethe, J. and L. Chittka (2003). Interindividual variation of eye optics and single object resolution in bumblebees. *Journal of Experimental Biology* 206(19): 3447–3453.

Srinivasan, M.V., M. Lehrer, W.H. Kirchner, and S.W. Zhang (1991). Range perception through apparent image speed in freely flying honeybees. *Visual Neuroscience* 6(5): 519–535.

Srinivasan, M.V., M. Lehrer, S.W. Zhang, and G.A. Horridge (1989). How honeybees measure their distance from objects of unknown size. *Journal of Comparative Physiology A: Neuroethology, Sensory, Neural, and Behavioral Physiology* 165(5): 605–613.

Srinivasan, M.V., M. Poteser, and K. Kral (1999). Motion detection in insect orientation and navigation. *Vision Research* 39(16): 2749–2766.

Srinivasan, M.V., S.W. Zhang, and N. Bidwell (1997). Visually mediated odometry in honeybees. *Journal of Experimental Biology* 200(19): 2513–2522.

Srinivasan, M.V., S.W. Zhang, and K. Chandrashekara (1993). Evidence for two distinct movement-detecting mechanisms in insect vision. *Naturwissenschaften* 80: 38–41.

Srinivasan, M.V., S.W. Zhang, M. Lehrer, and T. Collett (1996). Honeybee navigation en route to the goal: visual flight control and odometry. *Journal of Experimental Biology* 199(1): 237–244.

Ugolini, A. (1987). Visual information acquired during displacement and initial orientation in Polistes gallicus (L.) (Hymenoptera, Vespidae). *Animal Behaviour* 35(2): 590–595.

Zanker, J.M., M.V. Srinivasan, and M. Egelhaaf (1999). Speed tuning in elementary motion detectors of the correlation type. *Biological Cybernetics* 80(2): 109–116.